Design and performance evaluation methodology of thermal piles with large diameter and heat capacity (熱容量を持つ大口径基礎杭利用地中熱交換器の設計・性能評価手法に関する研究)

Supervisor　Prof. Takao Katsura

2024

Division of Human Environmental System
Graduate School of Engineering
Hokkaido University

Kunning Yang

Abstract

In today's world, the demand for energy is immense, leading to substantial annual energy consumption. The foremost environmental challenge facing humanity is global warming, largely attributed to the greenhouse effect caused by carbon dioxide (CO2) emissions. These significant CO2 emissions mainly stem from the extensive use of fossil fuels to meet diverse energy needs. Notably, building energy consumption represents about 40% of global energy usage, with heating and cooling in buildings accounting for 50%-60% of this figure. To substantially reduce greenhouse gas emissions, energy supplies for space cooling and heating must be shifted from fossil fuels to renewable energy sources.

Ground Source Heat Pump (GSHP) systems are increasingly being adopted in residential and commercial buildings worldwide due to their remarkable energy efficiency, environmental benefits, consistent operation, and seamless integration with other energy systems. However, their widespread application is hindered by the need for large land areas for boreholes when installing multiple Ground Heat Exchangers (GHEs).

Thermal piles, a novel type of vertical GHE, exhibit superior heat exchange capabilities because of their large diameter and high thermal capacity. Their primary advantage is the elimination of the need for additional land, as they are integrated directly beneath buildings. This dual functionality provides both structural support and efficient heat exchange.

This doctoral thesis delves into the design and performance evaluation methods for large diameter, high capacity thermal piles, proposing optimal design strategies for their use in energy-efficient buildings. By combining theoretical innovation, empirical research, and practical implementation, this thesis positions itself as a valuable reference for future research and practical deployment in the field of thermal piles.

Chapter 1 presents the background of the study, setting the stage and underscoring the significance of the research. It emphasizes the critical role of thermal piles, an innovative class of vertical GHEs noted for their effective heat exchange properties. The chapter outlines the research objectives, concentrating on devising novel methodologies for the design and performance evaluation of thermal piles.

Chapter 2 offers a comprehensive literature review of the existing research on spiral tube GHEs and their integration into thermal piles. This chapter sets the foundation for the development of novel design and evaluation methods proposed in this thesis, aiming to bridge the identified research gaps.

Chapter 3 introduces a novel computational approach for double spiral tube GHEs, designed to enhance the precision and efficiency of heat transfer calculation. This method employs the Capacity and Resistance Model (CaRM) approach, offering a comprehensive examination of the heat transfer dynamics in thermal piles. A key innovation is the integration of fin efficiency, which substantially streamlines heat transfer calculations for spiral pipes. The chapter also provides a detailed introduction to a Zero-Energy Building (ZEB) in Sapporo, which serves as the data collection site for method validation. This new calculation method has successfully integrated into the GroundClub and rigorously validated within a GSHP system for winter heating and summer cooling applications. Simulation results demonstrate a close correlation with actual measured data, characterized by a low Root Mean Squared Error (RMSE) and highly precise fluid temperature variations. The method's superiority in terms of precision and practicality is further underscored by a comparative analysis with another model employed in studying spiral tube GHEs. The comparison reveals that the application of fin efficiency for simplified heat transfer in this model results in more precise calculated outcomes.

Chapter 4 provides an empirical analysis of the performance of double spiral tube GHEs in the ZEB, based

on nearly two years of operational data. This chapter improves upon previous research by introducing a novel, comprehensive metric: the coefficient of heat extraction/injection, for a more precise evaluation of GHE performance. The chapter describes the methodology employed to calculate this metric, offering a more precise evaluation of GHE performance. The methodology for calculating this metric is detailed, with a focus on assessing the heat exchange capability of GHEs. An extensive analysis of the measurement data is carried out, employing linear regression and histograms for data simplification and clearer visualization. This method determines an efficiency rate for thermal piles with double spiral tube GHEs at approximately 4 W/m·K, significantly higher than conventional U-tube GHEs. These results demonstrate the effectiveness of the new evaluation metric and affirm its practical applicability.

Furthermore, the chapter assesses the performance of the GSHP system. This involves calculating the System Coefficient of Performance (SCOP), Seasonal COP, and the annual heat extraction/injection rates of GHEs using the gathered data. The study observes that climate warming, characterized by rising summer temperatures in colder regions, leads to an increased cooling demand, sometimes surpassing winter heating needs. This imbalance in heat extraction and injection causes fluctuations in underground temperatures, affecting heat pump efficiency. These findings emphasize the necessity of incorporating climatic considerations in the design and implementation of future GSHP systems.

Chapter 5 combines the computational methods for double spiral tube GHE, introduced in Chapter 3 with the performance evaluation metrics for GHEs discussed in Chapter 4. It develops an optimal design approach for thermal piles used in GSHP systems. This approach enables rapid calculation of the ideal pitch length for double spiral tube GHEs and aids in determining the most cost-effective installation techniques for thermal piles. This chapter comprehensively explains the detailed calculation procedures of this optimized design method.

Furthermore, the chapter includes simulations of this design methodology under a range of conditions, including daily operating hours, undisturbed ground temperature, underground soil conductivity, underground depth, and the diameter of thermal piles. These factors are crucial in the design of GSHP systems. The results reveal that the spiral length of double spiral GHEs has a significant impact on its thermal efficiency. Several variables markedly affect the optimization process, leading to considerable variations in optimal spiral length and total investment costs under different scenarios. Based on the simulation results, this chapter summarizes patterns in thermal pile design that could guide future projects. It offers practical insights and recommendations, thereby contributing to the effective deployment of thermal piles in energy-efficient buildings.

Chapter 6 summarizes the key findings from the previous chapters, recognizing the limitations of the research and outlines potential directions for future studies. The chapter concludes by emphasizing the significance of the methodologies developed in evaluating the energy efficiency of thermal piles and their optimal design, offering both academic insights and practical solutions for GSHP systems.

Contents

Chapter 5

Chapter 6

Chapter 1

Introduction

1.1. Research Background

1.1.1. Global Primary Energy Consumption and Dependence on Fossil Fuels

Since the advent of the Industrial Revolution, human civilization has witnessed rapid progress, achieving remarkable accomplishments and considerable advancements in various fields. It is universally acknowledged that the evolution of society is intrinsically linked to energy resources. In contemporary society, energy needs are extensive, covering a wide array of applications. Each year, considerable amounts of energy are consumed to power a diverse range of vehicles, from small cars to large trucks, and to generate electricity in facilities like thermal power stations, hydroelectric plants, and nuclear reactors. The absence of energy resources would abruptly halt the advancement of human civilization.

Energy serves as a fundamental pillar in powering diverse modes of transportation, driving manufacturing processes, and providing lighting and heating in industrial, commercial, and residential sectors. **Fig.1.1** illustrates the global primary energy consumption trends from 1965 to 2020 [1], demonstrating that, in parallel with global development, energy consumption in 2020 has escalated to approximately four times that of 1965. Notably, the data indicates a relatively stable energy consumption in North America, primarily in the United States, without significant increases. In Europe, following approximately two decades of growth, energy consumption has tended to stabilize and even decrease. Conversely, the most rapid escalation in energy consumption is currently being observed in Asia, where it continues to rise. **Fig.1.1** also indicate that the increase in global energy consumption is largely positively correlated with the growth in the GDP per capita [2]. This correlation is particularly evident in many Asian countries, which, amidst rapid economic expansion in recent years, have experienced an exponential increase in energy usage, soaring by 15.6 times and showing a continuous upward trend.

Fig.1.2 illustrates the changes in global primary energy consumption by source from 1950 to 2020 [3], highlighting the dependency on fossil fuels. Additionally, **Fig.1.3** presents the latest data on the distribution of global primary energy consumption by source in 2022 [4]. These figures underscore a longstanding global reliance on fossil fuels, including oil, coal, and natural gas. This dependence is largely attributable to their high energy density and the ease of accessibility and usability. For instance, oil is particularly convenient due to its simple storage and transportation, and the current global transportation system is predominantly driven by petroleum derivatives. This extensive dependence on fossil fuels not only underscores its critical role in sustaining current societal functions but also highlights the escalating pressure on energy resources. It is becoming increasingly clear that human consumption rates are surpassing the Earth's capacity to produce these

resources and absorb the resultant waste. To amend this dire situation, a substantial reduction in fossil fuel consumption is imperative, coupled with the implementation of sustainable development practices across various societal activities.

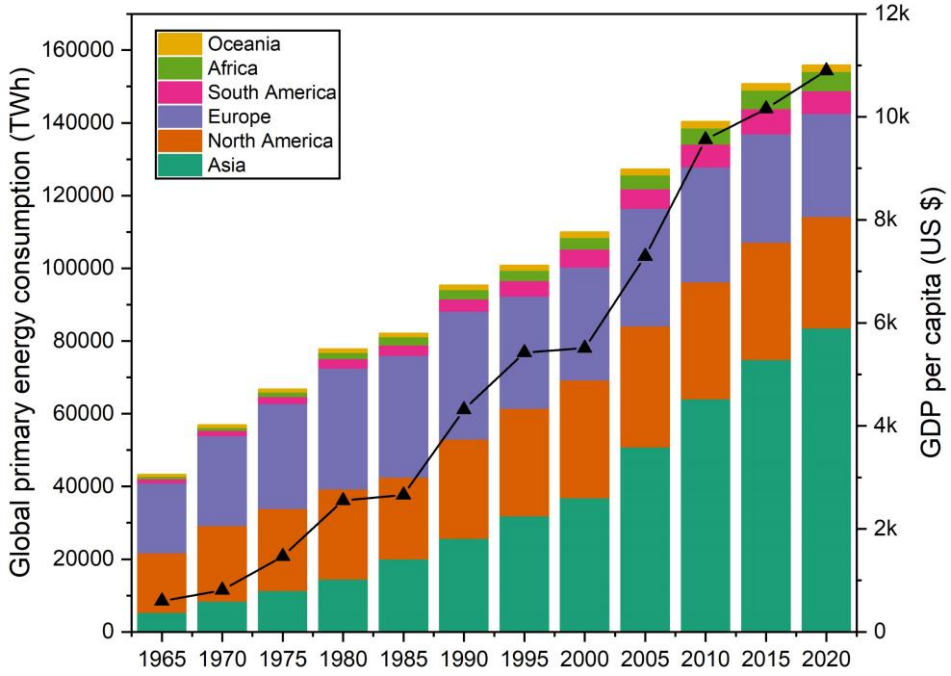

Fig.1.1 Global primary energy consumption and World GDP Per Capita from 1965 to 2020.

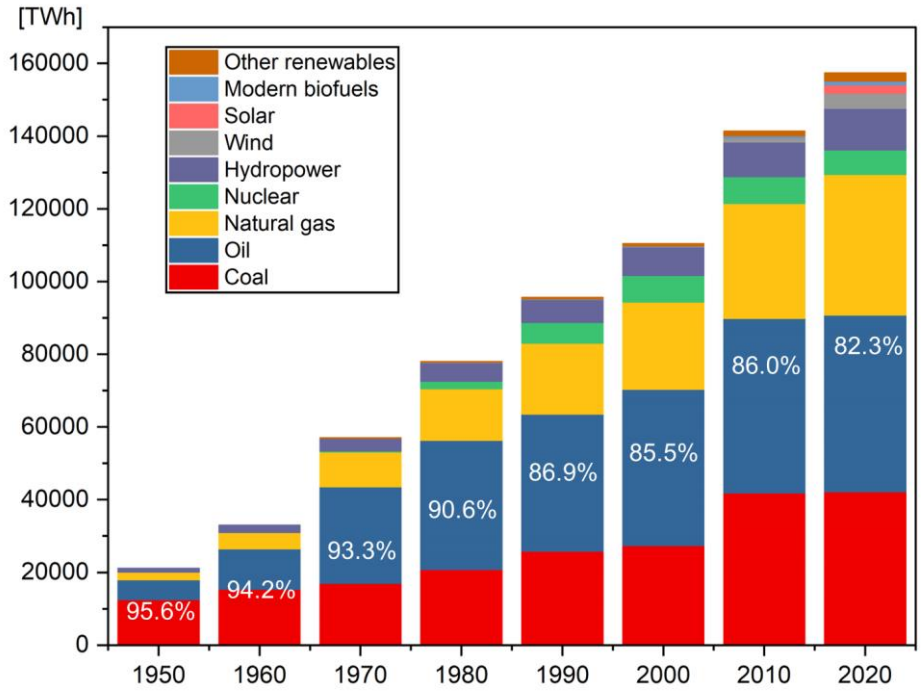

Fig.1.2 Global primary energy consumption from 1950 to 2020.

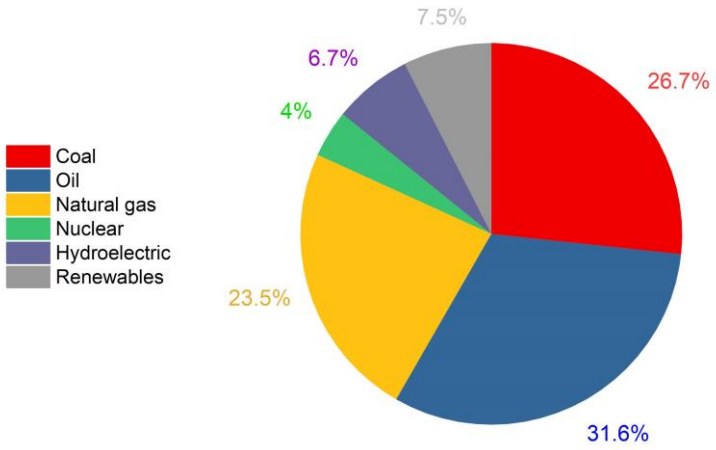

Fig.1.3 Global primary energy consumption by source in 2022.

1.1.2. Global Warming and Climate Change

Section 1.1.1 reveals that the global energy consumption is predominantly reliant on fossil fuels, a dependency that poses significant threats to the Earth, including the depletion of fossil fuel reserves and the generation of environmental issues, particularly global warming.

The Earth continuously receives solar radiation, a significant proportion of which is reflected back into space. The majority, primarily in the form of visible light, reaches the Earth's surface, where it is either absorbed or re-emitted as thermal radiation. However, the atmosphere contains minor but significant quantities of greenhouse gases (GHGs), predominantly carbon dioxide, which are opaque to thermal radiation. This property makes the atmospheric layer resemble a greenhouse covering the Earth, trapping a certain amount of heat. In the absence of this atmospheric layer, the Earth's surface would exhibit an average temperature of -18 °C. It is the greenhouse effect that maintains the Earth's average temperature at approximately 15 °C. Nevertheless, the current excess of greenhouse gases is leading to an increase in global surface temperatures, exacerbating the greenhouse effect and contributing to global warming.

Historically, atmospheric carbon dioxide levels, largely generated from the combustion or oxidation of organic matter, have remained relatively stable over thousands of years. Over the 5,000 years preceding the Industrial Revolution, atmospheric CO2 concentrations fluctuated only within a narrow range of 250-290 parts per million (ppm). However, since the late 18th century and the onset of the Industrial Era, atmospheric carbon dioxide levels have been on the rise due to the increased burning of fossil fuels. **Fig.1.4** illustrates the global atmospheric CO2 concentrations observed each January 15th from 1979 to 2023 [5]. This data clearly indicates that the excessive utilization of fossil fuels has contributed to a rapid escalation in global CO2 concentrations in recent

decades, surpassing the threshold of 400 ppm. Notably, it's not only the level of change in atmospheric CO2 that is of concern but also the unprecedented rate of this alteration. While historical changes in CO2 concentrations tended to occur over centuries or even thousands of years, the recent changes have occurred within mere decades.

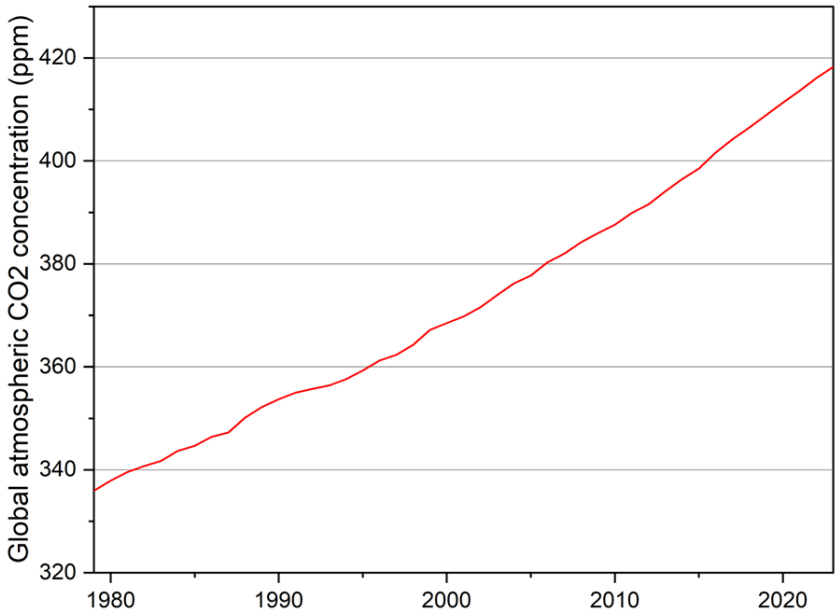

Fig.1.4 Global atmospheric CO_2 concentration, World.

Fig.1.5 illustrates the global average temperature relative to the average of the period between 1961 and 1990 [6]. This graph clearly demonstrates the influence of the greenhouse effect on global temperature rise. Notably, since the onset of the 21st century, escalating population growth and rapid industrial development have led to greater utilization of fossil fuels, resulting in a rise of over 0.6 degrees in global temperatures within the last two decades.

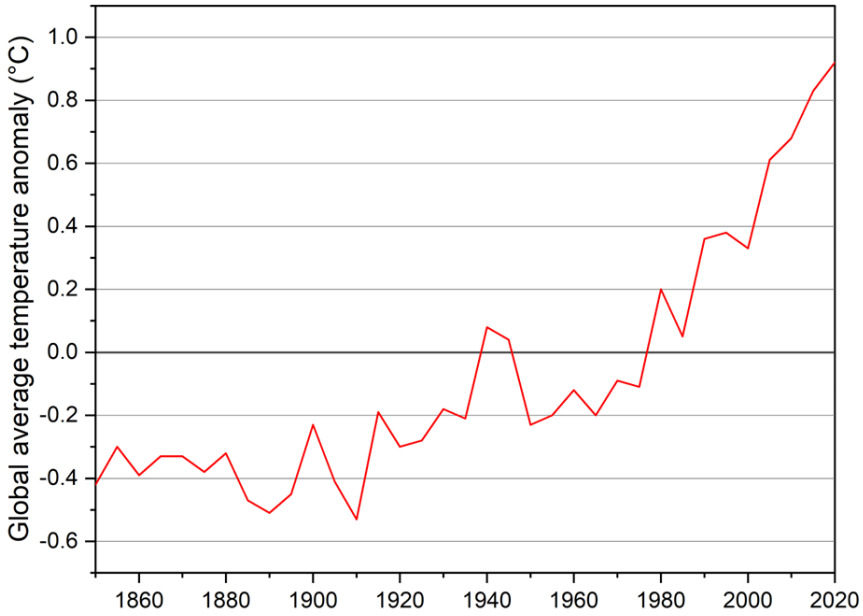

Fig.1.5 Average temperature anomaly, Global

Global warming is precipitating severe climatic changes. These changes encompass a range of potential ecological, physical, and health impacts, including extreme weather events like floods, droughts, storms, and heatwaves; rising sea levels; and disrupted water systems. It is estimated that over 90% of the thermal radiation reflected by GHGs is absorbed by the oceans, leading to an increase in ocean volume and a corresponding rise in sea levels. This absorption of heat by the oceans not only leads to an elevation in ocean temperatures but also accelerates the rate of seawater evaporation. The resulting increase in atmospheric humidity is closely associated with more frequent occurrences of heavy rainfall and flooding. Concurrently, the heightened temperatures cause increased evaporation, leading to soil dryness and subsequent drought conditions. Moreover, with rising temperatures, the extension of summer seasons and the consequent dryness of vegetation enhance the flammability of forests and facilitating the rapid spread of wildfires. **Fig.1.6** illustrates the annual frequency of natural disasters since 1950 [7]. While the incidence of earthquakes remains relatively constant, there is a noticeable surge in flood events and extreme weather occurrences, reflecting the profound impact of climate change.

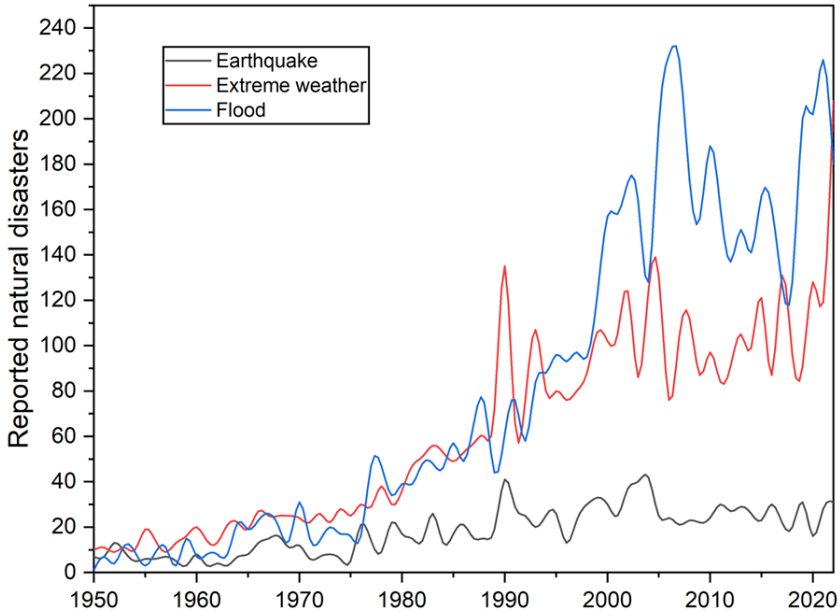

Fig.1.6 Number of recorded natural disaster events since 1950.

Climate change has escalated into a matter of human survival. In response to this environmental crisis, various international climate change treaties, including the Kyoto Protocol, Copenhagen Accord, and Paris Agreement, have been established to mitigate GHG emissions. A critical aim within these efforts is to achieve is the long-term temperature goal of limiting the increase in mean global temperature to 1.5 °C above pre-industrial levels.

1.1.3. Renewable Energy

Many of the Earth's resources are non-renewable, diminishing with use and inevitably facing depletion. Even if the actual reserves of fossil fuel resources are much larger than current estimates suggest, they are insufficient to sustain our society as the primary energy source for several centuries. Furthermore, the rapid and severe global warming, which is closely linked to fossil fuel combustion, may force an accelerated transition to renewable energy sources. A critical strategy in mitigating the release of greenhouse gases into the atmosphere involves reducing the combustion of fossil fuels across major sectors such as transportation, electricity generation, and heating. Transitioning to renewable energy sources is particularly impactful, as these resources emit far less carbon dioxide throughout their lifecycle compared to fossil fuels.

By definition, “renewable energy” refers to those energy sources that are either replenishable or inexhaustible, thereby remaining available for future human utilization. Most renewable energies, such as wind, wave, hydro, solar, and biomass, originate from solar radiation absorbed by the Earth. Tidal energy, on the other hand, originates from the gravitational interplay between the Earth, the Sun, and the Moon, whereas geothermal energy is sourced from the internal heat of the Earth's core. Despite certain challenges associated with their utilization,

the ability of renewable energy sources to produce end-use forms of energy such as electricity with considerably lower emissions, has led to their global recognition as sustainable and clean energy alternatives, thereby accelerating their adoption worldwide. **Fig. 1.7** illustrates the electricity generation from renewable sources since 1965 [8], revealing a steady growth in hydropower over an extended period. Notably, after 2000, driven by the heightened awareness of using renewable energy to reduce greenhouse gas emissions, there has been a rapid expansion in the generation of wind and solar power.

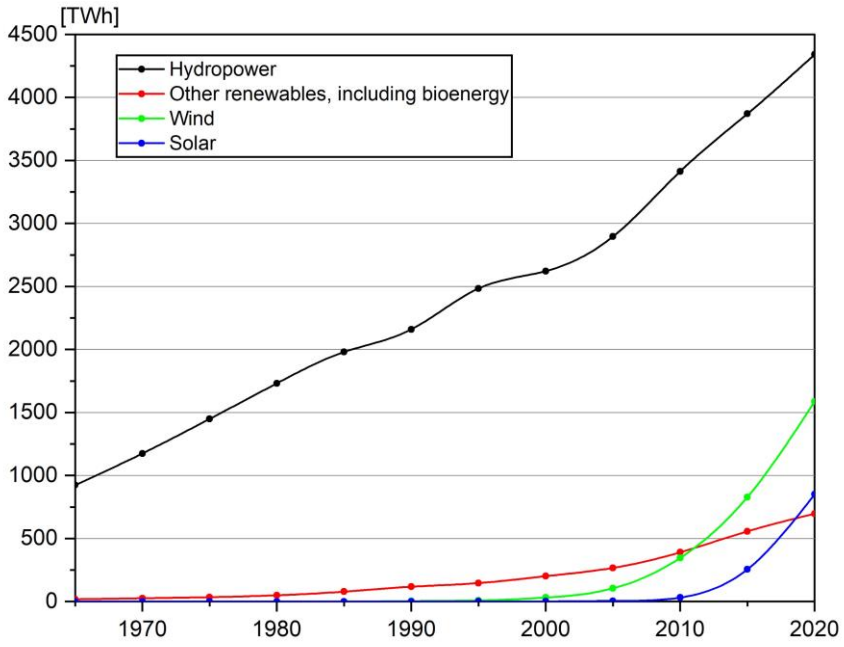

Fig. 1.7 Modern renewable energy generation by source, World.

Renewable energy sources, while offering numerous benefits, are accompanied by a range of challenges.

Hydropower, a long-utilized renewable resource, is associated with considerable ecological impacts. The construction of large dams, essential for many hydropower plants, leads to considerable environmental disruptions. These include flooding vast areas, altering natural water flow, obstructing fish migration, and requiring the resettlement of many people. Additionally, the sedimentation in many reservoirs causes submerged vegetation to decay, turning these areas into sources of greenhouse gas emissions, notably carbon dioxide and methane.

In contrast to hydropower and geothermal energy, wind and solar power provide energy in an intermittent and somewhat unpredictable manner. The inconsistency of wind energy arises from the variability in wind speeds, which proves challenging to forecast accurately over both short and long timescales. This unpredictability makes wind energy a less reliable source for meeting the consistent base load and peak electricity demands of contemporary societies. Additionally, wind turbines can cause noise pollution and pose risks to migrating birds

due to their blades.

Solar energy, while a promising renewable resource, faces challenges related to the environmental impact of its components and efficiency issues. The production of solar collectors and batteries often involves materials like copper and lead, raising concerns about environmental toxicity from waste accumulation. Market adoption of photovoltaic power generation remains limited, primarily due to the relatively low efficiency of photovoltaic conversion and the high cost of equipment. Although high-purity silicon crystal photovoltaic cells can achieve laboratory conversion efficiencies of nearly 25%, their efficiency in field applications frequently drops below 15% and further degrades over time to below 10%.

These pressing challenges continue to act as barriers to the widespread adoption of renewable energy technologies, necessitating further research and innovation to address these issues effectively.

1.1.4. Energy Consumption of Japan

Fig.1.8 showed the primary energy consumption of Japan and its dependency on fossil fuels from 1965 to 2020 [9]. Japan’s energy self-sufficiency ratio has consistently been low, heavily dependent on imported oil, coal, natural gas, and other fossil fuels. During the 1960s, Japan's rapid economic growth rate positioned it as the world's largest importer of oil at the time. Up to the present day, the share of fossil fuels in its energy mix has persistently exceeded 80%, indicating a continued high dependency on fossil fuels. Since 1980, Japan had made significant advancements in nuclear energy development. However, the Fukushima nuclear disaster in 2011 resulted in the abandonment of plans for new nuclear reactors and a marked decrease in nuclear energy utilization. This shift is evident in **Fig.1.9**, which depicts Japan's energy generation by source from 2012 to 2021 [10], highlighting the complete halt of nuclear power generation in 2014. In terms of renewable energy, Japan has sustained a steady level of hydroelectric power production, and there has been a significant shift towards solar power development, with its contribution to the energy mix rising from 0.63% in 2012 to 9.28% by 2021. Nevertheless, the country remains considerably behind in wind energy production, consistently accounting for less than 1%.

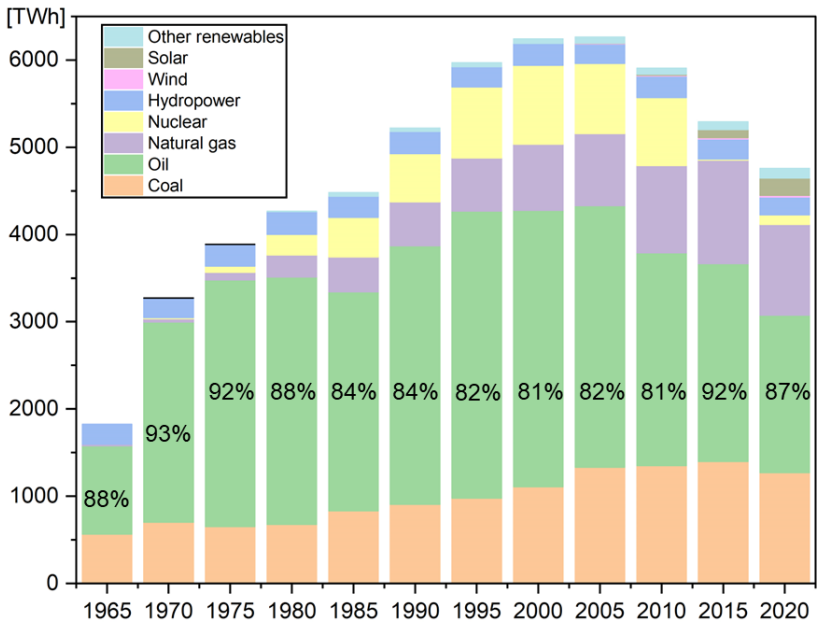

Fig.1.8 Japan's primary energy consumption by source from 1965 to 2020

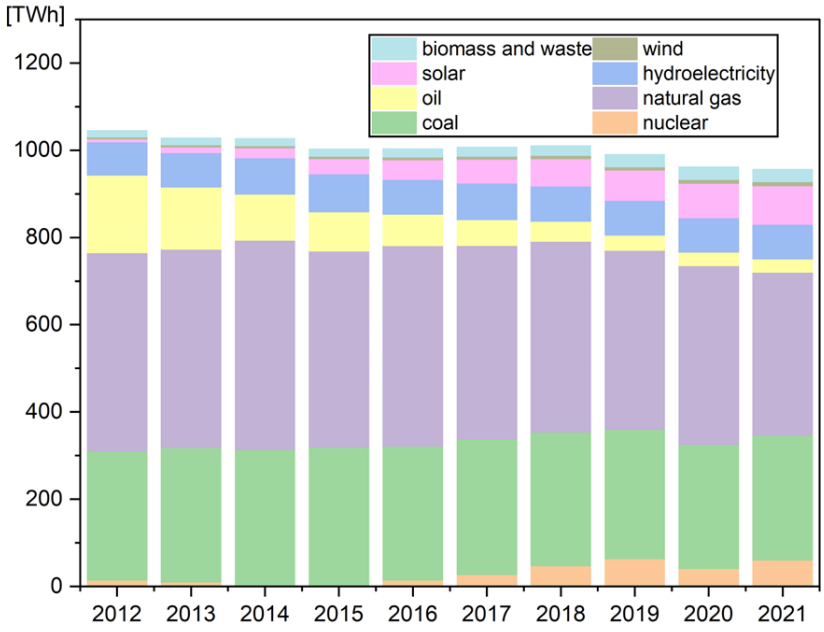

Fig.1.9 Japan's energy generation by source from 2012 to 2021

1.2. Ground Source Heat Pump (GSHP) System

1.2.1. Building Energy Consumption

The buildings sector, which include energy use for constructing, heating, cooling, lighting of residential and commercial buildings, as well as the appliances and equipment installed in them, represents a major energy consumer. In 2021, Operational energy demand in buildings, encompassing space heating and cooling, water

heating, lighting, cooking and other uses, accounts for around 34% of global final energy consumption, rising to 135 EJ. Furthermore, operational energy-related CO2 emissions from buildings exceeded 10 Gt CO2, constituting 37% of global energy-related emissions [11]. Within this sector, space heating in residential and commercial buildings contributes 32% and 33% to their total energy usage, respectively. Additionally, domestic hot water consumption contributes to 24% in residential buildings and 12% in commercial buildings [12]. Given the escalating impacts of climate change and the increasing frequency of heatwaves, there is a rising global demand for space cooling, which also constitutes a significant share of energy consumption in buildings. To achieve a substantial reduction in greenhouse gas emissions, there is a pressing need to transition the energy sources for space cooling and heating from fossil fuels to renewable energy sources.

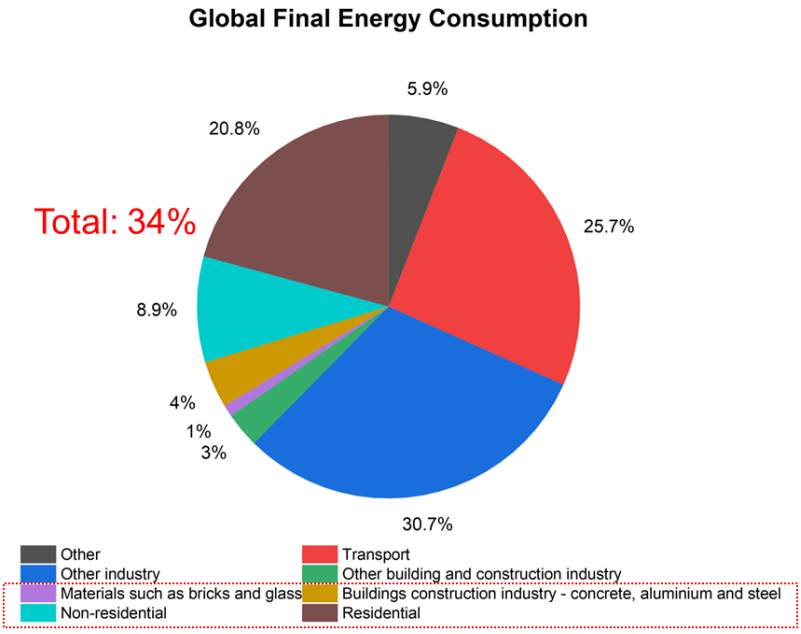

Fig.1.10 Share of buildings in total final energy consumptions in 2021.

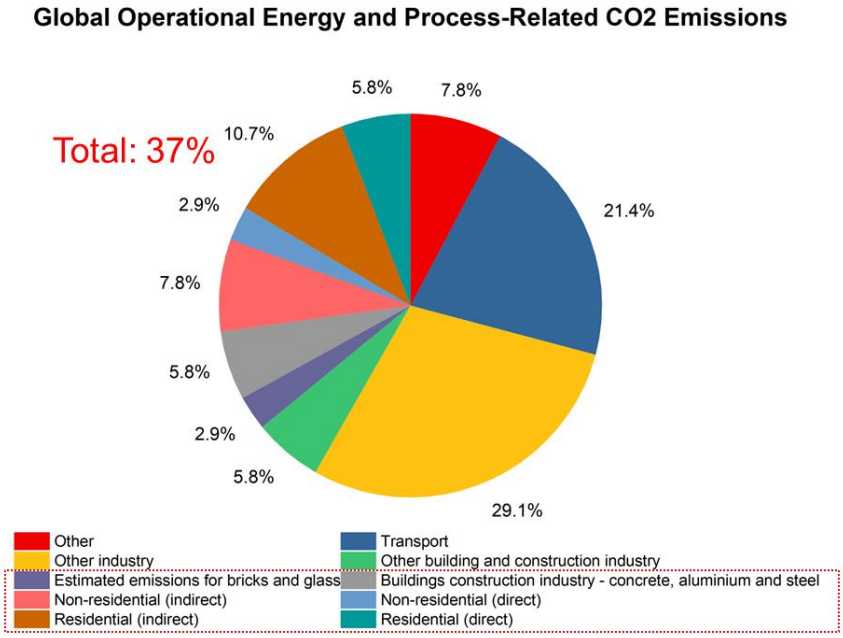

Fig.1.11 Share of buildings in global energy and process emissions in 2021.

1.2.2. Geothermal Energy

Geothermal energy, sourced from the Earth's internal heat, represents an important source of renewable energy, unique in its independence from solar-derived sources. Characteristically, geothermal energy offers consistent base-load generation, largely unaffected by weather conditions and devoid of seasonal fluctuations. It is exploited through two primary methods: large-scale power generation and smaller-scale direct heating applications.

In large-scale applications, geothermal power plants exploit subterranean hot water and steam, found in rock reservoirs and in vapor or liquid forms at temperatures exceeding 100 °C, to drive turbines for electricity generation and provide heating and cooling. As of 2022, the installed capacity of geothermal plants worldwide was approximately 14,877 MW, which, although growing, represents only a small fraction of global electricity production. According to the International Energy Agency's "Technology Roadmap: Geothermal Heat and Power", with dedicated efforts, geothermal power has the potential to contribute up to 3.5% of global electricity generation by 2050 [13].

Small-scale geothermal systems utilize subsurface heat for building heating and various industrial applications. Around half of these applications involve Ground Source Heat Pumps (GSHPs), which use the groundwater, ground, or surface water as a heat source/sink for space heating and cooling, and for providing domestic hot water. GSHP systems have gained increasing popularity in residential and commercial buildings globally, attributed to their high energy efficiency (surpassing that of widely used air-source heat pumps), environmental friendliness, consistent operation (as opposed to intermittently functioning systems), and compatibility with

other energy systems, such as photovoltaics.

1.2.3. GSHP systems

Heat pumps operate on the fundamental principle that gases and liquids expand and contract in response to temperature changes. Their increasing popularity for heating and cooling stems from their efficiency: heat pumps require less energy to transfer heat from a source to a sink than to generate heat from primary energy sources. The working principle, as illustrated in **Fig.1.12**, involves circulating a refrigerant through a closed-loop pipeline, where a compressor and an expansion valve modify the pressure along the path. This process enables the refrigerant to absorb heat in one area and release it in another. In winter, heat pumps transfer heat from the outdoors into a building, and in summer, they reverse this process to eject indoor heat outside. Utilizing heat pumps for building heating and cooling can largely reduce primary energy consumption.

Heat pumps are becoming essential for heat decarbonization, receiving substantial policy support worldwide in recent years. Modern models are 3-5 times more energy-efficient than traditional gas boilers. In 2022, heat pumps had the potential to satisfy approximately 60% of the global demand for space and water heating, offering lower CO_2 emissions than traditional gas boilers [14]. The International Energy Agency (IEA) projects that heat pumps could reduce global CO_2 emissions by at least 500 million tonnes by 2030.

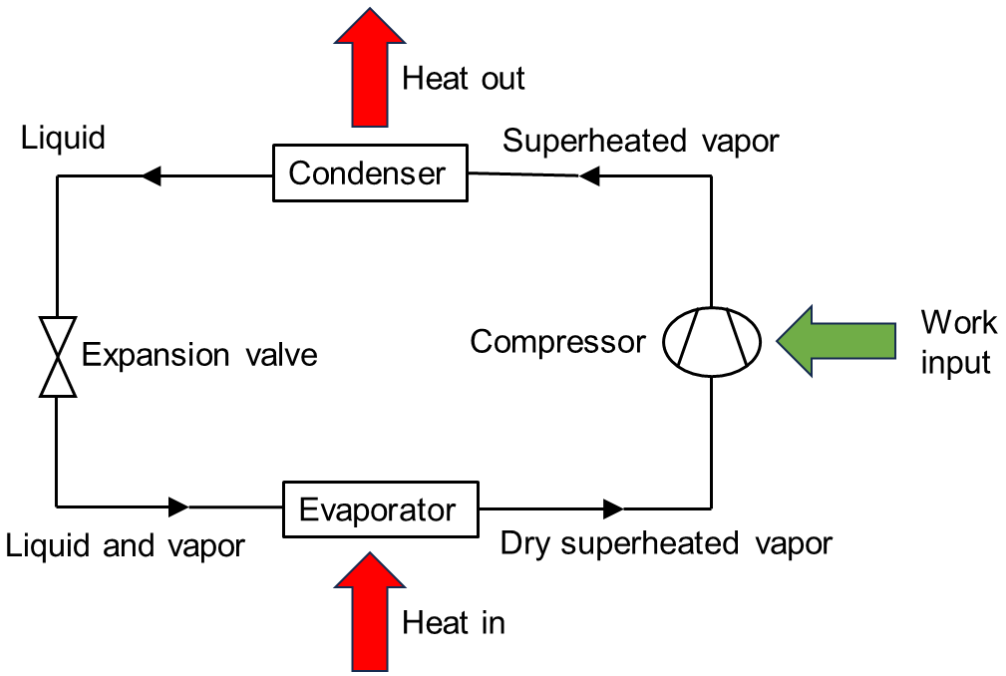

Fig.1.12 A conceptual model of a heat pump.

Ground-source heat pump (GSHP) comprise a broad range of systems utilizing the ground, groundwater, or surface water as a heat source and sink. These pumps are generally categorized into three types based on their

external heat exchange systems: ground-coupled heat pumps (GCHPs) with closed-loop piping systems underground, groundwater heat pumps (GWHPs) with open-loop systems using water wells, and surface-water heat pumps (SWHPs) with either closed-loop coils or open-loop systems linked to bodies of water like lakes and streams. In residential buildings, GCHP systems are most prevalent. These systems involve transferring heat to or from the ground via a closed-loop ground heat exchanger (GHE), which circulates either pure water or an antifreeze fluid. The GSHP system discussed in this study specifically refers to the GCHP system.

As depicted in **Fig. 1.12**, the relatively stable temperature of the shallow ground (in the undisturbed layer) throughout the year [15] facilitates the use of GSHP systems. These systems exploit the ground as a heat source or sink, employing GHEs to efficiently heat and cool buildings. These GHEs are installed at depth ranging from 20 to 300 meters, with diameters between 100 and 200 mm, utilizing circulating fluids such as ethylene glycol. Compared to traditional air conditioning methods, GSHP systems can substantially lower CO2 emissions. In winter, the underground space is warmer than the outside air, making it possible to extract heat from the ground via circulating fluid to heat buildings. Similarly, in summer, the cooler underground temperatures allow for circulating fluid to convey the heat from indoor to outdoor and inject them into the ground. Thus, GSHP systems maintain high efficiency across all seasons and climate types.

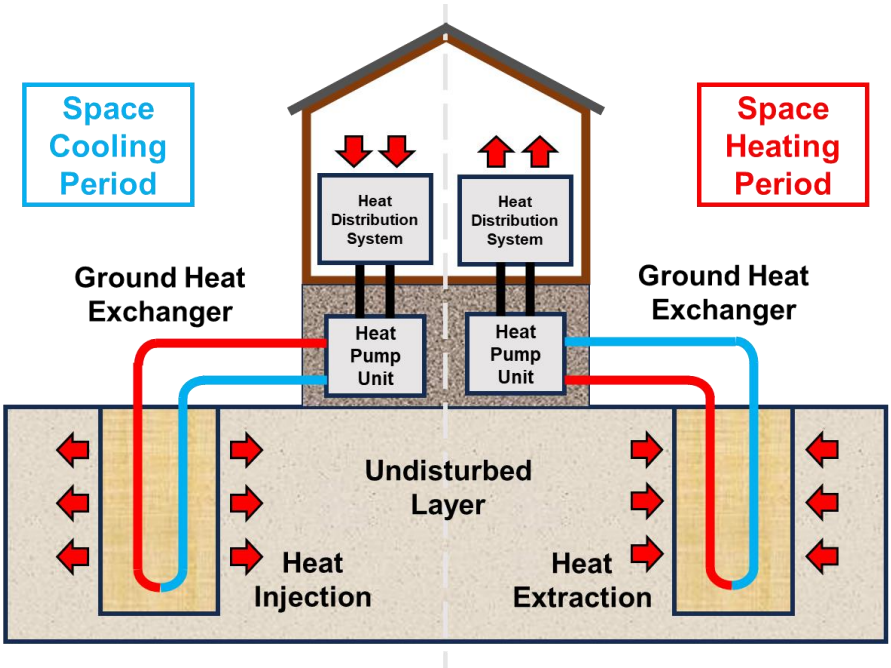

Fig. 1.12 A typical ground-source heat pump (GSHP) system providing space cooling and heating in a building.

Despite the considerable initial investment, the adoption of GSHPs has seen a consistent global increase, positioning them among the most effective heating and cooling systems in use. As shown in **Fig. 1.13**, GSHP

systems have gain popularity worldwide both in utilization and installed capacity in recent years [16]. The International Energy Agency projects that by 2050, direct geothermal heating could supply nearly 4% of the energy required for heating purposes. Moreover, as electrically driven heat pumps, GSHP systems can be integrated with renewable electricity sources, like solar photovoltaics, to achieve carbon-neutral heating and cooling. Additionally, GSHP systems have the capability to store heat extracted during summer, which can be subsequently utilized in winter heating modes.

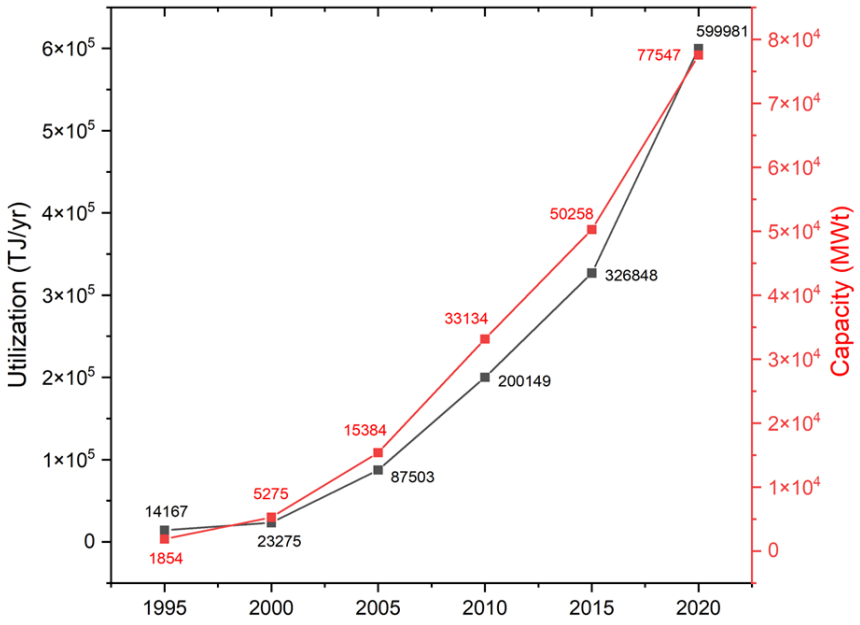

Fig. 1.13 The installed capacity and annual utilization of GSHP systems from 1995 to 2020.

1.2.4. Thermal Piles

GSHP systems offer several benefits: they are in contact with soil that varies very little in temperature and thermal properties, demand the least piping and pump energy, and can yield the most efficient thermal performance. The disadvantage is that they are typically higher in cost because of limited availability of appropriate equipment and trained installation personnel. Additionally, in recent years, as energy demands have increased, the usage of large-scale multiple GHEs has also risen. Nevertheless, their large-scale implementation faces a substantial obstacle, as they require extensive land area for borehole installation during the setup of multiple GHEs.

To overcome this limitation, an innovative approach has been developed: vertical GHEs with large diameter and heat capacity, commonly referred to as “thermal piles.” These are integrated into the foundation elements of buildings, thereby eliminate the need for additional installation space. This approach has become increasingly popular in energy-efficient residential and commercial buildings (as illustrated in **Fig. 1.14**). These dual-purpose

elements not only provide structural support to buildings but also serves as efficient heat exchangers. This integration effectively resolves the land space challenges associated with traditional Borehole Heat Exchangers (BHEs).

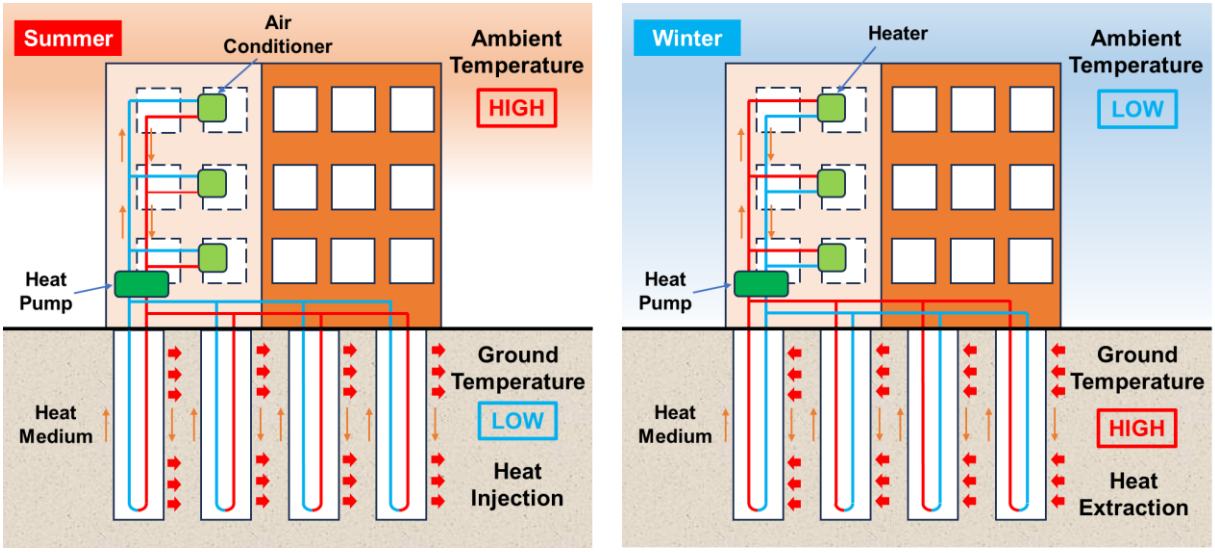

Fig.1.14 Operation of a building equipped with thermal piles during summer and winter.

In a thermal pile, heat exchanger pipes are integrated with the reinforcement cage of the pile prior to the pouring of concrete. Given concrete's high thermal conductivity, large heat capacity and good heat storage properties, foundation piles are an ideal medium for heat transfer to the surrounding soil. The primary focus of this doctoral thesis is to assess the performance of thermal piles, particularly addressing the heat transfer issues associated with thermal piles. It aims to establish a methodology for designing and evaluating the performance of thermal piles with large diameter and heat capacity.

The most used thermal piles are categorized into four types: H-shaped steel piles, cast-in-place concrete piles, prestressed high-strength concrete (PHC) piles, and steel piles. In recent years, there has been a significant increase in the utilization of thermal piles in many countries, including the United Kingdom and Japan. This increase is observable in the growing number of thermal piles used, the increasing quantity of buildings integrating this technology, and the substantial growth in CO2 savings. **Fig. 1.15** and **Fig. 1.16** [17][18] illustrate these trends.

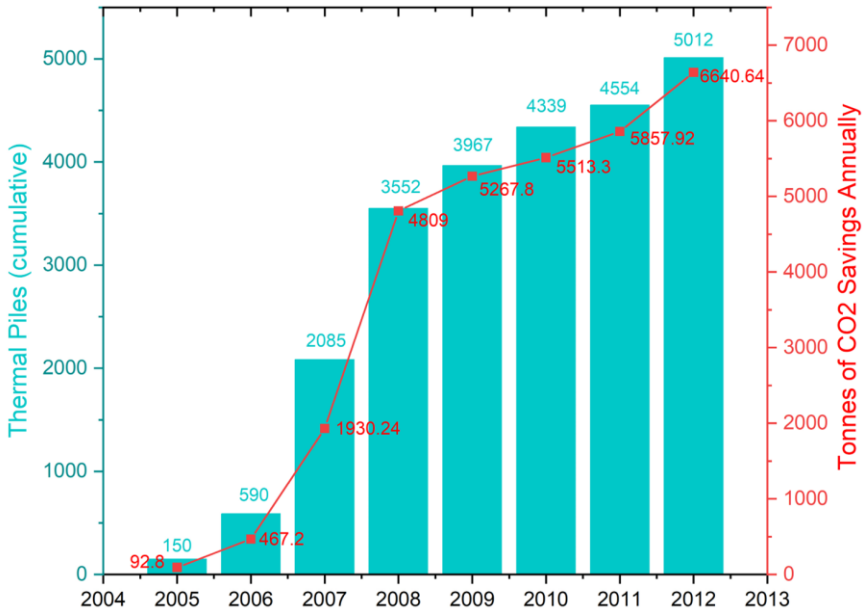

Fig.1.15 The resultant annual CO2 savings from thermal piles installed in the UK.

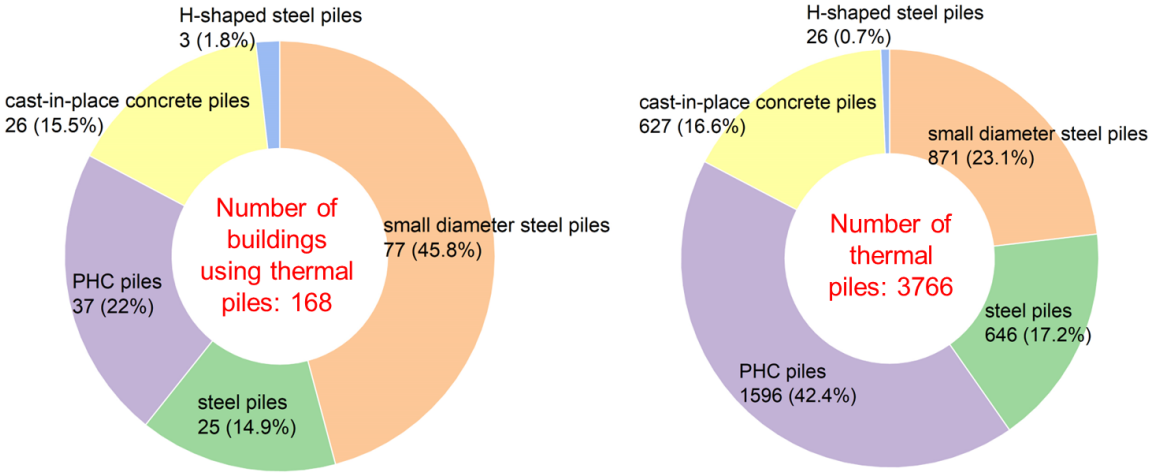

Fig.1.16 Categories of thermal piles being used in Japan, 2019.

1.2.5. Double Spiral tube GHEs

In early years, thermal piles were mainly built primarily consisted of driven precast concrete piles equipped with integrated heat exchange tubes. The technology has since evolved to incorporate large-diameter, deep-bored piles. These allow for the installation of multiple U-shaped loops of pipes, which circulate the carrier fluid. While U-tube GHEs have predominantly been used in thermal piles, this study focuses on the more complex double spiral tube GHEs.

Historically, U-tube GHEs have been the predominant choice, largely due to their simplicity in manufacturing. However, the installation of U-tube GHEs requires deep-borehole drilling, which is very costly. Addressing this, the Japan Pile Corporation, a Japanese construction company, innovated a new GHE type with double spiral

pipes and devised the Geothermal Tornado Method for its installation [19]. **Fig.1.17** illustrates the three types of GHEs: single and double U-shaped and double spiral tube. The double-spiral tube, at an equivalent borehole depth, offers a greater extended length than the conventional U-tube configuration, leading to an increased heat transfer surface area between the ground and the circulating fluid within the GHE. Moreover, the larger diameter of thermal piles, compared to conventional borehole GHEs, results in a higher thermal capacity, thereby allowing for increased heat exchange with the ground. Overall, this results in a significant boost in thermal efficiency.

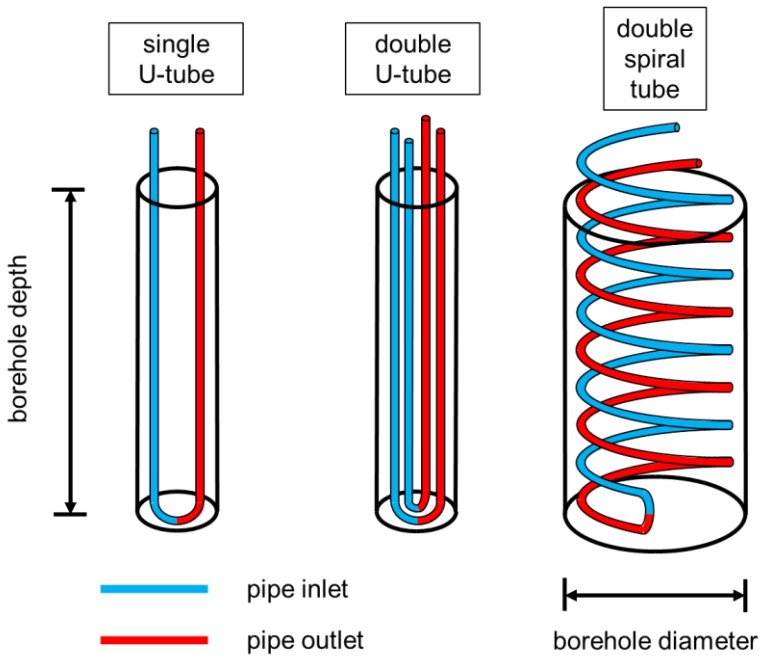

Fig.1.17 GHE configurations: (a) single U-tube; (b) double U-tube; (c) double spiral tube

The installation of double spiral tube GHEs used to be challenging, but the recent introduction of the "geothermal tornado method" by Japan Pile Corporation has effectively resolved these issues, ensuring safety and ease of installation. Here's a concise summary of the installation process, as illustrated in **Fig. 1.18** and **Fig. 1.19**:

1) Insert the compressed spiral pipe into the hollow section of the pile.
2) When the spiral pipe is half-extended, connect its lower joint to the bottom of the borehole.
3) Secure the fully extended spiral pipe at the pile head.
4) Begin rotating and embedding the pile into the ground.
5) After installation, trim and remove the excess spiral pipe from the pile head.

This technique not only succeeded in reducing installation time and labor, but also reduced the risks associated with damage, drilling work and initial costs.

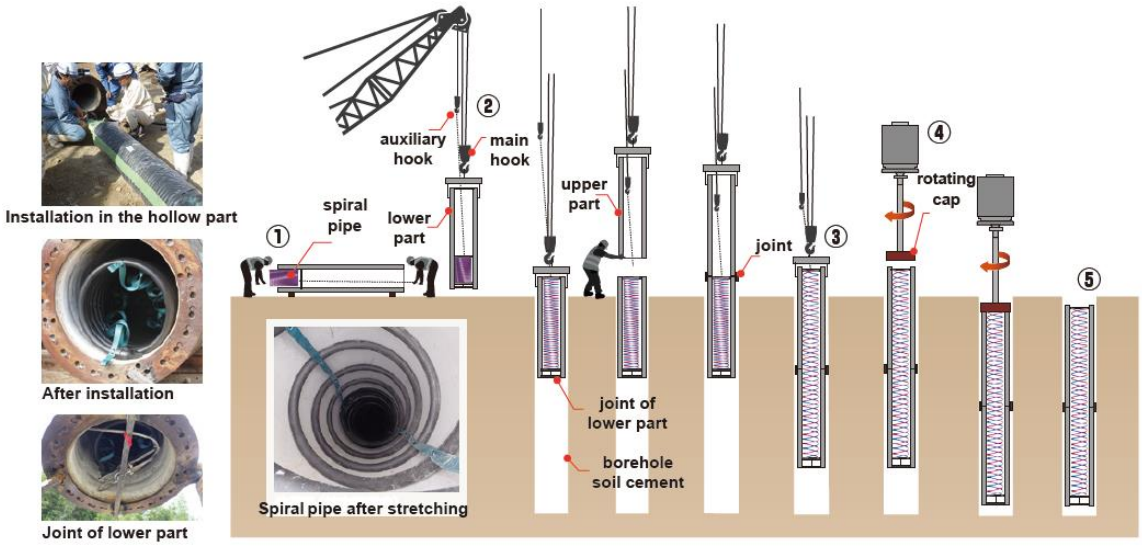

Fig.1.18 Installation process of "geothermal tornado method".

Fig.1.19 Installation process from the construction site.

1.3. Study Objective

The existing knowledge and design considerations for thermal pile performance are limited, more research work is necessary to build confidence in the utilization of thermal piles. Once clear design guidelines are established, the adoption of thermal piles is anticipated to surpass its current rate. Additionally, research on GHEs in spiral pipes is scarce, especially regarding the calculation and evaluation of their thermal efficiency.

The thermal behavior of thermal piles differs from that of borehole heat exchangers (BHEs), with several key factors to consider:

1) **Small length-diameter ratios in thermal piles**: Unlike conventional boreholes for GHEs, thermal piles typically have larger diameters, resulting in varying pipe geometry and layout. Traditional BHE designs often use temperature response functions, such as g-functions, for feasible design. However, these functions, originally based on heat sources with small diameter and large depth/spacing ratios, are not suitable for thermal pile design. In contrast, the length-diameter ratio of thermal piles is relatively small compared that of conventional BHEs. The smaller length-diameter ratio of thermal piles, compared to BHEs, means that applying these functions to thermal piles might underestimate temperature changes at shorter timescales.
2) **Delayed heat transfer in large diameter thermal piles**: Simple heat source models assume a steady-state temperature within the pile when predicting ground temperature changes. While effective in BHE design, this approach may not be suitable for large piles due to their substantial concrete cross-sectional area. Short-term heat transfer analysis should consider the concrete's thermal mass and the varying thermal properties between the pile and surrounding soil.

3) **Complexities in pile heat exchanger geometries**.

The objectives of this study are:

1) **Developing a simpler calculation method**: This involves adapting the method used for hot water floor heating systems to double spiral tube GHEs, aiming for a concise yet accurate heat transfer calculation.
2) **Introducing a new performance metric for GHEs**: This metric, validated for effectiveness and accuracy, incorporates the temperature of the undisturbed layer and circulating fluid. It will be based on approximately two years of data from a Zero Energy Building (ZEB), effectively evaluating the thermal efficiency of double spiral tube GHEs.
3) **Formulating design methods based on new calculation method and performance metric**: This will aid in optimizing thermal piles equipped with double spiral GHEs, crucial for their future application and promotion.

Reference

[1] “Primary energy consumption by source, 2022.” Accessed: Dec. 02, 2023. [Online]. Available: https://ourworldindata.org/grapher/primary-energy-source-bar

[2] “GDP per capita (current US$) | Data.” Accessed: Dec. 02, 2023. [Online]. Available: https://data.worldbank.org/indicator/NY.GDP.PCAP.CD

[3] “Global primary energy consumption by source.” Accessed: Dec. 02, 2023. [Online]. Available: https://ourworldindata.org/grapher/global-energy-consumption-source

[4] bp, “Statistical Review of World Energy 2022”.

[5] N. G. M. L. US Department of Commerce, “Global Monitoring Laboratory - Carbon Cycle Greenhouse Gases”.

[6] C. P. Morice *et al.*, “An Updated Assessment of Near-Surface Temperature Change From 1850: The HadCRUT5 Data Set,” *Journal of Geophysical Research: Atmospheres*, vol. 126, no. 3, Feb. 2021, doi: 10.1029/2019JD032361.

[7] “Number of recorded natural disaster events, 1900 to 2023.” Accessed: Dec. 02, 2023. [Online]. Available: https://ourworldindata.org/grapher/number-of-natural-disaster-events

[8] “Modern renewable energy generation by source, World.” Accessed: Dec. 02, 2023. [Online]. Available: https://ourworldindata.org/grapher/modern-renewable-prod

[9] “Brochures｜Agency for Natural Resources and Energy.” Accessed: Dec. 02, 2023. [Online]. Available: https://www.enecho.meti.go.jp/en/category/brochures/#pamph

[10] “International - U.S. Energy Information Administration (EIA).” Accessed: Dec. 02, 2023. [Online]. Available: https://www.eia.gov/international/analysis/country/jpn

[11] “2022 Global Status Report for Buildings and Construction | UNEP - UN Environment Programme.” Accessed: Dec. 03, 2023. [Online]. Available: https://www.unep.org/resources/publication/2022-global-status-report-buildings-and-construction

[12] D. Ürge-Vorsatz, L. F. Cabeza, S. Serrano, C. Barreneche, and K. Petrichenko, “Heating and cooling energy trends and drivers in buildings,” *Renewable and Sustainable Energy Reviews*, vol. 41. 2015. doi: 10.1016/j.rser.2014.08.039.

[13] “Technology Roadmap - Geothermal Heat and Power – Analysis - IEA.” Accessed: Dec. 03, 2023. [Online]. Available: https://www.iea.org/reports/technology-roadmap-geothermal-heat-and-power

[14] “Heat Pumps - Energy System - IEA.” Accessed: Dec. 04, 2023. [Online]. Available: https://www.iea.org/energy-system/buildings/heat-pumps

[15] G. Florides and S. Kalogirou, “Ground heat exchangers-A review of systems, models and applications,”

Renewable Energy, vol. 32, no. 15. 2007. doi: 10.1016/j.renene.2006.12.014.

[16] J. W. Lund and A. N. Toth, “Direct utilization of geothermal energy 2020 worldwide review,” *Geothermics*, vol. 90, 2021, doi: 10.1016/j.geothermics.2020.101915.

[17] A. Amis and F. Loveridge, “Energy piles and other thermal foundations for GSHP – developments in UK practice and research,” 2014.

[18] “1-10.初期費用を下げる対策としてどの様なことが考えられているのでしょうか？ | 地中熱利用促進協会.” Accessed: Dec. 03, 2023. [Online]. Available: http://www.geohpaj.org/introduction/qa/1-10

[19] “地熱トルネード工法 (地中熱利用技術) | 周辺技術 | 施工・製品情報 | ジャパンパイル株式会社.” Accessed: Dec. 07, 2023. [Online]. Available: https://www.japanpile.co.jp/method/othertech/tornado/

Chapter 2

Prior Research on Spiral Tube Ground Heat Exchangers and Thermal Piles

2.1. Simulation Models of Spiral Tube Ground Heat Exchangers

In this study, the primary focus is on the spiral tube Ground Heat Exchangers (GHEs), which is more complicated than conventional U-tube GHEs. Accurately modeling the heat transfer in spiral tube GHEs is of great importance. Prior research and experimental studies have extensively explored spiral tube GHEs. Yang et al. [1] established a model experimental apparatus for an energy pile with spiral tube GHEs based on the principle of similarity. Their investigation covered the impact of variables such as inlet water temperature, intermittent operation mode, spiral pitch, and pile material on the thermal performance of spiral tube GHEs, as well as the effect on the temperature distribution in the surrounding soil of the energy pile. Kim et al. [2] proposed a design method for horizontal spiral tube GHEs by modifying the boundary conditions of an existing equation. They validated their model through a laboratory thermal response test (TRT), finding that their numerical modeling closely matched the experimental data. Dinh et al. [3] conducted an indoor TRT test to evaluate the heat transfer performance of spiral tube GHEs. Their results revealed that spiral tube GHEs exhibit higher heat exchange rate (twice that of U-tube GHEs), and shorter payback period.

The approaches to analyze the heat transfer in spiral tube GHEs can be classified into three categories: numerical model, analytical model, capacity and resistance model (CaRM).

2.1.1. Numerical Model

Numerical models comprise numerous mathematical equations consist of a multitude of mathematical equations that utilize computers and simulation software to approximate solutions to fundamental physical problems. This enables highly detailed 2D or 3D modeling of substantial complexity. However, these models require extensive computation time and deep understanding due to their significant complexity. Recent advancements in computer science and improved computing power have enabled numerical models to accurately represent the heat transfer process in various GHEs through complex modeling over long-term operation.

Carotenuto et al. [4] analyzed the heat transfer performance of the thermal piles using various GHEs, including U-shaped, double U-shaped, triple U-shaped, and spiral tubes. Their findings indicated that spiral tubes exhibit the best heat transfer performance. In a comparative study by Zhao et al. [5], different GHE types in thermal piles were analyzed, revealing that spiral tube GHEs have better thermal performance than the others in both short-term and long-term operations. Serageldin et al. [6] utilized ANSYS Workbench to simulate a 3D model of double spiral tube GHEs. Their simulation results showed that double spiral tube GHEs have better thermal efficiency, a higher heat transfer rate, and lower thermal resistance under turbulent flow conditions compared to

single U-shaped pipes. Yoon et al. [7] combined experimental and numerical methods to study spiral tube GHEs, assessing the thermal conductivity of the ground through TRT test and created a three-dimensional finite element model of the spiral tube GHE to compare numerical and experimental results.

Park et al. [8] explored heat transfer around helical tube GHEs through both experimental and numerical research, applying axisymmetric finite element analyses. They improved the heat source models for helical tube GHEs by incorporating a finite-length line source solution, which considered the vertical return pipe at the center of the helical tube GHEs. Dehghan [9] employed COMSOL software to develop mathematical models for nine different arrangements of spiral tube GHEs. These models investigated various factors, such as performance decay, GHE spacing, and thermal interactions under different working fluid temperatures. These models examined factors like performance decay, GHE spacing, and thermal interactions at varying working fluid temperatures, suggesting a minimum spacing of 6 meters between spiral tube GHEs, with a 2-meter embedding depth below the ground surface. Lastly, Suzuki et al. [10] utilized TOUGH2/EOS1 for the development of spiral tube GHEs and double U-tube GHEs for GSHP system, focusing on the accuracy of temperature field formation and heat flow and calculating the initial cost per unit of heat exchange capacity. Their simulation results indicated that spiral tube GHEs are approximately 30% more cost-effective than double U-tube GHEs in both gravel and clay layers, highlighting the advantages of spiral tube GHEs.

2.1.2. Analytical Model

Analytical models, which offer solutions to the diffusivity equation, require a multitude of simplifying assumptions. These assumptions are often complex to derive and analyze, yet they aim to provide precise closed-form expressions for specific characteristics. Despite the complexity of their derivation, analytical models are highly advantageous for calculating the heat transfer process in various GHEs. They are not only suitable for academic research but also highly applicable for engineering applications.

Cui et al. [11] developed a transient ring-coil heat source model to investigate transient heat conduction around buried spiral tube GHEs. However, a limitation of their model is the neglect of the pipe's size, resulting in simulated temperatures that frequently deviate from the actual conditions. Zhang et al. [12] refined this by simplifying calculations and accounting for the spiral tube's arrangement and pitch. However, their model falls short when the grouting material varies from the surrounding soil. Subsequently, Park et al. [13] introduced an efficient spiral coil source model with an analytical solution, although its long-term efficiency remains unconfirmed.

Man et al. [14], [15] then proposed a solid cylindrical source model for pile foundations, considering both the radial dimension and heat capacity of the borehole or pile. Li et al. [16], [17] further enhanced this model by

employing the Green's function method to derive analytical solutions for 1D and 2D models in infinite or semi-infinite anisotropic media with a line, spiral-line, or cylindrical-surface heat sources. This provided new temperature response functions for pile GHEs with spiral coils and borehole GHEs with single or double U-shaped pipes. Leroy et al. [18] innovated further with a model for spiral tube GHEs incorporating axial effects using the Green's function approach, simulating fluctuating thermal reactions in spiral tube GHEs by combining heat sources at different locations. To overcome the limitations of existing analytical models for spiral tube GHEs, especially when the thermal properties of pile material and soil vary, Lei et al. [19] developed a hybrid analytical model. This model, utilizing a decomposition algorithm, effectively addresses the challenges of a coil line source embedded in a composite cylinder, with error analysis confirming its suitability for engineering applications.

2.1.3. Capacity and Resistance Model (CaRM)

The Capacity and Resistance Model (CaRM), also recognized as the Lumped Thermal Capacity Model, is a simplified method for analyzing thermal systems, particularly useful in transient heat conduction analysis. This model reduces the complexity of thermal systems into discrete entities, based on the assumption of minimal temperature variations within each entity. The CaRM utilizes a network connecting temperature nodes, thermal resistances, and thermal capacities to streamline the complex differential equations typically involved in heat transfer. The model's primary advantages are its simplicity and practical applicability. This model facilitates the resolution of various transient heat transfer problems, such as:

1) Estimating the time required to either cool or heat a solid from its initial temperature to a certain temperature.
2) Calculation of temperature of the solid at any given time.
3) Determining the total energy transferred to or from the solid.
4) Calculation of heat transfer coefficient between the solid surface and surrounding fluid

These capabilities make the CaRM an essential tool for thermal analysis, particularly in scenarios where a simplified yet effective approach is necessary.

In the field of borehole heat exchangers (BHEs), Bauer et al. [20] developed two-dimensional thermal resistance and capacity models, considering all thermal resistances between the fluid in the pipes, grout capacities, and borehole wall. Their models, when validated against fully discretized Finite Element Method (FEM) models, showed high accuracy. Minaei et al. [21] further advanced this approach by devising an analytical method for modeling heat transfer in BHEs over short periods, incorporating thermal resistance and capacity circuits and accounting for radial heat transfer in the surrounding ground, as well as the thermal capacities of fluid and grout. Their analytical results closely matched reference numerical outcomes.

The CaRM model was notably applied by Zarrella et al. [22] to analyze the heat transfer of spiral tube GHEs. Their comparative analysis between spiral tube and double U-tube GHEs for long- and short-term operations revealed that despite being 33% shorter, spiral tube GHEs exchanged the same amount of heat with the ground as double U-tube GHEs, suggesting potential installation cost reductions. In short-term operations, spiral tube GHEs supported higher peak loads due to the greater heat capacity of thermal pile. Furthermore, field experiments and numerical analyses [23] compared spiral tube and triple U-tube GHEs in a foundation pile, with the spiral tube GHEs showing a 23% increase in peak thermal performance.

2.2. Factors Affect Thermal Efficiency of Ground Heat Exchangers

A critical component of any GSHP system is the GHEs. In designing GSHP systems, a critical question is the appropriate size of the GHEs. Incorrect sizing can lead to early system failure or reduced efficiency. If the GHE is too small, the system may fail soon after starting or after several years of operation. Conversely, an oversized GHE results in unnecessary expense and potential selection of less energy-efficient alternatives. The thermal efficiency of the GHEs is a key factor in the performance of GSHP system; hence, accurate evaluation of heat transfer in GHEs is essential for the design and operational efficiency of GSHP systems.

The thermal efficiency of GHEs can be influenced by various factors. Extensive research, encompassing both numerical simulations and experimental tests (laboratory and field studies), has been conducted to understand the heat transfer behavior of GHEs. These studies have addressed various performance measurement and analysis concerns. Additionally, numerous studies have assessed the efficiency of GHEs using a variety of parameters and methodologies, as detailed below:

2.2.1. Material of ground and grout

In thermal piles with large diameters, it is crucial to account for the thermal mass and varying thermal properties of both the grouting material and the surrounding soil during heat transfer analysis. The temperature difference between the circulating fluid and ground can substantially impact heat transfer, influenced by factors like medium type, undisturbed ground temperature, and thermal conductivity. Although a greater temperature differential can lead to more efficient heat exchange, maintaining ground temperature within safe limits is essential to avoid long-term system performance degradation.

Chen et al. [24] developed a numerical model for in-depth analysis of Deep Borehole Heat Exchanger (DBHE) systems, finding that soil thermal conductivity greatly affects the specific heat extraction rate (W/m). Tang et al. [25] employed numerical simulations to determine the primary factors affecting the GSHP system's coefficient of performance (COP). They noted that changing from clay to sand and operating in warmer climates

(meteorological conditions) can substantially boost system efficiency. Cao et al. [26] performed experimental tests on flat-panel GHEs and discovered that the choice of backfill material substantially affects the overall operating efficiency of the system, with a water–sand mixture markedly improving the heat transfer rate (W) compared to dry sand. Zhang et al. [27] studied a DBHE system and observed that increased thermal conductivity in geological formations resulted in higher heat extraction and injection rates during winter and summer, respectively. Congedo et al. [28] analyzed horizontal GHEs using FLUENT, reporting that the surrounding ground's thermal conductivity is the key parameter affecting heat transfer performance, with optimal ground types possessing the highest conductivity. Lastly, Zhang et al. [29] combined field experiments and numerical simulations to investigate the long-term thermal properties of a prestressed high-strength concrete (PHC) pile in a layered foundation. Their work showed that enhancing the backfill soil's thermal conductivity can significantly improve the heat exchange rate (W/m) of a PHC pile.

2.2.2. Temperature of the pipe inlet and outlet

The temperatures at the inlet and outlet of the GHEs can considerably influence the heat exchange capacity of the GSHP systems.

Jalaluddin et al. [30] explored the thermal performance (W/m) of spiral tube GHEs, uncovering that variations in the pipe inlet temperature can markedly alter the rate of heat exchange. Moreover, Huang et al. [31] and Cai et al. [32] developed an analytical model to evaluate the efficiency of heat exchange in deep geothermal systems under nonuniform ground conditions. This model, based on reliability theory, indicates that a greater temperature differential between the pipe inlet and the undisturbed ground layer can notably boost the system's heat exchange efficiency.

2.2.3. Configurations and materials of GHEs

The design and materials of GHEs are crucial in determining their thermal efficiency. Optimized designs enhance the interaction between the ground and the circulating fluid, leading to improved performance. Additionally, the use of materials with high thermal conductivity is crucial in these systems.

Serageldin et al. [33] explored an oval U-tube GHE, employing computational fluid dynamics simulations to show a reduction in thermal resistance and an increase in the COP of GHEs. Jahanbin [34] proposed a single U-tube GHE design, demonstrating through three-dimensional finite element simulations that elliptical U-tubes significantly boost heat transfer and lower borehole thermal resistance, compared to traditional single U-tubes. Majeed et al. [35] assessed GHEs made of different materials like polyvinyl chloride (PVC), copper, and galvanized materials. Their findings indicate copper pipes have the highest heat exchange rate (W/m), while

PVC pipes have the lowest. Kerme and Fung [36] compared single and double U-tube BHEs, concluding that double U-tube BHEs offer superior performance and lower resistance. Kim et al. [37] developed a stainless-steel BHE, finding it to have a maximum heat capacity and gain (kW) 160% and four times higher, respectively, than conventional GHEs made of high-density polyethylene, indicating a superior ground heat extraction capacity. Zou et al. [38] developed a three-dimensional heat transfer model for three types of Horizontal Ground Heat Exchangers (HGHEs), showing that spiral-coil HGHEs have the best performance in terms of COP and heat transfer rate (W/m).

2.2.4. Diameter and depth of borehole

The depth and diameter of boreholes can substantially enhance the thermal efficiency and performance of GHEs in GSHP systems, facilitating improved heat transfer. However, the increased costs associated with deeper and wider borehole drilling must be considered.

Luo et al. [39] analyzed the thermal load of BHEs with three borehole diameters installed in GSHP systems, revealing that larger diameters can slightly improve the thermal performance of the BHEs. Dehghan [40] conducted both experimental and computational studies on the thermal dynamics of spiral tube GHEs, finding that the heat transfer rate is heavily reliant on the borehole's vertical length. Additionally, the distances between multiple GHEs leads to thermal interactions that have a minor effect. Li et al. [41] examined various factors affecting a GSHP system's energy efficiency, concluding that the operation mode and depth of the buried GHEs are more influential than other variables. They also noted that intermittent operation of the GSHP system enhances heat exchange efficiency of GHEs, and deeper pipe installation correlates with higher energy efficiency coefficients.

Beyond these considerations, other variables also must be considered. Walch et al. [42] assessed the potential (kWh/m2) of GSHP systems for district heating and cooling, noting that seasonal regeneration considerably reduces thermal interference between boreholes, thus impacting the maximum achievable geothermal potential. Guo et al. [43] analyzed how groundwater flow affects the thermal performance of BHEs in Tangshan, China, finding that natural groundwater flow has a negligible effect on enhancing heat transfer. Tu et al. [44] developed a thermal resistance and capacity model to study the interaction between vertical single U-tube GHEs and frozen soil in extremely cold climates, demonstrating that frozen soil can increase the GHE’s heat transfer capacity (W/m) by 30%.

2.3. Research of spiral tube GHEs Integrated into Thermal Piles

Section 2.1 and 2.2 discussed how the performance of spiral tube GHEs are susceptible to various influences and have lacked a suitable design method. Numerous studies have been conducted on the design, modeling, and simulation of spiral tube GHEs.

For instance, Xiang et al. [45] introduced a one-dimensional numerical model considering different thermal properties between the pile material and surrounding soil, employing a capacity resistance method for enhanced computational speed. Go et al. [46] examined borehole thermal resistance in thermal piles with spiral tube GHEs, developing a numerical model whose predictions matched in situ thermal response test results. Yang et al. [1] undertook experimental research on spiral tube GHEs, investigating factors like inlet temperature, intermittent operation modes, and spiral pitch on thermal performance. Park et al. [47] used Computational Fluid Dynamics (CFD) simulations to e assess spiral pitch and thermal interference effects on the thermal performance of spiral tube GHEs, validating their accuracy against field-test data. You et al. [48] proposed a model for thermal piles with spiral tube GHEs, considering seepage, geometric variations, and thermal interactions between the piles. Huang et al. [49] developed a numerical model for thermal piles with double spiral tube GHEs, showing that this innovative GHE design can effectively improve thermal balance and ensured heat transfer. Dehghan et al. [50][9] conducted a parametric study on spiral tube GHEs, finding that spacing, pitch length, vertical length, and diameter impact the heat transfer rate (HTR). They also compared various configurations for spiral tube GHEs using experimental and numerical methods. Cui et al. [11] presented an enhanced analytical model for transient heat conduction around spiral tube GHEs, focusing on the impact of pitch length and internal temperature distribution. Zhang et al. [51] created a heat transfer model to explore groundwater effects spiral tube GHEs in pile foundations, and they also examined the effects of varying pitch lengths. Wang et al. [52][53] investigated groundwater's influence on spiral tube GHEs in thermal piles, developing an analytical model for precise heat transfer characterization. Jalaluddin et al. [54] analyzed different pitch lengths on the thermal performance and pressure drop of spiral tube GHEs, highlighting spiral tubes' superiority over straight ones. Zarrela et al. [22][55] applied a capacitance-resistance model (CaRM) to spiral tube GHEs, validated with field measurements. Lei et al. [19] devised a hybrid analytical model considering different thermal properties of pile and soil, assessing pitch length variations' impact. Saeidi et al. [56] introduced aluminum rods into spiral tube GHEs to enhance thermal efficiency, using simulations to examine pitch length and borehole depth effects. Park et al. [57] studied the construction and thermal performance of spiral tube GHEs in large-diameter thermal piles, noting that reduced pitch length could improve thermal efficiency but highlighted the need to consider adjacent spiral loops' thermal interference. Finally, Kim et al. [58][2] validated a numerical model for spiral tube GHEs through a

thermal response test (TRT) and proposed a broadly applicable design method.

2.4. Prior Studies in Our Laboratory

In our laboratory's previous research, we introduced an innovative simulation model for Vertical Spiral Ground Heat Exchangers (VSGHEXs) in Ground Source Heat Pump (GSHP) systems, as referenced in publication [59]. This model ingeniously merges the Infinite Cylindrical Source (ICS) model with the Capacity Resistance Model (CaRM), enabling efficient simulation of the heat capacity within VSGHEXs. It offers dynamic, rapid, and precise calculations.

Furthermore, the research includes validation of the simulation tool by comparing its results with actual measurements from a residential property in Miyagi, Japan, equipped with a GSHP system utilizing VSGHEXs. The comparison confirmed the tool's high accuracy in predicting system performance.

The study also investigated the correlation between the heating/cooling demand and the required number of VSGHEXs for residential homes in Japan. It provides a simplified equation for quick estimation, highlighting the critical need for precise thermal performance assessments of spiral tube GHEs, particularly due to their increasing adoption in real-world applications.

However, the initial model was limited to spiral tube GHEs with a pitch (spiral distance) of less than 150 mm. Addressing this limitation, the current study introduces a novel calculation method for the heat transfer of thermal piles using double spiral tube GHEs, accommodating various pitch sizes.

2.5. Position of Current Study

This study made improvements in the following aspects:

2.5.1. Limitations of prior research and improvement in this study

Despite their functionality, models for heat transfer in spiral tube GHEs present certain challenges. Simulations that span a few hours can be computationally demanding for time-intensive numerical models, rendering them impractical for extended simulations. Most available analytical models presuppose uniformity in the materials of grouting, pile body, and ground soil, which limits their applicability when material differences exist. Notably, while many analytical models concentrate on single-point temperature calculations, they are slow in deriving results when averaging temperatures across multiple points.

This calculation method for double spiral tube GHEs proposed in **Chapter 3** leverages the CaRM and

integrates the principle of fin efficiency. A novel simulation tool is devised by combining this temperature change calculation method within the thermal pile with a ground temperature simulation program for GSHP systems, addressing external temperature variations of the thermal pile. This tool has proven effective for temperature simulations in thermal piles equipped with double spiral tube GHEs. Its simulation accuracy remains consistent irrespective of the spiral pitch, accommodating material discrepancies between grouting and soil.

The benefits of this new approach include:

- Compared to numerical models that use dense grid cells and are slower, this method saves on computational time and lessens the extensive pre-processing required. While many numerical models offer precise results, few are suitable for long-term simulations. This method, however, retains acceptable accuracy and aligns well with empirical measurements.
- Compared to numerous existing analytical models, which often consist of multiple integrals that impose substantial computational demands and create concerns regarding numerical stability, this method offers a simplified and innovative approach to examining heat transfer within thermal piles containing double spiral GHEs.

2.5.2. Limitations of models for spiral tube GHEs

Numerous studies have been conducted to analyze the factors that influence the thermal performance of spiral tube GHEs, but they mainly focus on laboratory tests and computer simulations. with limited exploration in real-world applications. A key limitation of these studies is their short-term nature and reliance on idealized conditions, which don't reflect actual usage. As a result, the operational data obtained are confined to lab and simulated environments. Additionally, many studies fail to accurately represent the heat exchange capabilities of spiral tube GHEs. They typically use watts or watts per meter as metrics for thermal performance, overlooking the temperature differential between the ground and the circulating fluid within the GHEs. Furthermore, these studies often consider deep ground depths, which do not align with the conditions of large-scale applications that mostly use shallow ground layers.

Moreover, few studies have addressed the performance of thermal piles and spiral tube GHEs, which are primarily installed in shallow grounds. Therefore, accurately assessing the thermal performance of spiral tube GHEs is crucial, especially given the recent widespread adoption of GSHP systems that utilize thermal piles.

In **Chapter 4**, this study investigated the thermal performance of double spiral tube GHEs integrated into the thermal piles of an energy-efficient building in Sapporo, Japan. By using actual data from the site and a new metric, the coefficient of heat extraction/injection, a more precise evaluation is provided. The findings

demonstrate the effectiveness of the thermal piles and double spiral tube GHEs. The advantages of this novel GHE for practical use is also highlighted. The results indicate that GSHP systems with double spiral tube GHEs outperform conventional GHEs in efficiency. Additionally, they maintain consistent efficiency over long-term operation, with the circulating fluid maintaining thermal balance, thus preventing performance degradation even in cold regions.

2.5.3. Limitations of prior research and improvement in this study

Prior research has identified various factors influencing the thermal efficiency of spiral tube GHEs, such as borehole depth, soil conductivity, spiral pitch, and intermittent operation modes. However, these studies also exhibit limitations. Often, the pitch length was invariable, lacking options for modification. Most research was confined to laboratory settings without empirical validation, and the methodologies generally suited only short-term operations. Additionally, while some design methodologies for spiral tube GHEs were proposed, they primarily focused on horizontal configurations, neglecting vertical types. There was also a notable scarcity of comprehensive design principles, especially those linking pitch length or other parameters to construction costs.

The limited number of established programs for the precise design of vertical spiral GHEs highlights the need for a specialized design tool. This tool should facilitate a thorough, systematic assessment of spiral tube GHEs' thermal efficiency, addressing the specific requirements of GSHP systems in various locations. Many studies have used the heat transfer rate (HTR), expressed in W/m, which inadequately represents the true heat exchange capacity of GHEs. As noted in **Section 2.5.2**, considering the temperature differential between underground and circulating fluids is crucial for a more complete understanding.

In **Chapter 5** of this study, a novel methodology for optimally designing thermal piles and double-spiral GHEs is introduced. by utilizing a simulation tool based on a novel thermal efficiency evaluation index. This method employs a simulation tool based on a new thermal efficiency evaluation index introduced in **Chapter 4**, incorporating an innovative calculation method for heat transfer in double spiral tube GHEs within thermal piles, a concept developed in **Chapter 3**.

Distinctively, while most studies on thermal piles and spiral tube GHEs focused on modeling and analyzing heat transfer, this research establishes a comprehensive design methodology and a strategy for identifying optimal solutions. This method, characterized by robust applicability and precision, accounts for various factors, including underground soil thermal properties, intermittent operation modes, and spiral pitch. Furthermore, this study emphasizes the importance of optimizing GSHP system designs, suggesting broader applicability of the

findings to other large-diameter GHEs.

Reference

[1] W. Yang, P. Lu, and Y. Chen, “Laboratory investigations of the thermal performance of an energy pile with spiral coil ground heat exchanger,” *Energy Build*, vol. 128, 2016, doi: 10.1016/j.enbuild.2016.07.012.

[2] M. J. Kim, S. R. Lee, S. Yoon, and J. S. Jeon, “An applicable design method for horizontal spiral-coil-type ground heat exchangers,” *Geothermics*, vol. 72, 2018, doi: 10.1016/j.geothermics.2017.12.010.

[3] B. H. Dinh, Y. S. Kim, and S. Yoon, “Experimental and numerical studies on the performance of horizontal U-type and spiral-coil-type ground heat exchangers considering economic aspects,” *Renew Energy*, vol. 186, 2022, doi: 10.1016/j.renene.2022.01.001.

[4] A. Carotenuto, P. Marotta, N. Massarotti, A. Mauro, and G. Normino, “Energy piles for ground source heat pump applications: Comparison of heat transfer performance for different design and operating parameters,” *Appl Therm Eng*, vol. 124, 2017, doi: 10.1016/j.applthermaleng.2017.06.038.

[5] Q. Zhao, B. Chen, and F. Liu, “Study on the thermal performance of several types of energy pile ground heat exchangers: U-shaped, W-shaped and spiral-shaped,” *Energy Build*, vol. 133, 2016, doi: 10.1016/j.enbuild.2016.09.055.

[6] A. A. Serageldin, A. Radwan, T. Katsura, Y. Sakata, S. Nagasaka, and K. Nagano, “Parametric analysis, response surface, sensitivity analysis, and optimization of a novel spiral-double ground heat exchanger,” *Energy Convers Manag*, vol. 240, 2021, doi: 10.1016/j.enconman.2021.114251.

[7] S. Yoon, S. R. Lee, G. H. Go, and S. Park, “An experimental and numerical approach to derive ground thermal conductivity in spiral coil type ground heat exchanger,” *Journal of the Energy Institute*, vol. 88, no. 3, 2015, doi: 10.1016/j.joei.2014.10.002.

[8] H. Park, S. R. Lee, S. Yoon, H. Shin, and D. S. Lee, “Case study of heat transfer behavior of helical ground heat exchanger,” *Energy Build*, vol. 53, 2012, doi: 10.1016/j.enbuild.2012.06.019.

[9] B. Dehghan B., “Experimental and computational investigation of the spiral ground heat exchangers for ground source heat pump applications,” *Appl Therm Eng*, vol. 121, 2017, doi: 10.1016/j.applthermaleng.2017.05.002.

[10] M. Suzuki, K. Yoneyama, S. Amemiya, and M. Oe, “Development of a Spiral Type Heat Exchanger for Ground Source Heat Pump System,” in *Energy Procedia*, 2016. doi: 10.1016/j.egypro.2016.09.091.

[11] P. Cui, X. Li, Y. Man, and Z. Fang, “Heat transfer analysis of pile geothermal heat exchangers with spiral coils,” *Appl Energy*, vol. 88, no. 11, 2011, doi: 10.1016/j.apenergy.2011.03.045.

[12] W. Zhang, H. Yang, L. Lu, P. Cui, and Z. Fang, “The research on ring-coil heat transfer models of pile foundation ground heat exchangers in the case of groundwater seepage,” *Energy Build*, vol. 71, 2014, doi: 10.1016/j.enbuild.2013.12.016.

[13] Sk. Park, S. R. Lee, H. Park, S. Yoon, and J. Chung, "Characteristics of an analytical solution for a spiral coil type ground heat exchanger," *Comput Geotech*, vol. 49, pp. 18–24, Apr. 2013, doi: 10.1016/J.COMPGEO.2012.11.006.

[14] Y. Man, H. Yang, N. Diao, P. Cui, L. Lu, and Z. Fang, "Development of spiral heat source model for novel pile ground heat exchangers," *HVAC and R Research*, vol. 17, no. 6, 2011, doi: 10.1080/10789669.2011.610281.

[15] Y. Man, H. Yang, N. Diao, J. Liu, and Z. Fang, "A new model and analytical solutions for borehole and pile ground heat exchangers," *Int J Heat Mass Transf*, vol. 53, no. 13–14, 2010, doi: 10.1016/j.ijheatmasstransfer.2010.03.001.

[16] M. Li and A. C. K. Lai, "Heat-source solutions to heat conduction in anisotropic media with application to pile and borehole ground heat exchangers," *Appl Energy*, vol. 96, pp. 451–458, 2012, doi: 10.1016/j.apenergy.2012.02.084.

[17] M. Li and A. C. K. Lai, "New temperature response functions (G functions) for pile and borehole ground heat exchangers based on composite-medium line-source theory," *Energy*, vol. 38, no. 1, 2012, doi: 10.1016/j.energy.2011.12.004.

[18] A. Leroy and M. Bernier, "Development of a novel spiral coil ground heat exchanger model considering axial effects," *Appl Therm Eng*, vol. 84, 2015, doi: 10.1016/j.applthermaleng.2015.03.032.

[19] F. Lei, P. Hu, and X. P. Huang, "Hybrid analytical model for composite heat transfer in a spiral pile ground heat exchanger," *Appl Therm Eng*, vol. 137, 2018, doi: 10.1016/j.applthermaleng.2018.04.019.

[20] D. Bauer, W. Heidemann, H. Müller-Steinhagen, and H. J. G. Diersch, "Thermal resistance and capacity models for borehole heat exchangers," *Int J Energy Res*, vol. 35, no. 4, 2011, doi: 10.1002/er.1689.

[21] A. Minaei and M. Maerefat, "A new analytical model for short-term borehole heat exchanger based on thermal resistance capacity model," *Energy Build*, vol. 146, 2017, doi: 10.1016/j.enbuild.2017.04.064.

[22] A. Zarrella, A. Capozza, and M. De Carli, "Analysis of short helical and double U-tube borehole heat exchangers: A simulation-based comparison," *Appl Energy*, vol. 112, 2013, doi: 10.1016/j.apenergy.2013.06.032.

[23] A. Zarrella, M. De Carli, and A. Galgaro, "Thermal performance of two types of energy foundation pile: Helical pipe and triple U-tube," *Appl Therm Eng*, vol. 61, no. 2, 2013, doi: 10.1016/j.applthermaleng.2013.08.011.

[24] C. Chen, H. Shao, D. Naumov, Y. Kong, K. Tu, and O. Kolditz, "Numerical investigation on the performance, sustainability, and efficiency of the deep borehole heat exchanger system for building heating," *Geothermal Energy*, vol. 7, no. 1, 2019, doi: 10.1186/s40517-019-0133-8.

[25] F. Tang and H. Nowamooz, "Factors influencing the performance of shallow Borehole Heat Exchanger," *Energy Convers Manag*, vol. 181, 2019, doi: 10.1016/j.enconman.2018.12.044.

[26] J. Cao, M. Bottarelli, M. Bortoloni, and G. Pei, "Small-scale lab analysis of the ground freezing effect on the thermal performance of a Flat-Panel ground heat exchanger," *Geothermics*, vol. 74, 2018, doi: 10.1016/j.geothermics.2018.03.013.

[27] J. Zhang, X. Lu, W. Zhang, J. Liu, W. Yue, and F. Ma, "Investigation of a Novel Deep Borehole Heat Exchanger for Building Heating and Cooling with Particular Reference to Heat Extraction and Storage," *Processes*, vol. 10, no. 5, 2022, doi: 10.3390/pr10050888.

[28] P. M. Congedo, G. Colangelo, and G. Starace, "CFD simulations of horizontal ground heat exchangers: A comparison among different configurations," *Appl Therm Eng*, vol. 33–34, no. 1, 2012, doi: 10.1016/j.applthermaleng.2011.09.005.

[29] G. Zhang, Z. Cao, Y. Liu, and J. Chen, "Field test and numerical simulation on the long-term thermal response of phc energy pile in layered foundation," *Sensors*, vol. 21, no. 11, 2021, doi: 10.3390/s21113873.

[30] Jalaluddin, A. Miyara, R. Tarakka, A. A. Mochtar, and I. R. Muhammad Anis, "Thermal performance of shallow spiral-tube ground heat exchanger for ground-source cooling system," in *IOP Conference Series: Materials Science and Engineering*, 2019. doi: 10.1088/1757-899X/619/1/012012.

[31] X. Huang, Z. Yao, H. Cai, X. Li, and H. Chen, "Performance evaluation of coaxial borehole heat exchangers considering ground non-uniformity based on analytical solutions," *International Journal of Thermal Sciences*, vol. 170, 2021, doi: 10.1016/j.ijthermalsci.2021.107162.

[32] W. Cai *et al.*, "Long-term performance evaluation for deep borehole heat exchanger array under different soil thermal properties and system layouts," *Energy*, vol. 241, 2022, doi: 10.1016/j.energy.2021.122937.

[33] A. A. Serageldin, Y. Sakata, T. Katsura, and K. Nagano, "Thermo-hydraulic performance of the U-tube borehole heat exchanger with a novel oval cross-section: Numerical approach," *Energy Convers Manag*, vol. 177, 2018, doi: 10.1016/j.enconman.2018.09.081.

[34] A. Jahanbin, "Thermal performance of the vertical ground heat exchanger with a novel elliptical single U-tube," *Geothermics*, vol. 86, 2020, doi: 10.1016/j.geothermics.2020.101804.

[35] S. H. Majeed, A. S. Abdul-Zahra, and D. G. Mutasher, "Performance evaluation of different types of ground source heat exchangers in a hot and dry climate," *Heat Transfer*, vol. 51, no. 6, 2022, doi: 10.1002/htj.22566.

[36] E. D. Kerme and A. S. Fung, "Heat transfer analysis of single and double U-tube borehole heat exchanger with two independent circuits," *J Energy Storage*, vol. 43, 2021, doi: 10.1016/j.est.2021.103141.

[37] J. W. Kim, Y. M. Kim, Y. J. Ko, Q. Chen, C. Xin, and S. J. Oh, "Study on an advanced borehole heat exchanger for ground source heat pump operating in volcanic island: Case study of Jeju island, South Korea," *Front Built Environ*, vol. 8, 2022, doi: 10.3389/fbuil.2022.1061760.

[38] H. Zou, P. Pei, C. Wang, and D. Hao, "A numerical study on heat transfer performances of horizontal ground

heat exchangers in ground-source heat pumps," *PLoS One*, vol. 16, no. 5 May, 2021, doi: 10.1371/journal.pone.0250583.

[39] J. Luo, J. Rohn, M. Bayer, and A. Priess, "Thermal performance and economic evaluation of double U-tube borehole heat exchanger with three different borehole diameters," *Energy Build*, vol. 67, 2013, doi: 10.1016/j.enbuild.2013.08.030.

[40] B. Dehghan B., "Experimental and computational investigation of the spiral ground heat exchangers for ground source heat pump applications," *Appl Therm Eng*, vol. 121, 2017, doi: 10.1016/j.applthermaleng.2017.05.002.

[41] B. Li, M. Zheng, M. Shahrestani, and S. Zhang, "Driving factors of the thermal efficiency of ground source heat pump systems with vertical boreholes in Chongqing by experiments," *Journal of Building Engineering*, vol. 28, 2020, doi: 10.1016/j.jobe.2019.101049.

[42] A. Walch *et al.*, "Shallow geothermal energy potential for heating and cooling of buildings with regeneration under climate change scenarios," *Energy*, vol. 244, 2022, doi: 10.1016/j.energy.2021.123086.

[43] L. Guo, J. Zhang, Y. Li, J. McLennan, Y. Zhang, and H. Jiang, "Experimental and numerical investigation of the influence of groundwater flow on the borehole heat exchanger performance: A case study from Tangshan, China," *Energy Build*, vol. 248, 2021, doi: 10.1016/j.enbuild.2021.111199.

[44] S. Tu, X. Yang, X. Zhou, M. Luo, and X. Zhang, "Experimenting and modeling thermal performance of ground heat exchanger under freezing soil conditions," *Sustainability (Switzerland)*, vol. 11, no. 20, 2019, doi: 10.3390/su11205738.

[45] Y. Xiang *et al.*, "A new practical numerical model for the energy pile with spiral coils," *Int J Heat Mass Transf*, vol. 91, 2015, doi: 10.1016/j.ijheatmasstransfer.2015.08.028.

[46] G. H. Go, S. R. Lee, S. Yoon, and H. byul Kang, "Design of spiral coil PHC energy pile considering effective borehole thermal resistance and groundwater advection effects," *Appl Energy*, vol. 125, 2014, doi: 10.1016/j.apenergy.2014.03.059.

[47] S. Park, S. Lee, D. Lee, S. S. Lee, and H. Choi, "Influence of coil pitch on thermal performance of coil-type cast-in-place energy piles," *Energy Build*, vol. 129, 2016, doi: 10.1016/j.enbuild.2016.08.005.

[48] T. You and H. Yang, "Feasibility of ground source heat pump using spiral coil energy piles with seepage for hotels in cold regions," *Energy Convers Manag*, vol. 205, 2020, doi: 10.1016/j.enconman.2020.112466.

[49] G. Huang *et al.*, "A novel independent heat extraction-release double helix energy pile: Numerical and experimental investigations of heat extraction effect," *Energy Convers Manag*, vol. 254, 2022, doi: 10.1016/j.enconman.2022.115249.

[50] B. Dehghan, A. Sisman, and M. Aydin, "Parametric investigation of helical ground heat exchangers for heat

pump applications," *Energy Build*, vol. 127, 2016, doi: 10.1016/j.enbuild.2016.06.064.

[51] W. Zhang, H. Yang, P. Cui, L. Lu, N. Diao, and Z. Fang, "Study on spiral source models revealing groundwater transfusion effects on pile foundation ground heat exchangers," *Int J Heat Mass Transf*, vol. 84, 2015, doi: 10.1016/j.ijheatmasstransfer.2014.12.036.

[52] D. Wang, L. Lu, W. Zhang, and P. Cui, "Numerical and analytical analysis of groundwater influence on the pile geothermal heat exchanger with cast-in spiral coils," *Appl Energy*, vol. 160, 2015, doi: 10.1016/j.apenergy.2015.04.037.

[53] D. Wang, L. Lu, and P. Cui, "A novel composite-medium solution for pile geothermal heat exchangers with spiral coils," *Int J Heat Mass Transf*, vol. 93, 2016, doi: 10.1016/j.ijheatmasstransfer.2015.10.055.

[54] Jalaluddin and A. Miyara, "Thermal performance and pressure drop of spiral-tube ground heat exchangers for ground-source heat pump," *Appl Therm Eng*, vol. 90, 2015, doi: 10.1016/j.applthermaleng.2015.07.035.

[55] A. Zarrella and M. De Carli, "Heat transfer analysis of short helical borehole heat exchangers," *Appl Energy*, vol. 102, 2013, doi: 10.1016/j.apenergy.2012.09.012.

[56] R. Saeidi, Y. Noorollahi, and V. Esfahanian, "Numerical simulation of a novel spiral type ground heat exchanger for enhancing heat transfer performance of geothermal heat pump," *Energy Convers Manag*, vol. 168, 2018, doi: 10.1016/j.enconman.2018.05.015.

[57] S. Park, D. Lee, H. J. Choi, K. Jung, and H. Choi, "Relative constructability and thermal performance of cast-in-place concrete energy pile: Coil-type GHEX (ground heat exchanger)," *Energy*, vol. 81, 2015, doi: 10.1016/j.energy.2014.08.012.

[58] M. J. Kim, S. R. Lee, S. Yoon, and G. H. Go, "Thermal performance evaluation and parametric study of a horizontal ground heat exchanger," *Geothermics*, vol. 60, 2016, doi: 10.1016/j.geothermics.2015.12.009.

[59] T. Katsura *et al.*, "A new simulation model for vertical spiral ground heat exchangers combining cylindrical source model and capacity resistance model," *Energies (Basel)*, vol. 16, no. 3, Mar. 2020, doi: 10.3390/en13061339.

Chapter 3

Development and Application of a New Calculation Method for Double Spiral Tube Ground Heat Exchangers

3.1. Establishment of A Novel Calculation Method

3.1.1. CaRM model for double spiral tube GHEs

As outlined in Chapter 2, for Ground Heat Exchangers (GHEs) utilizing spiral pipes, existing literature has provided 3 major models to access the temperature variations in 2 parts: circulating fluid inside the GHEs, and surrounding soil. These models are categorized as follows: Numerical models, which generally necessitate extensive computational efforts, often requiring advanced simulation software and high-performance computing resources. Analytical models, in contrast, simplify the computational process but require significant theoretical derivation. The Capacity and Resistance Model (CaRM), though not yet widely adopted, presents a more intuitive and easily comprehensible approach. In this study, the CaRM has been employed to evaluate the thermal performance of thermal piles equipped with double spiral tube GHEs.

The overall thermal efficiency of a thermal pile is influenced by the arrangement of pipes within the pile, as well as the size of the concrete part of the pile in relation to the size of the pipes. In the design of thermal piles, it is essential to account for the distinctions between thermal piles and borehole heat exchangers (BHEs). Due to the larger diameters of thermal piles compared to BHEs, a thorough evaluation of the heat capacities of both grouting and pile materials is imperative for accurate thermal performance assessment. Therefore, it is necessary to segment the internal space of the thermal pile for detailed analysis. **Fig. 3.1 (a)** and **Fig. 3.1 (b)** gave 2 sectional views of thermal pile with double spiral tube GHE inside. The volume of the thermal pile is divided into three distinct sections:

1. “core” sections: grouting material
2. double spiral tube GHEs (illustrated in blue) along with the grouting material between each spiral loop
3. “shell” sections: thermal pile material between double spiral GHEs and borehole boundary

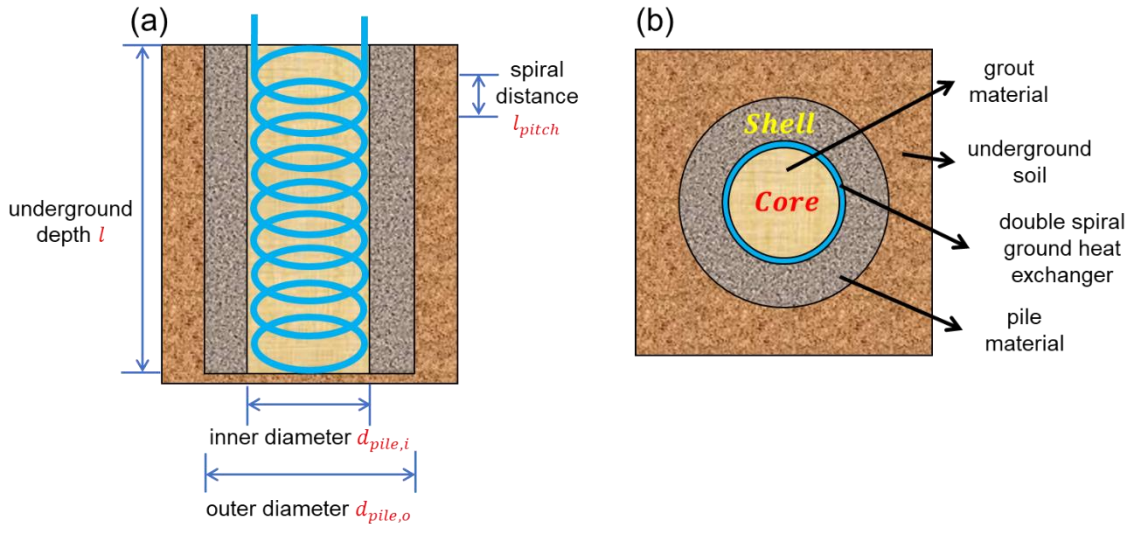

Fig. 3.1 (a) Sectional view of thermal pile, (b) Top view of thermal pile.

Utilizing the CaRM model, as depicted in **Fig. 3.2 (a)**, six temperature nodes were established to represent corresponding temperature zones: 1. T_{core}, positioned at the midpoint between the center of thermal pile and innermost sides of the spiral pipe's surface; 2. $T_{surface,sp}$, located at both the innermost and outermost sides of the spiral pipe's surface (referring to **Fig. 3.2 (a)**); 3. $T_{fluid,sp}$, within the circulating fluid inside the spiral pipe; 4. T_{shell}, at the midpoint between outermost sides of the spiral pipe's surface and the boundary of the thermal pile; 5. T_{ground}, at the boundary of the thermal pile [1]. The heat transfer process within a thermal pile can be divided into 3 parts: heat conduction within the "core" sections, heat convection between the circulating fluid and spiral pipe's surface, and heat conduction within the "shell" sections.

As indicated in **Fig. 3.4**, the outer diameter of the pipe, denoted as $d_{pipe,o}$ is much smaller than the diameter of thermal pile. Consequently, the double spiral pipe is treated as a linear heat source or sink, depending on the season, injecting or absorbing heat into/from the ground during summer and winter, respectively. This allows for the simplification of heat transfer to a one-dimensional, steady-state process across a multi-layer cylindrical wall [2]. Moreover, the two temperature nodes $T_{surface,sp}$ shown in **Fig. 3.2 (a)** are simplified as a single point due to the consideration of the double spiral pipe as a line. **Fig. 3.2 (b)** presents a detailed thermal network, demonstrating the temperature, thermal resistance, and thermal capacity of each section within the thermal pile.

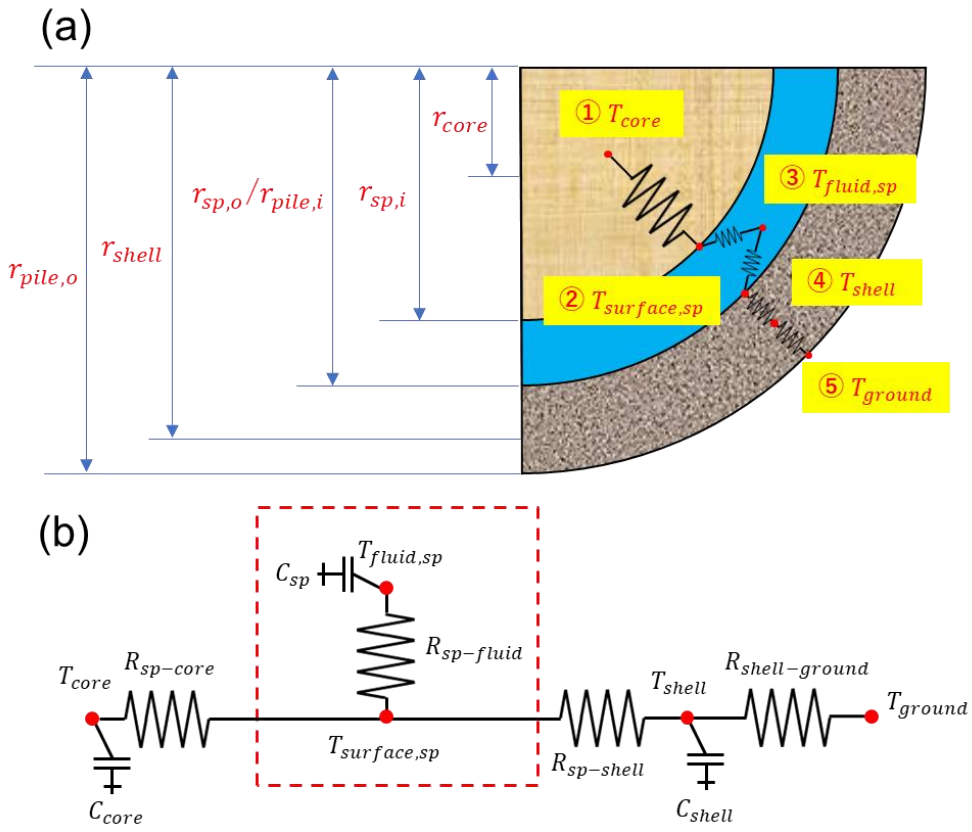

Fig. 3.2 (a) Partial detail of thermal pile, (b) Thermal network

The thermal resistances between "core" section and double spiral pipe $R_{sp-core}$, double spiral pipe and "shell" section $R_{sp-shell}$, "shell" section and surrounding soil $R_{shell-ground}$ can be respectively expressed in form of equations as under:

$$R_{sp-core} = \frac{1}{2\pi \cdot l \cdot \lambda_{core}} \cdot ln\left(\frac{r_{sp,i}}{r_{core}}\right) \tag{3.1}$$

$$R_{sp-shell} = \frac{1}{2\pi \cdot l \cdot \lambda_{shell}} \cdot ln\left(\frac{r_{shell}}{r_{sp,o}}\right) \tag{3.2}$$

$$R_{shell-ground} = \frac{1}{2\pi \cdot l \cdot \lambda_{shell}} \cdot ln\left(\frac{r_{pile,o}}{r_{shell}}\right) \tag{3.3}$$

where l is the underground depth of the thermal pile, λ_{core} and λ_{shell} are the thermal conductivity of grouting and pile materials, respectively; r_{core} and r_{shell} are the distances from center point of the thermal pile to the temperature nodes within the "core" and "shell" sections, respectively; $r_{pile,o}$ is the outer radius of thermal pile; $r_{sp,i}$ and $r_{sp,o}$ represent the distances from the center point of the thermal pile to the innermost

and outermost sides of spiral pipe's surface, as illustrated in **Fig. 3.2 (a)**.

3.1.2. Calculation for Heat Transfer Rate Using Kollmar-Liese Method

In previous research, a method was proposed for calculating the thermal emission of flat floor heating panels equipped with a cylindrical heat source. This methodology is fundamentally based on the Kollmar-Liese method, which utilizes the concept of fin efficiency and is extensively employed in the design of hot water floor heating systems [3]. In this approach, it is assumed that a virtual fin, with a width (d) equal to the outer diameter ($d_{pipe,o}$)) of the pipe, is integrated [refer to **Fig. 3.3** (b)].

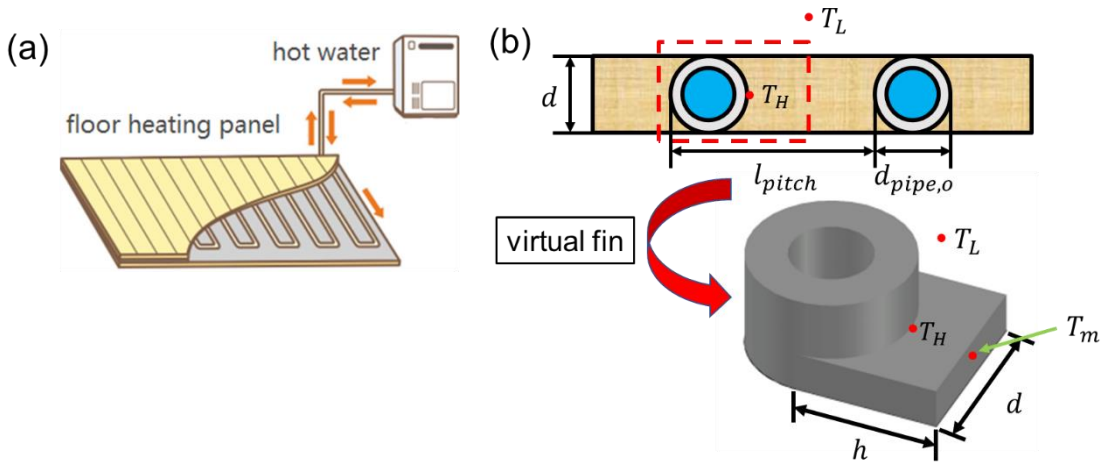

Fig. 3.3 (a) A typical radiant floor heating system (b) Principle of Kollmar-Liese method

Fig. 3.3 (b) illustrates the integration of a virtual fin with a short segment of pipe. The fin efficiency η of the virtual fin can be calculated using the equation provided, where α represents the convective heat transfer coefficient between the floor and ambient air, and λ denotes the thermal conductivity of the floor material:

$$m = \sqrt{\frac{2\alpha}{\lambda \cdot d}}; h = \frac{l_{pitch} - d_{pipe,o}}{2}; \eta = \frac{tanh(m \cdot h)}{m \cdot h} \tag{3.4}$$

Assuming that T_H represents the pipe's surface temperature and T_L denotes the ambient temperature, the average temperature T_m of the virtual fin can be calculated using the Kollmar-Liese method [4]:

$$T_m = T_L + \eta \cdot (T_H - T_L) \tag{3.5}$$

The rate of heat transfer from the lower floor to the upper air can be expressed using the following equation:

$$Q = \alpha \cdot \eta \cdot (T_H - T_L) = \alpha \cdot (T_m - T_L) \tag{3.6}$$

Drawing inspiration from earlier research on hot water floor heating systems, it was noted that the vertical section of the double spiral pipe closely resembles a "vertical" floor heating panel, as illustrated in **Fig. 3.4**. This panel facilitates heat exchange with both the "core" and the "shell" sections. As a result, the heat transfer rate can be precisely estimated using a methodology similar to the one used for flat floor heating panels.

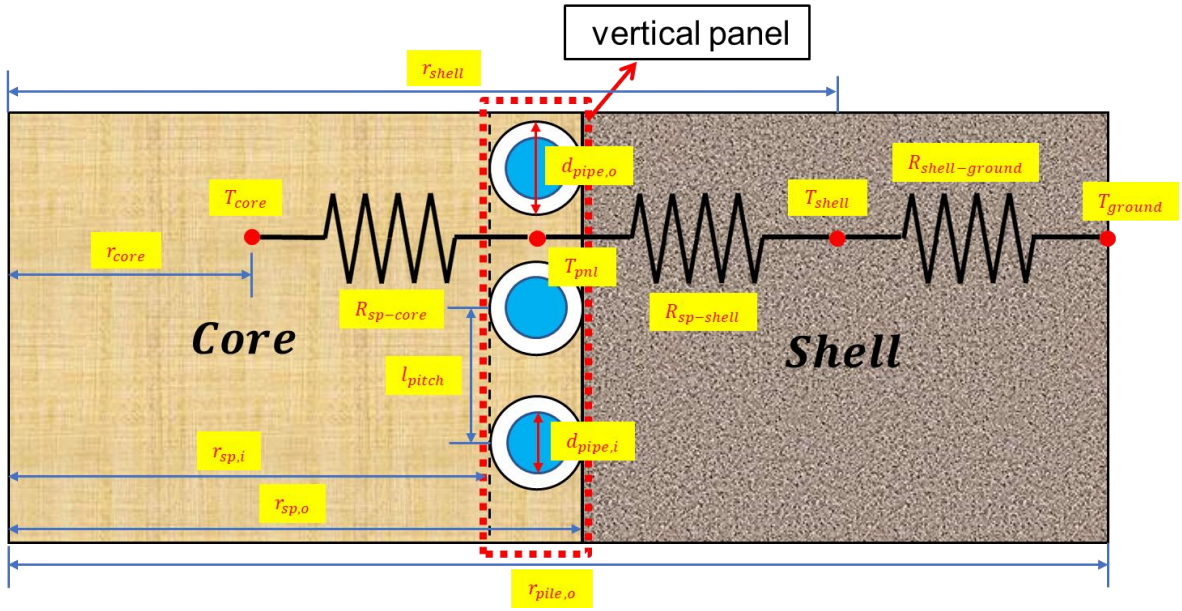

Fig. 3.4 Similarity between floor heating panel and double spiral tube GHE

By analogy, the temperature T_{pnl} of the approximate line (which correlates with the mean temperature T_m of the virtual fin depicted in **Fig. 3.3 (b)**) can be formulated in terms of the surface temperature $T_{surface,sp}$ of the spiral pipe (corresponding to the pipe's surface temperature T_H) and the temperature in "core" and "shell" sections (corresponding to the ambient temperature T_L). The relations among these temperatures can be expressed as:

$$T_{pnl} = T_{core} + \eta_{core} \cdot \left(T_{surface,sp} - T_{core}\right) \tag{3.7}$$

$$T_{pnl} = T_{shell} + \eta_{shell} \cdot \left(T_{surface,sp} - T_{shell}\right) \tag{3.8}$$

Integrating **Eq. (3.7)** and **Eq. (3.8)**, the expression for temperature of the approximate line T_{pnl} can be formulated as follows:

$$T_{pnl} = \frac{1}{2}\left[\left(T_{surface,sp} - T_{core}\right) \cdot \eta_{core} + T_{core}\right] + \frac{1}{2}\left[\left(T_{surface,sp} - T_{shell}\right) \cdot \eta_{shell} + T_{shell}\right] \quad (3.9)$$

3.1.3. Calculation of Heat Transfer Rate

Using parameters of the double spiral tube GHE, the fin efficiency for determining the heat transfer rate from "vertical" floor heating panel to both the "core" section η_{core} and "shell" section η_{shell} can be using Eq. (3.4). The convective heat transfer coefficient, α_{core}, between "vertical" floor heating panel and "core" section, α_{shell} between "vertical" floor heating panel and "shell" section, are calculated by employing the thermal resistance $R_{sp-core}$, $R_{sp-shell}$, the heat transfer area A_{core} for the "core" section and A_{shell} for the "shell" section:

$$\alpha_{core} = \frac{R_{sp-core}}{A_{core}} = \frac{R_{sp-core}}{2\pi \cdot l \cdot r_{sp,i}} \quad (3.10)$$

$$\alpha_{shell} = \frac{R_{sp-shell}}{A_{shell}} = \frac{R_{sp-shell}}{2\pi \cdot l \cdot r_{sp,o}} \quad (3.11)$$

Subsequently, the fin efficiency of heat transfer in both directions can be expressed as follows:

$$\eta_{core} = \frac{tanh\left(\sqrt{\frac{2\alpha_{core}}{\lambda_{core} \cdot d_{pipe,o}}} \cdot \frac{l_{pitch} - d_{pipe,o}}{2}\right)}{\sqrt{\frac{2\alpha_{core}}{\lambda_{core} \cdot d_{pipe,o}}} \cdot \frac{l_{pitch} - d_{pipe,o}}{2}} \quad (3.12)$$

$$\eta_{shell} = \frac{tanh\left(\sqrt{\frac{2\alpha_{shell}}{\lambda_{core} \cdot d_{pipe,o}}} \cdot \frac{l_{pitch} - d_{pipe,o}}{2}\right)}{\sqrt{\frac{2\alpha_{shell}}{\lambda_{core} \cdot d_{pipe,o}}} \cdot \frac{l_{pitch} - d_{pipe,o}}{2}} \quad (3.13)$$

Based on **Eq. (3.6)**, the heat transfer rate (W) of the circulating fluid across the pipe surface to the to the "core" and "shell" sections can be respectively expressed by following equations:

$$Q_{core} = \alpha_{core} \cdot A_{core} \cdot (T_{pnl} - T_{core}) \quad (3.14)$$

$$Q_{shell} = \alpha_{shell} \cdot A_{shell} \cdot (T_{pnl} - T_{shell}) \quad (3.15)$$

Fig 3.5 presents a detailed illustration of heat transfer within the thermal pile, ranging from the central point on the left to the boundary on the right. The temperatures of the three sections, as segmented in **Section 3.1.1**, are labeled as T_{core}, T_{pnl}, and T_{shell}, respectively.

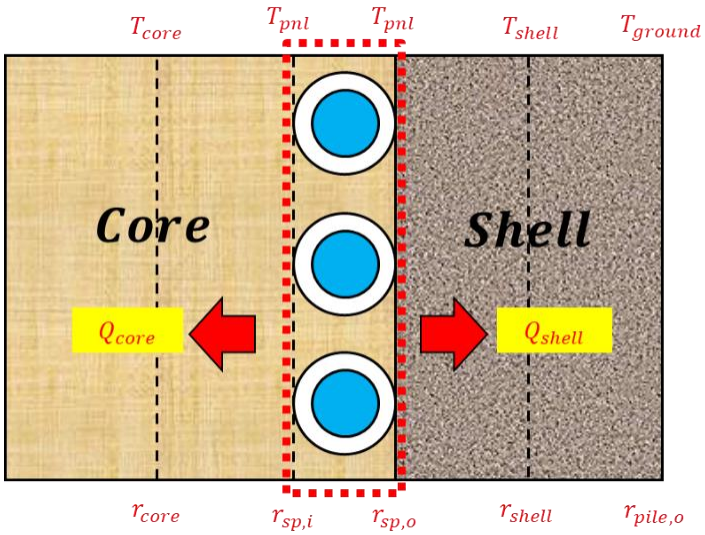

Fig. 3.5 Heat transfer rate from "vertical" panel to "core" and "shell" sections

3.1.4. Calculations for convective thermal resistance

Three thermal resistances of heat conduction processes shown in **Fig. 3.2** has been computed in **Section 3.1.1**. Now the convection heat resistance between the fluid and the pipe surface remains to be calculated. Upon determining the temperature of the approximate line T_{pnl}, it is essential to establish the relationship between the pipe surface temperature $T_{surface,sp}$ and the circulating fluid temperature $T_{fluid,sp}$. The impact of centrifugal force on the fluid flow within the double spiral pipe must be considered for accurately calculating the convective heat transfer coefficient α_f between the circulating fluid and the pipe surface. The Reynolds number Re and Prandtl number Pr of the circulating fluid flowing in double spiral pipe can be calculated using its thermophysical properties, such as density ρ, kinematic viscosity ν, and thermal diffusivity α.

Based on the obtained Reynolds number Re and Prandtl number Pr, prior research has established the formulation of the Nusselt number Nu applicable to both laminar and turbulent flow conditions:

- Historically, the calculation of the Nusselt number for laminar flow has been predominantly based on

equations pertinent to straight pipes. However, this study highlights a critical observation: the centrifugal force induced by the circulating fluid in spiral pipes markedly impacts the Reynolds number. Consequently, this investigation adopts Dravid's formula [5] specifically designed for single-phase laminar flow in spiral pipes:

$$De = Re \cdot \sqrt{\frac{d_{pipe,o}}{d_{sp,o}}}, Nu = (0.76 + 0.65De^{0.5}) \cdot Pr^{0.175} \tag{3.16}$$

- Gnielinski's formula was applied to analyze turbulent flow [6][7]:

$$f = 4C_f = 4\left(0.0791Re^{-1/4}\right), Nu = \frac{(f/8) \cdot (Re - 1000) \cdot Pr}{1 + 12.7(f/8)^{1/2} \cdot (Pr^{2/3} - 1)} \tag{3.17}$$

Fig. 3.6 illustrates results indicating that the Nusselt number calculated using Dravid's formula exceeds that obtained from Gnielinski's formula in both the laminar and most of the turbulent flow regions. Therefore, the Nusselt number calculation curve used in this study is represented by the red line shown in the figure, which is applicable for both laminar and turbulent flow regions.

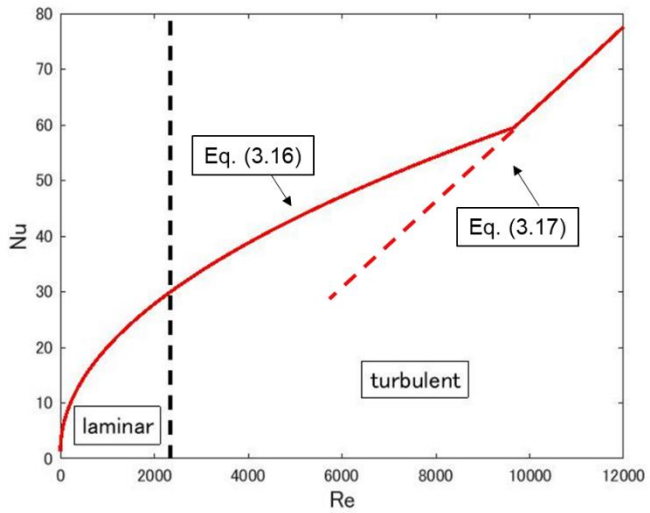

Fig. 3.6 Nusselt number calculated for laminar and turbulent flow.

Then, the convective heat transfer coefficient for the fluid, denoted as α_{fluid} can be expressed as:

$$\alpha_{fluid} = \frac{Nu \cdot \lambda_{fluid}}{d_{pipe,i}} \tag{3.18}$$

where λ_{fluid} represents the fluid's thermal conductivity, $d_{pipe,o}$ and $d_{pipe,i}$ denote the outer and inner diameters of the pipe, respectively.

The length of double spiral pipe l_{sp} can be calculated using the following formula:

$$l_{sp} = \frac{l}{l_{pitch}} \cdot \sqrt{l_{pitch}^2 + \left(\pi \cdot \frac{d_{sp,i} + d_{sp,o}}{2}\right)^2} \tag{3.19}$$

Convective thermal resistance $R_{sp-fluid}$ between circulating fluid and pipe surface can be expressed as:

$$R_{sp-fluid} = \frac{1}{2\pi \cdot r_{pipe,i} \cdot l_{sp} \cdot \alpha_{fluid}} + \frac{1}{2\pi \cdot \lambda_{pipe} \cdot l_{sp}} \cdot ln\left(\frac{r_{sp,o}}{r_{sp,i}}\right) \tag{3.20}$$

3.1.5. Heat balance equations for each section

The volume of each section can be expressed by following equations:

Circulating fluid in double spiral pipe:

$$V_{fluid} = \pi \cdot r_{pipe,i}^2 \cdot l_{sp} \tag{3.21}$$

"core" section:

$$V_{core} = \pi \cdot r_{sp,i}^2 \cdot l \tag{3.22}$$

"shell" section:

$$V_{shell} = \pi \cdot (r_{pile,o}^2 - r_{sp,o}^2) \cdot l \tag{3.23}$$

Utilizing the aforementioned parameters, the heat balance within the circulating fluid in the double spiral pipe, as well as in the "core" and "shell" sections, can be quantified for each time interval ($dt = 60s$). This can be expressed through **Eq. (3.24)**, **(3.25)**, and **(3.26)**, corresponding to each respective section.

The circulating fluid in the double spiral pipe is characterized as follows:

$$\begin{aligned} c_{fluid} \cdot \rho_{fluid} \cdot V_{fluid} \cdot \frac{dT_{fluid}}{dt} \\ = c_{fluid} \cdot \rho_{fluid} \cdot v_{fluid} \cdot \left(T_{fluid,in} - T_{fluid,out}\right) \\ - \frac{T_{fluid,sp} - T_{surface,sp}}{R_{sp-fluid}} \end{aligned} \tag{3.24}$$

The "core" section:

$$c_{core} \cdot \rho_{core} \cdot V_{core} \cdot \frac{dT_{core}}{dt} = \frac{T_{pnl} - T_{core}}{R_{sp-core}} \tag{3.25}$$

The "shell" section:

$$c_{shell} \cdot \rho_{shell} \cdot V_{shell} \cdot \frac{dT_{shell}}{dt} = \frac{T_{pnl} - T_{shell}}{R_{sp-shell}} - \frac{T_{shell} - T_{ground}}{R_{shell-ground}} \tag{3.26}$$

where c_{fluid}, c_{core}, c_{shell}, ρ_{fluid}, ρ_{core}, ρ_{shell} represent the heat capacities and densities of circulating fluid, grouting material, and pile material, respectively. T_{core}, T_{shell}, T_{ground} denote the temperatures at the temperature nodes in the "core" section, "shell" section, and the boundary of the thermal pile, respectively.

In this context, the inlet temperature of the double spiral pipe equals to the inflow temperature of the circulating fluid $T_{fluid,in} = T_{pipe,in}$. Similarly, the outlet temperature of the double spiral pipe equals to the outflow temperature of the circulating fluid $T_{fluid,out} = T_{pipe,out}$.

3.1.6. Combination of new calculation method and simulation tool for GSHP systems

GroundClub, a GSHP system simulation program created by the Environmental System Research Laboratory at Hokkaido University [8], is based on the analytical model of Infinite Line Source (ILS) and Infinite Cylindrical Source (ICS) models., A novel simulation tool was developed by incorporating the above innovative calculation method into GroundClub in MATLAB, the flow calculations f for this integration are depicted in **Fig. 3.7**.

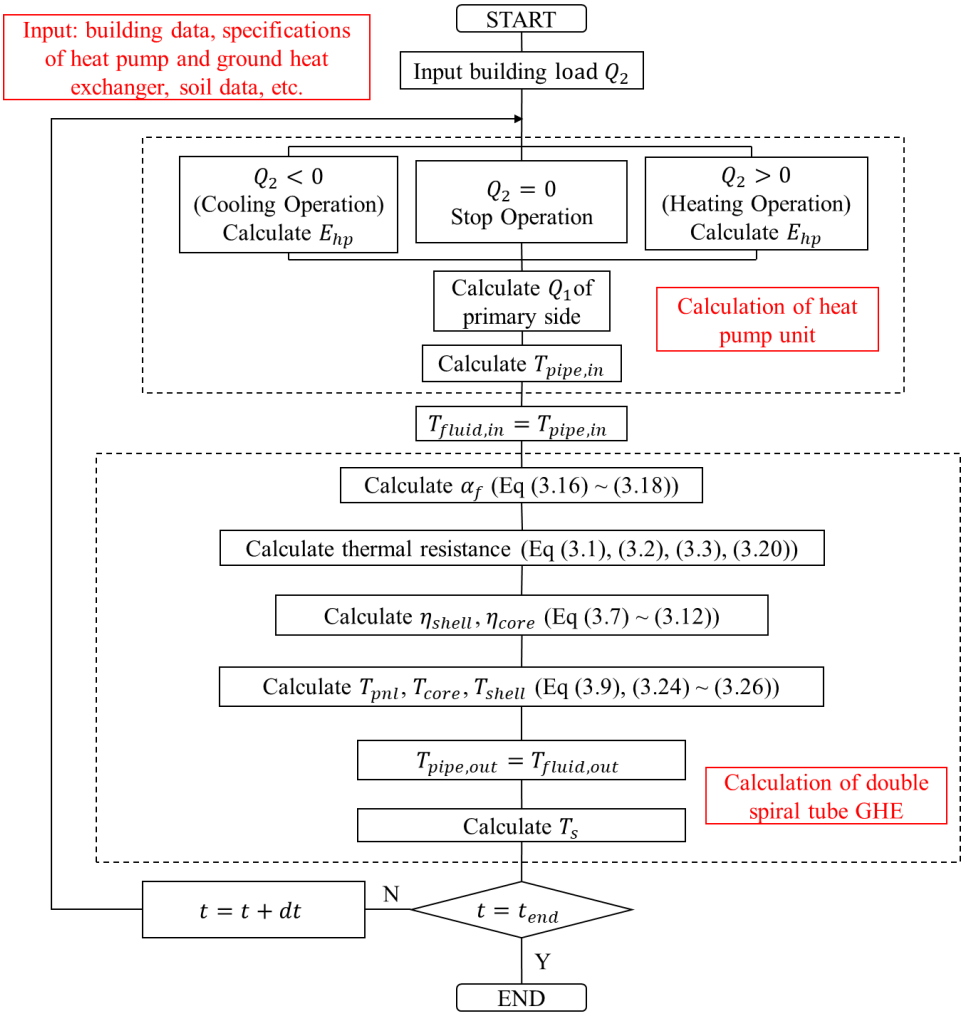

Fig. 3.7 Calculation flowchart for the GSHP system with double spiral pipe GHEs

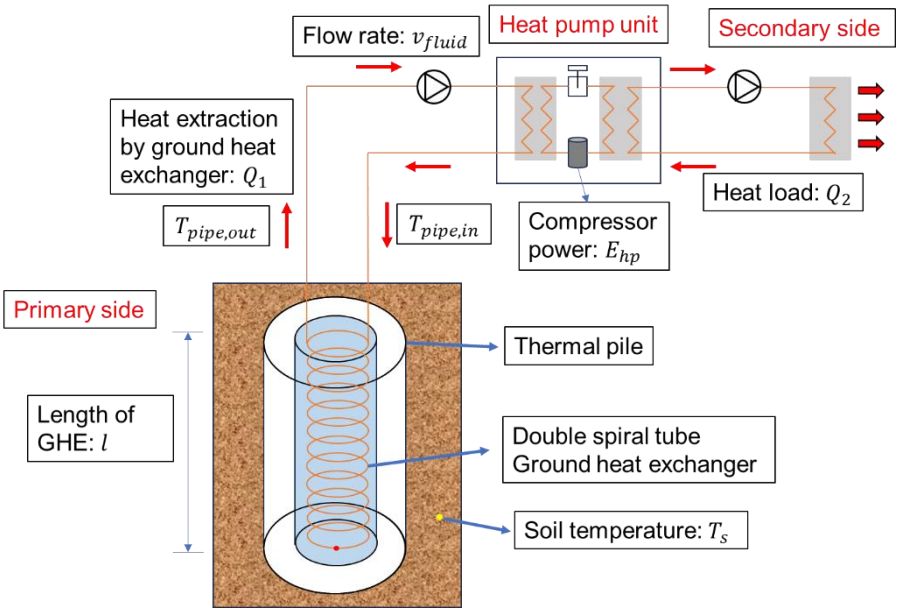

Fig. 3.8 Schematic of the GSHP system using thermal pile with double spiral tube GHE.

For a clearer understanding of the calculation flows, please refer to **Fig. 3.8**. The calculation procedures in a single time step of $dt = 60s$ are as follows:

1. The electricity consumption E_{hp} of the heat pump unit and fluid temperature $T_{1,out}$ flowing out of the heat pump unit are determined using empirical formulas. These calculations are based on the building load Q_2 (secondary side) and the heat extraction or injection into/from the ground Q_1 (primary side). $T_{1,out}$ is equal to the inlet temperature of the double spiral pipe $T_{pipe,in}$.
2. The heat transfer processes within the thermal pile and the outlet temperature of the double spiral pipe $T_{pipe,out}$ are calculated using the new method that has been proposed above. $T_{pipe,out}$ is equal to the fluid temperature $T_{1,in}$ flowing into the heat pump unit, which will be used for the calculation of next time step.
3. The surrounding soil temperature T_s (outside the thermal pile) is calculated in GroundClub. This temperature T_s is equal to the thermal pile boundary temperature T_{ground}, which is also utilized for the calculation of next time step.

By conducting continuous step-by-step simulations of temperature changes at the pipe inlet $T_{pipe,in}$, outlet $T_{pipe,out}$, and ground T_{ground}, long-term operation results for the GSHP system can be obtained. Notably, the simulation tool's speed is much faster than that of traditional numerical tools. For example, in **Section 3.3.1**, simulations of 3019 hours for space heating were completed in approximately 7 seconds. This calculation method's simplicity and efficiency significantly reduce computation time compared to many numerical methods.

3.2. Field Experiment of Thermal Response Test

3.2.1. Experimental Site

The verification was conducted in a nearly zero energy building (NZEB), situated in Sapporo, Japan. This three-story building serves as a company office and incorporates a variety of energy-saving technologies. The first floor houses stores and control rooms for the overall system, the second floor contains office spaces, and the third floor is dedicated to conference and meeting rooms. Operational since July 2021, the building features an array of energy-saving technologies, including photovoltaic (PV) panels for electricity generation, fan coil units, materials with high thermal insulation properties, heat recovery ventilation systems, GSHP systems, and radiant air-conditioning systems. The basic information about the house is detailed in **Table 3.1**.

Fig. 3.8 Subject of this research study: the energy-efficient house in Sapporo, Japan.

Table 3.1 Basic information of the house

Building	**Energy saving technologies**
Location: Sapporo, Japan	Heat recovery ventilation system
Floor area: 650.85 m^2	High thermal insulation
Number of floors: 3	PV system
Operation time: 2021/7 ~ now	Radiant air conditioning system
Structure: Wooden	GSHP system

Three GSHP units, each with a rated power of 10 kW, provide space heating and cooling across all the rooms

on each floor and facilitate snow melting around the building during winter. During operation, the indoor temperatures were consistently maintained at 22 °C in winter and 26 °C in summer. During periods when the rooms were unoccupied, such as at night or on weekends and holidays, the corresponding GSHP system remained inactive until required. **Fig. 3.9** illustrates the GSHP system layout for each floor.

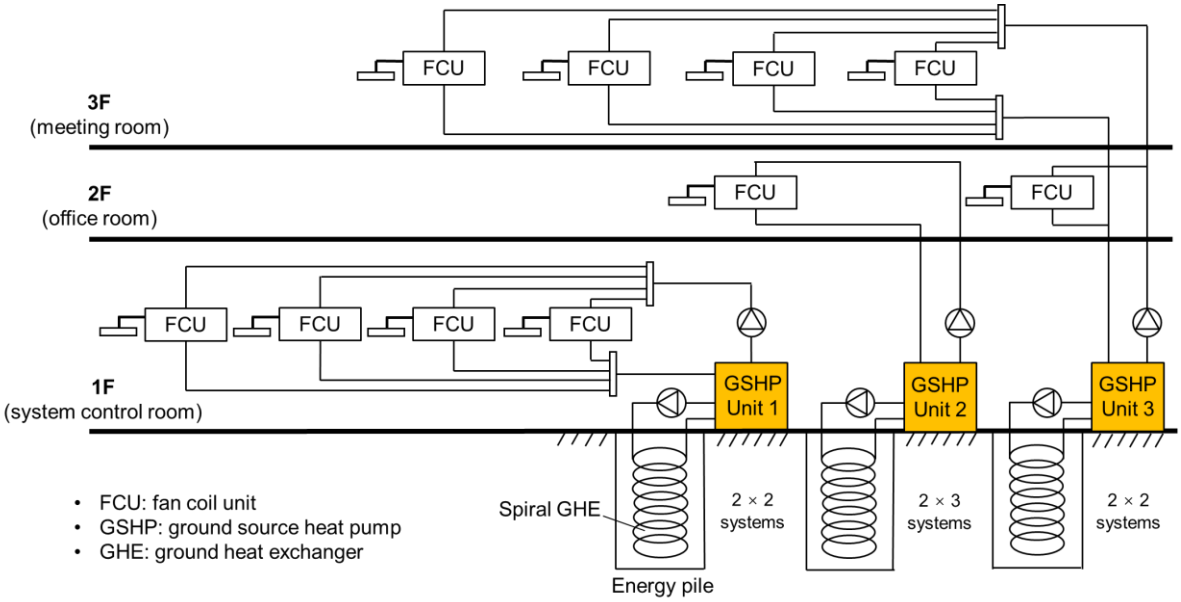

Fig. 3.9 Schematic diagram of the three-story building.

Fig. 3.10 Heat pump units on the first floor.

In this study, the GSHP-1040URX model of GSHP units were utilized in this house, manufactured by Sunpot Co., Ltd. The following are its technical specifications:

Table 3.2 Specifications of the heat pump units

Description		**Value**
Cooling	Capacity	10.0 kW
	Rated power consumption	2.50 kW
	Operating current	12.5 A
	COP	4
Heating	Capacity	10.0 kW
	Rated power consumption	2.50 kW
	Operating current	12.5 A
	COP	4
Rated voltage		Single-phase 200V (for the compressor and control circuit)
Rated frequency		50/60 Hz
Noise level		50 dB
Type of refrigerant		R32
Weight		67 kg

For the GHEs, 24 thermal piles were installed underneath the building, reaching a depth of 20 meters underground. This installation was guided by the innovative "Geothermal Tornado Method," as introduced in **Chapter 1**. The distribution of these thermal piles varied across different levels: the first, second, and third floors were equipped with four (arranged in two series of two piles each), six (two series of three piles each), and four (configured as 1 + 1 + 2) piles respectively. Additionally, the snowmelt systems were supported by ten thermal piles. This layout is illustrated in **Fig. 3.11**.

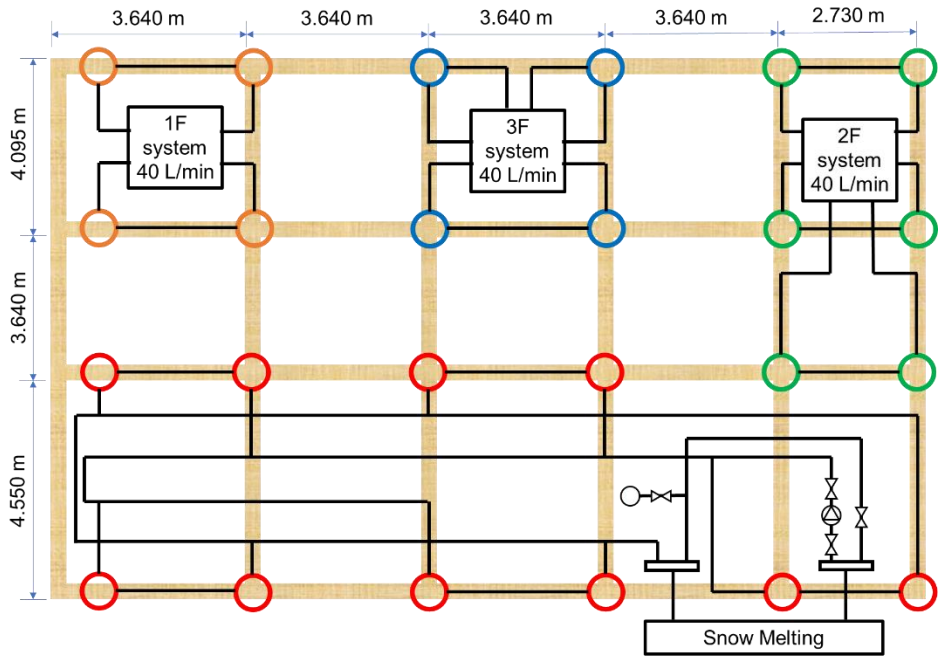

Fig. 3.11 Layout diagram of thermal piles installed underneath the building (orange circle: first floor system; green circle: second floor system; blue circle: third system; red circle: snowmelt system).

Each GSHP unit is equipped with temperature sensors (Pt100) and electromagnetic flow meters, enabling the real-time collection of data on the pipe inlet temperature $T_{pipe,in}$, outlet temperature $T_{pipe,out}$, circulating fluid flow rate v_{fluid}, and the power consumption of the heat pump unit E_{hp}. The measurement was started on 2021/08/27. All data were captured using a real-time measurement system, providing minute-by-minute measurements. These measurements are available for download in .csv (comma-separated values) file format. **Fig. 3.12** shows a schematic diagram of the GSHP system, including the locations of these measurements.

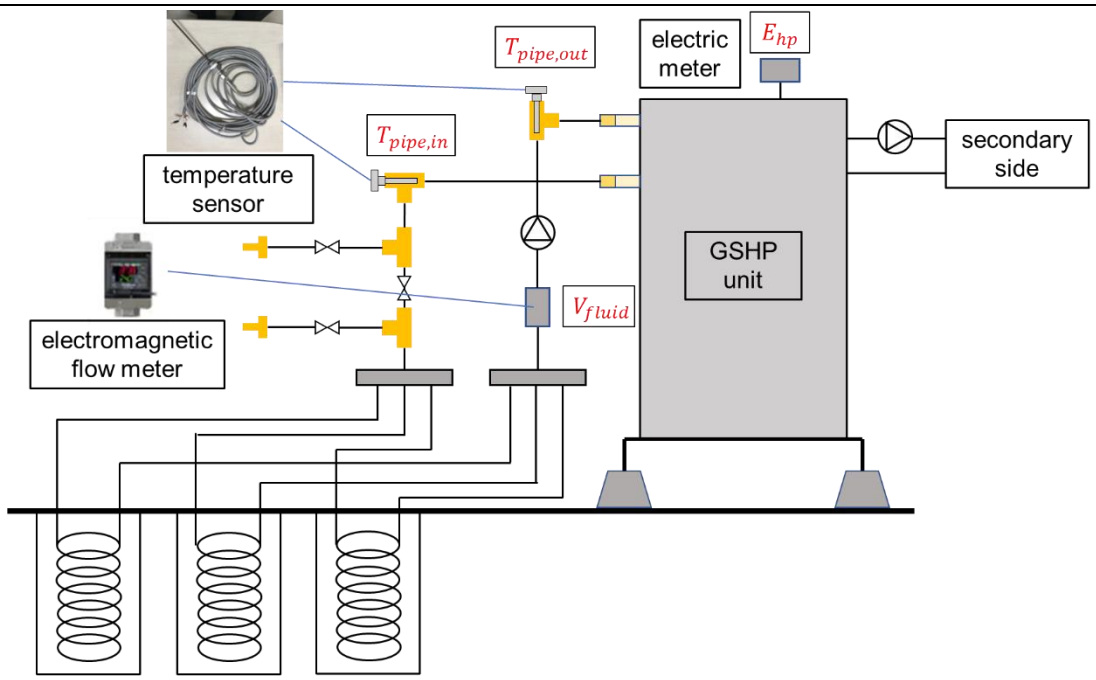

Fig. 3.12 Schematic diagram of the GSHP system and its associated measuring points.

The thermal characteristics of the grout and pile material, including thermal conductivity, specific heat capacity, and density, were determined using the "HC-10 Quick λ Thermal Conductivity Tester" from EKO Instruments [9]. The detailed parameters are presented in Table 3.3. Based on in situ underground temperature measurements conducted before construction began, the undisturbed ground temperature was established at 12 °C.

Table 3.3 GSHP system specifications

Description	**Unit**	**Value**
Thermal pile		
Depth l	m	20
Outer radius $r_{pile,o}$	m	0.3
Inner radius $r_{pile,i}$	m	0.2
"Core" part (cement & soil)		
Thermal conductivity λ_{core}	$W/m{\cdot}K$	0.6
Specific heat capacity c_{core}	$kJ/kg{\cdot}K$	0.9
Density ρ_{core}	kg/m^3	2100
"Shell" part (concrete)		
Thermal conductivity λ_{shell}	$W/m{\cdot}K$	2.0
Specific heat capacity c_{shell}	$kJ/kg{\cdot}K$	0.95

Density ρ_{shell}	kg/m^3	2500
Double spiral pipe		
Outer diameter $d_{pipe,o}$	m	0.032
Inner diameter $d_{pipe,\mathrm{i}}$	m	0.026
Spiral distance l_{pitch}	m	0.25
Thermal conductivity of pipe material λ_{pipe}	$W/m{\cdot}K$	0.38
Length of spiral pipe l_{sp}	m	94.63
Soil		
Specific heat capacity λ_s	$kJ/kg{\cdot}K$	2
Density ρ_s	kg/m^3	1500
Undisturbed ground temperature T_{ground}	℃	12

3.2.2. Thermal Response Test

In the design and construction of a GSHP system, certain parameters hold significant importance. While specific heat capacity, density, and temperature of the underground soil can be estimated from geological or soil-profile data, the effective thermal conductivity of the soil is crucial for precise simulation of a GSHP system. However, deriving accurate values for these parameters solely from geological data presents challenges.

To address this, an in-situ Thermal Response Test (TRT) was performed on a thermal pile from the third-floor system. The purpose of a TRT, essential for ascertaining ground thermal conductivity—a critical element in GSHP system design—is to evaluate the equivalent thermal conductivity of the tested ground volume. The main concept of the test involves monitoring the temperature changes in a borehole heat exchanger under a thermal load. By analyzing the rate of temperature variation over time, the thermal conductivity of the ground surrounding the borehole heat exchanger can be estimated. The Kelvin Line Theorem [10] is employed to interpret the test results and determine the underground soil's thermal conductivity at the specific site, considering various assumptions and simplifications. **Fig. 3.13** illustrates the schematic of the TRT test. In this test, a 40% ethylene glycol solution was used as the circulating fluid.

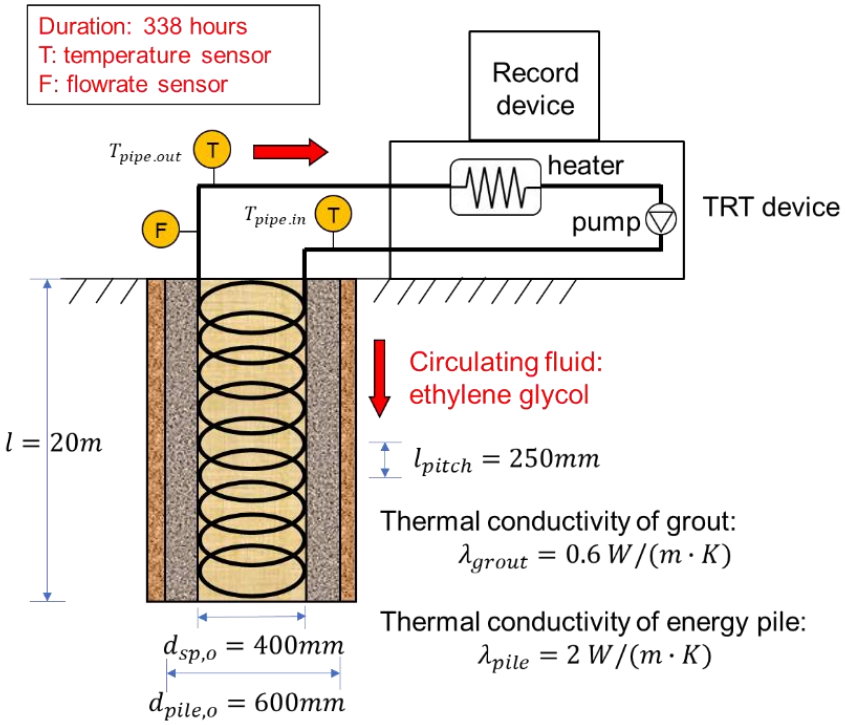

Fig. 3.13 Schematic diagram of TRT test.

Fig. 3.14 Devices used for TRT test.

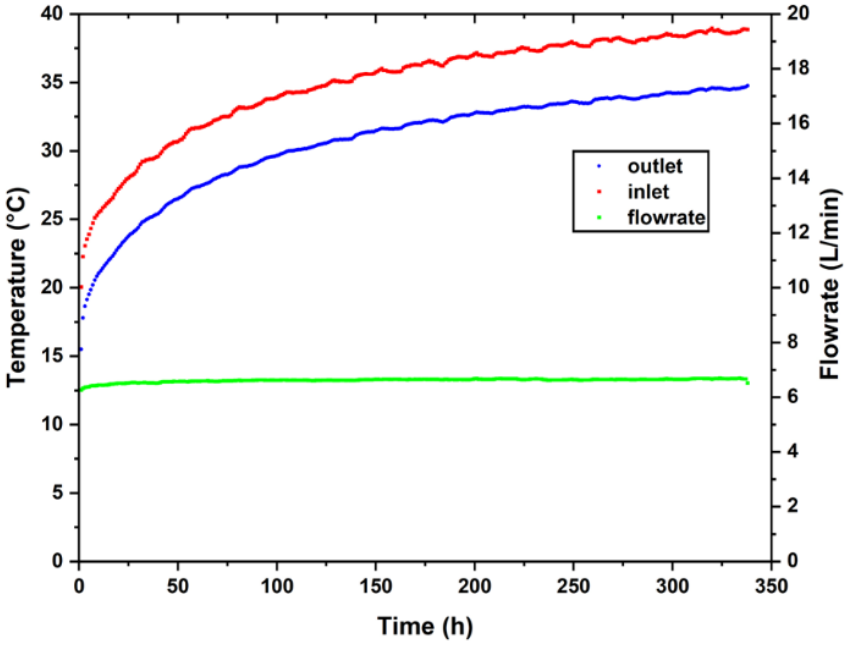

Fig. 3.15 338-h measurement from TRT test.

Fig. 3.15 shows the pipe inlet/outlet temperature and flowrate of the circulating fluid, as recorded over a duration of 338 hours (2021/10/06 13:00–2021/10/20 15:00). The effective thermal conductivity of the ground, where the house is situated, was determined using the subsequent methodology:

A transient 1D heat conduction analysis [11], provides the fluid temperature as a time-dependent variable:

$$T_{fluid}(t) = \frac{q}{4\pi \cdot \lambda_s} \cdot ln(t) + \frac{q}{4\pi \cdot \lambda_s} \cdot \left(ln\frac{4\alpha_s}{r_b^2} - \gamma \right) + q \cdot R_b + T_s \tag{3.27}$$

where T_{fluid} represents fluid temperature, T_s denotes the undisturbed ground temperature, q is the heat load per unit length, λ_s is the effective thermal conductivity of the ground, r_b is borehole radius, α_s is thermal diffusivity of the ground, γ represents Euler's constant, and R_b is the borehole thermal resistance.

By substituting the values of m' and b for the constants in Eq (3.27), the equation is transformed as follows:

$$T_f(t) = m' \cdot ln(t) + b; m' = \frac{q}{4\pi \cdot \lambda_s}; b = \frac{q}{4\pi\lambda_s}\left(ln\frac{4\alpha_s}{r_b^2} - \gamma \right) + qR_b + T_s \tag{3.28}$$

The equation above is only valid under the condition that the time is not too short, necessitating the fulfillment of the time criterion $t > 5 \cdot r_b^2/\alpha_s$. Given the thermal diffusivity of the ground $\alpha_s = 0.002\, m^2/s$, and the borehole radius $r_b = 0.3\, m$, this leads to the determination of the effective starting time for the TRT analysis as follows:

$$\frac{\alpha_s \cdot t}{r_b^2} > 5 \rightarrow \frac{0.002t}{0.3^2} > 5 \rightarrow t > 225\ h \tag{3.29}$$

Fig. 3.15 (a) and (b) respectively present the mean fluid temperature over time during the TRT test in both linear and logarithmic time scales.

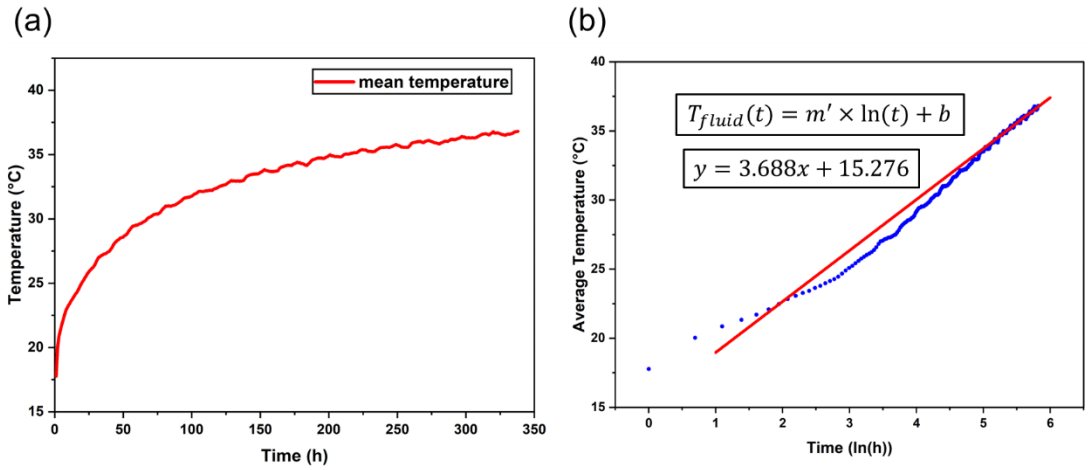

Fig 3.16 Mean fluid temperature in (a) linear time scale and (b) logarithmic time scale with the fitting linear function from start time of 225 h to end time of 338 h.

The thermal conductivity derived from the slope k of the approximate linear curve from the effective start time of 225 h to the end time of 338 h.

$$\lambda_s = \frac{q}{4\pi \cdot m'} \tag{3.30}$$

This analysis yielded an effective thermal conductivity of the ground, $\lambda_s = 1.846(W/m \cdot K)$. Utilizing this value in the simulation, the verification work was performed by comparing the measured and simulated data. This was executed under two different scenarios, which are discussed subsequently.

3.3. Verification and Analyses

3.3.1. Space Cooling in Summer

During the space cooling period, the indoor room temperatures were maintained at 26 °C. Notably, most rooms on the first floor were occupied, leading to the longest operational duration for GSHP unit 1 in the first-floor system. Therefore, this unit was chosen for detailed data analysis. The heat injection from the house to the ground can be calculated by using the hourly recorded temperatures at the pipe inlet and outlet, along with the flow rate data of the circulating fluid during the space cooling period. This calculation follows Eq 3.31, and the results are presented in **Fig. 3.17**.

$$Q_{injection} = \rho_{fluid} \cdot c_{fluid} \cdot v_{fluid} \cdot (T_{pipe,in} - T_{pipe,out}) \tag{3.31}$$

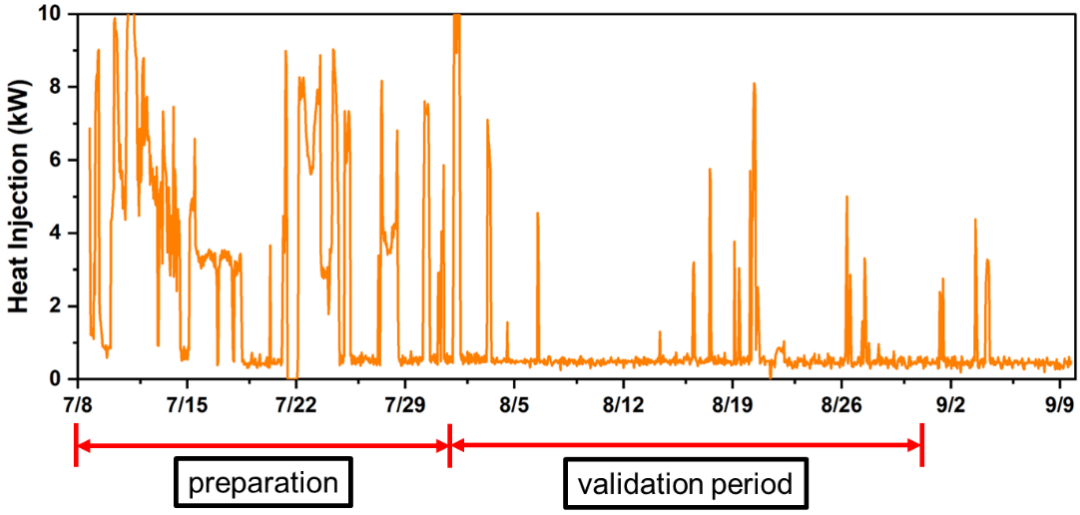

Fig. 3.17 Heat injection into the ground during space cooling period.

As depicted in **Fig. 3.17**, variations in heat injection into the ground were observed, correlating with the building's load. This load was affected by factors such as the preset indoor temperature, outdoor temperature fluctuations, and room occupancy. Notably, peak loads were observed during periods of maximum occupancy or extreme hot weather, while the load remained low for the majority of the time. The heat injection during this period served as the primary side load, Q_1, for subsequent simulations. Except for the preparation time, the verification period was designated from 2021/8/1 to 2021/8/31. **Fig. 3.18** presents a comparative analysis of the hourly variations in the pipe inlet temperature, $T_{pipe,in}$, showcasing a comparison of the measured data against the simulation results.

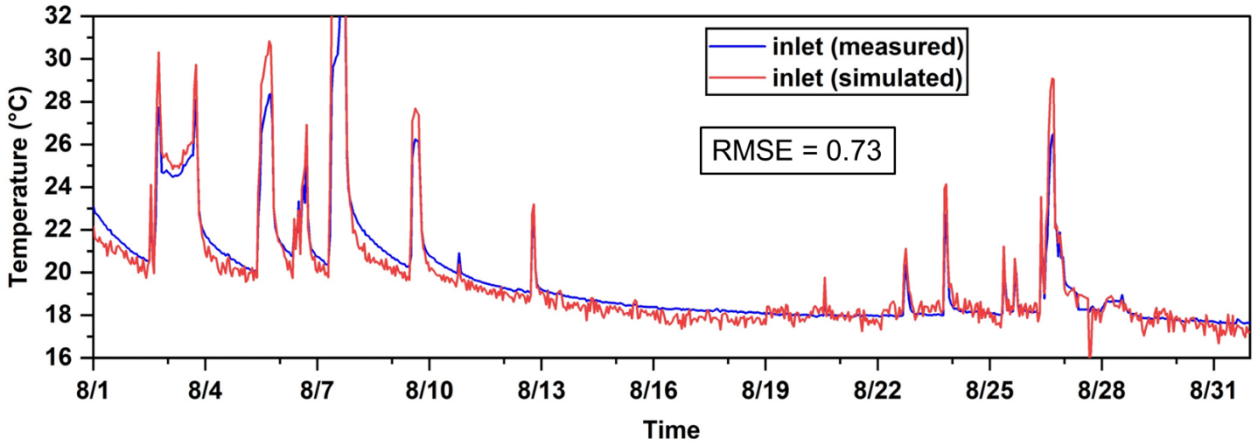

Fig. 3.18 Pipe inlet temperature during space cooling period from 8/1 to 8/31

Both temperatures exhibit similar trends, with minor discrepancies during periods of rapid temperature shifts. The maximum deviation between the simulated and observed temperatures was 4.34 °C, corresponding to a peak relative error of 13.06%. However, excluding moments of abrupt building load surges and swift temperature fluctuations, the temperature variance remained below 1 °C for 683 hours (91.80% of the total 744 hours). Furthermore, the relative error was maintained below 5% for 690 hours (92.74%) within the same timeframe. The average simulated and observed temperatures were recorded at 19.71 °C and 19.77 °C, respectively. The Root Mean Squared Error (RMSE) value between measurement and simulation data for the period from 8/1 to 8/31 was calculated to be 0.73, demonstrating the precision of the simulation tool.

3.3.2. Space Heating in Winter

All GSHP units were configured to deliver hot water at 45 °C throughout the space heating period, with the indoor room temperatures maintained at 22 °C. The collected data was utilized to determine the amount of heat extracted from the ground. This calculation adhered to **Eq. 3.32**, and the corresponding results are depicted in **Fig. 3.19**.

$$Q_{extraction} = \rho_{fluid} \cdot c_{fluid} \cdot v_{fluid} \cdot (T_{pipe,out} - T_{pipe,in}) \quad (3.32)$$

Fig. 3.20 presents a comparison between the observed and simulated data regarding the temperature at the pipe inlet. Excluding periods of maintenance and holidays, the verification phase was conducted from 1/7 to 2/7, coinciding with Sapporo's coldest period when space heating demand is at its peak. The findings indicate a strong correlation between measured and simulated temperatures, as evidenced by a RMSE of 1.06. This RMSE value

is within an acceptable range, affirming the reliability and effectiveness of the simulation tool employed.

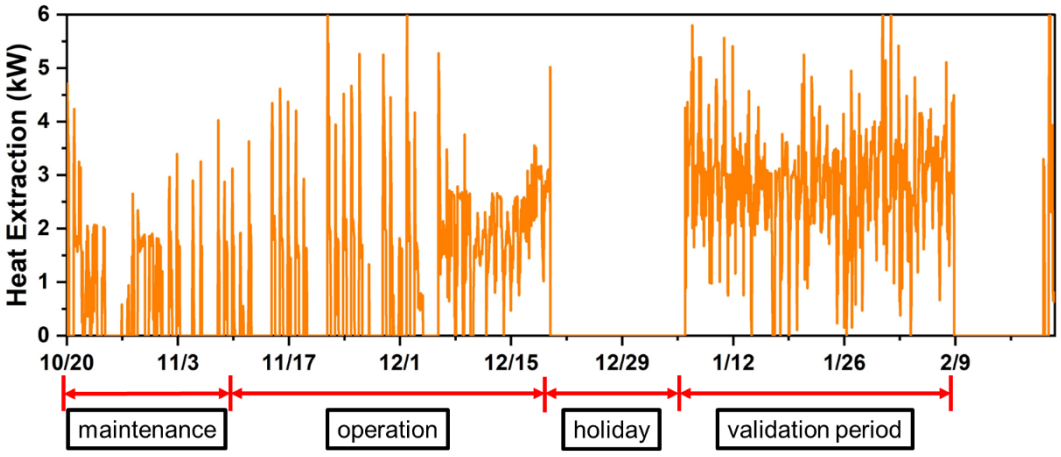

Fig. 3.19 Heat injection into the ground during space cooling period

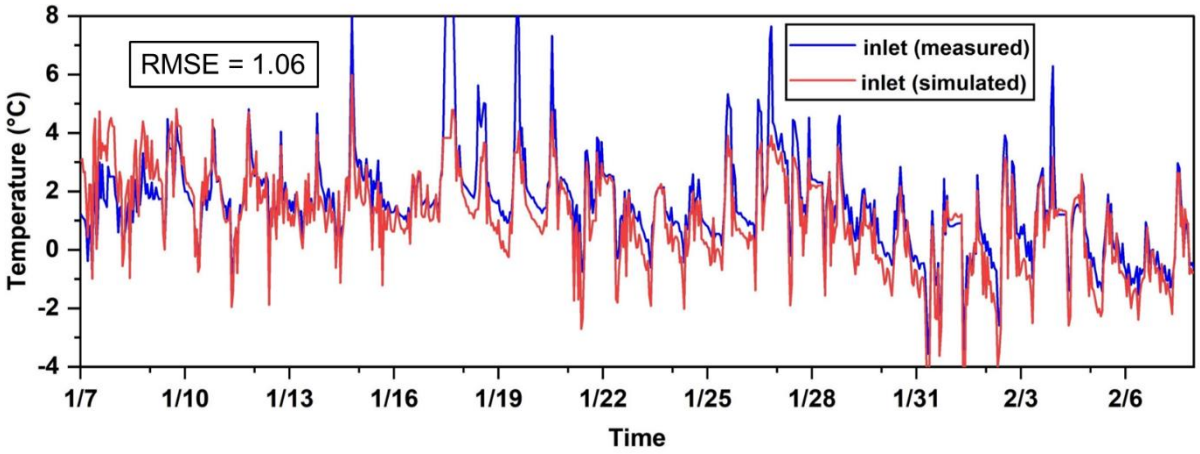

Fig. 3.20 Pipe inlet temperature during space cooling period from 8/1 to 8/31

This simulation tool is meticulously crafted to produce highly accurate results for performance assessment, enabling robust estimates that bolster early-stage decision-making. Verification in both summer and winter conditions demonstrates the tool's efficacy for performance prediction in the preliminary design phase of future GSHP systems employing thermal piles and double spiral tube GHEs.

3.4. Discussion

3.4.1. Superiority to another CaRM model

The analyses in this study indicate that the newly developed simulation tool can outperform the widely recognized CaRM-He model in predicting performance of GHEs. Contrasting with the CaRM-He model from

previous research [2], which analyzed the thermal behavior of helical GHEs, the approach in this study demonstrates notable advancements. As depicted in **Fig 3.21**, helical GHEs comprise an inner pipe (pipe 1) and a helical pipe (pipe 2), where the heat carrier fluid may circulate either in the inner or helical pipe. However, in this study, the double spiral tube GHE, benefiting from an innovative manufacturing method, eliminates the need for straight pipe, with both inlet and outlet of the heat carrier fluid employing spiral pipes, thereby enhancing efficiency.

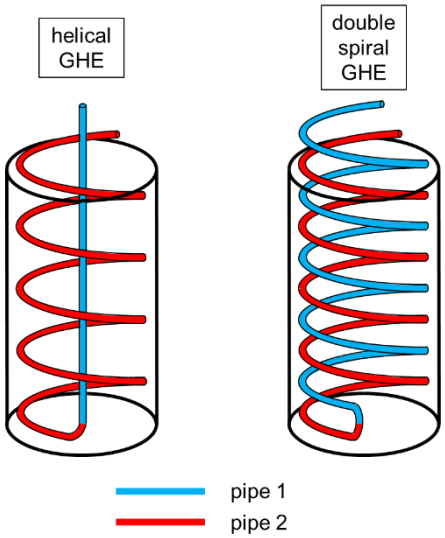

Fig 3.21 Comparison between helical GHE in previous study and double spiral tube GHE in this study

The new calculation method in this study, utilizing fin efficiency, conceptualizes the spiral pipe as a vertical panel for heat emission or absorption. In this model, the spiral pipe is simplified to a linear heat source, allowing temperature nodes to be positioned anywhere within the grout or pile. This method overcomes the limitations of aligning temperature nodes parallel to the spiral pipe, as shown in **Fig 3.22** (a). It also removes the constraint of their proximity to the pipe.

While the CaRM-He model accounts for heat transfer along the depth direction, it assumes that heat flow in and out of the temperature nodes nearest to the spiral pipe occurs in four directions: the pipe surface, the temperature nodes above and below, and the temperature nodes on the adjacent parallel line. However, CaRM-He model 's applicability is limited to scenarios with small-pitch spiral pipes, as in cases where the pitch (spiral distance) exceeds 100 mm, heat flow from the pipe surface to non-parallel temperature nodes is reduced, rendering the heat balance inapplicable for larger pitch distances.

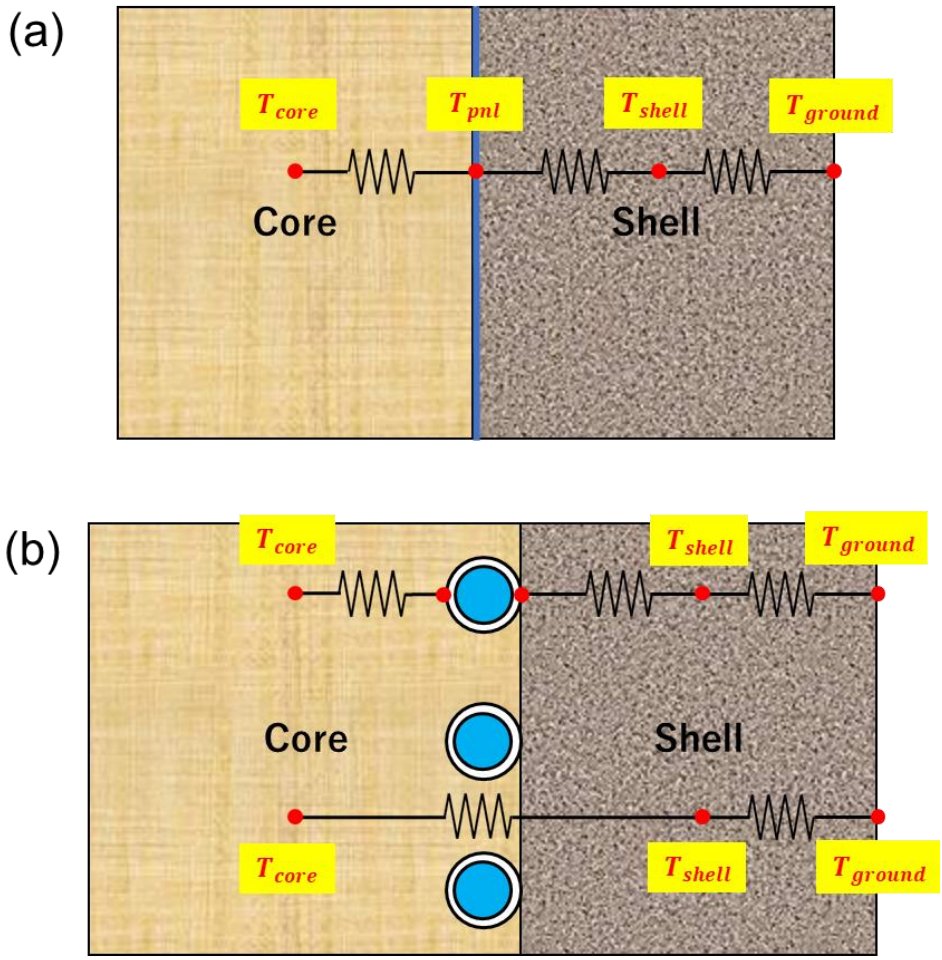

Fig. 3.22 Comparison of the new calculation method (a) and model CaRM-He (b)

A comparative analysis between the new method in this study and the CaRM-He model was conducted, focusing on a specific application scenario: a one-week period of summer cooling (2021/08/05 – 2021/08/12), as illustrated in **Fig. 3.23**. The comparison revealed that the simulation result by CaRM-He model consistently falls below the actual measurement. This discrepancy is attributed to its lower simulated heat flow from the pipe surface compared to the measured value. Key performance metrics for this period are as follows: the CaRM-He model predicted an average temperature of 19.72 °C, with a RMSE of 2.31, a maximum error of 18.55%, and a peak temperature difference of 6.21°C. In contrast, the simulations conducted using the new method reported an average temperature of 21.70 °C, aligning more closely with the actual measurements. This method demonstrated an RMSE of 1.07, a maximum error of 13.06%, and a reduced maximum temperature difference of 4.34°C. The marked improvements in these metrics underscore the new method's enhanced accuracy and its increased reliability for long-term operational simulations.

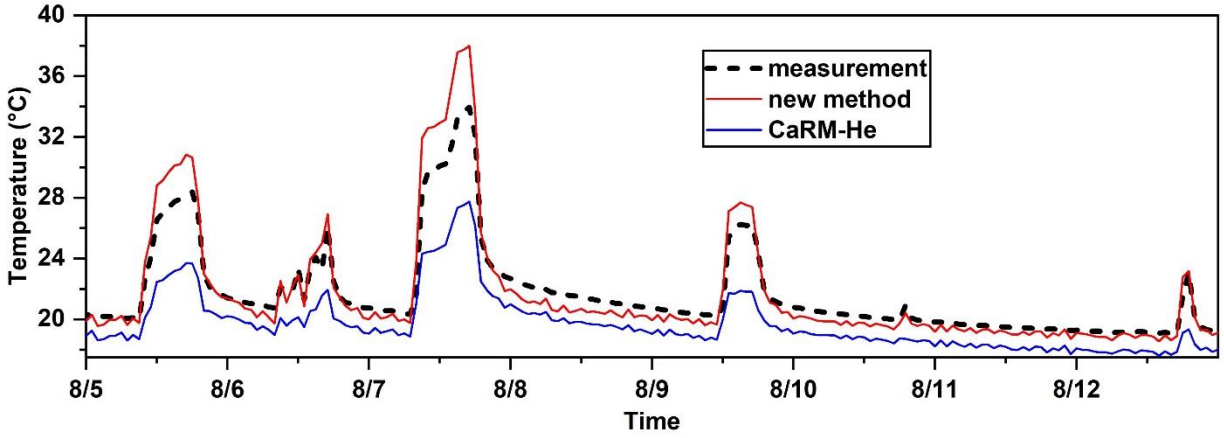

Fig. 3.23 Comparison of the simulation results of new calculation method (red) and model CaRM-He (blue) over a one-week period.

3.4.2. Coefficient of heat extraction/injection

The impact of varying pitch (spiral distance) on the performance of the double spiral tube GHE was investigated, given that the simulation tool in this study can be used for double spiral tube GHE with any pitch size. Additionally, a comparative efficiency analysis was conducted, including a single U-tube GHE with identical underground depth and pipe material, but a smaller borehole diameter, to contrast the efficiencies of GHEs with different designs.

To assess the performance of GHE, this study introduces the heat extraction/injection rate per unit length of GHE, which is defined as the coefficient of heat extraction/injection [12], and its comprehensive explanation will be presented in the subsequent chapter. The relevant formula for this metric is as follows:

$$\Delta T = \frac{T_{pipe,in} + T_{pipe,out}}{2} - T_{ground};\ q' = \frac{Q}{l \cdot \Delta T} \tag{3.33}$$

where $T_{pipe,in}$ and $T_{pipe,out}$ represent the pipe inlet and outlet temperature, T_{ground} denotes the undisturbed ground temperature, Q refers to the heat load, l is underground depth of thermal pile, q' is the coefficient of heat extraction/injection.

The parameters of the thermal pile, spiral pipe, soil, and circulating fluid were kept constant maintained constant, as detailed in Tables 3.3 and 3.4. Simulation outcomes illustrate variations in the coefficient of heat extraction/injection per 100 hours, as shown in **Fig. 3.24**. At the 100-hour mark, the efficiency of double spiral tube GHEs increased by 6.7%, 14.3%, 22.9%, 32.7%, and 39.6% corresponding to pitch alterations from 0.07 m to 0.1, 0.15, 0.2, 0.25, and 0.3 m. Moreover, at 800 h, the efficiency of double spiral tube GHE exhibited

increases of 4.6%, 9.5%, 14.8%, 20.7%, and 24.7% for corresponding pitch changes from 0.07 m to 0.1, 0.15, 0.2, 0.25, and 0.3 m.

Table 3.4 Simulation condition settings

Description	**Unit**	**Value**
Heat load Q	W	2000
Flow rate of circulating fluid v_{fluid}	L/min	6.5
Length of borehole for U-tube GHE and double spiral tube GHE l	m	20
Radius of borehole for U-tube GHE	m	0.06
Radius of thermal pile	m	0.3
Duration time t	h	800
Spiral distance of spiral pipe l_{pitch}	m	0.07, 0.1, 0.15, 0.2, 0.25, 0.3

The lowest efficiency of the double spiral tube GHE (pitch = 0.3m) is still far superior to the U-tube GHE. At 800 h, the efficiency of double spiral tube GHE (pitch = 0.3m) was observed to be 67.5% higher compared to the U-tube GHE, thereby highlighting its enhanced effectiveness.

In summary, for fixed underground depths, reducing the pitch size of the double spiral tube GHE enhances its efficiency, regardless of the operation duration. This finding aligns with the research of Zhao et al. [13]. Their study revealed that in both heating and cooling scenarios, a smaller spiral pitch leads to an increase in the average coefficient of performance. They proposed that thermal piles with smaller spiral pitches not only demonstrate higher energy efficiency but also have a wider range of applications.

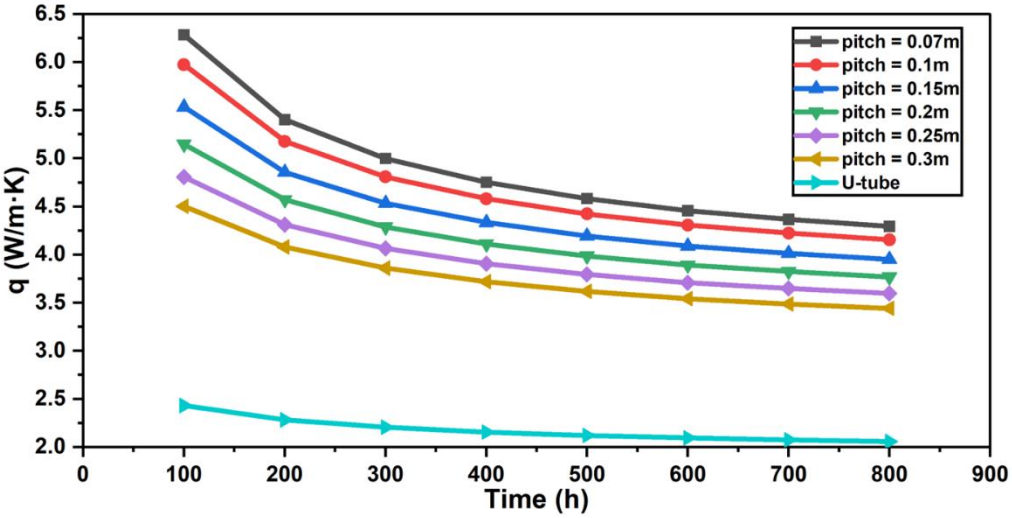

Fig. 3.24 Coefficient of heat extraction/injection for spiral pipe for varied pitches every 100 h.

3.5. Conclusion

The newly proposed calculation method, grounded in the CaRM model, represents a significant advancement over previous methodologies by incorporating the concept of fin efficiency and integrating a simulation program for GSHP system in MATLAB. This method showcases several key improvements:

1) Contrasting with the conventional U-tube GHE, the innovative double spiral tube GHE utilizes shorter underground depth while offering a more extensive heat exchange area between the ground and circulating fluid. This enhancement is achieved without necessitating additional drilling, thereby reducing the initial costs of the GSHP system and fostering its future adoption.
2) The method introduces a novel approach by substituting the spiral pipe with a vertical heat generating/absorbing panel. This modification simplifies the process of determining temperature variations across different sections of the thermal pile, reducing the computational burden.
3) Verification work conducted in an energy-efficient house has demonstrated that the simulation tool yields accurate and precise results for the long-term operation of GSHP systems across both summer and winter seasons. This reliability is pivotal for the preliminary design stages of future GSHP systems.

When compared to the established CaRM-He model, this novel simulation tool exhibits superior performance. Originating from a calculation method for floor heating systems, its effectiveness is not constrained by the pitch size of spiral pipes, enhancing its versatility.

In conclusion, the simulation outcomes indicate a substantial enhancement in thermal efficiency when employing the double spiral tube GHE with a reduced pitch size, marking a notable step forward in the field of

GSHP system design and optimization.

NOMENCLATURE

c	: specific heat capacity [J/(kg·K)]
d	: diameter [m]
E	: electricity consumption [kW]
l	: length/depth [m]
Q	: thermal load [kW]
q	: thermal load per unit length [W/m]
q'	: coefficient of heat extraction/injection [W/m·K]
R	: heat resistance [k/W]
r	: radius [m]
T	: temperature [°C]
V	: volume [m^3]
v	: flow rate [m^3/s]

GREEK SYMBOLS

α	: heat transfer coefficient [$W/m^2 \cdot K$]
η	: fin efficiency [-]
λ	: thermal conductivity [W/m·K]
ρ	: density [kg/m^3]

SUBSCRIPTS

core	: "core" section
fluid	: circulating fluid
ground	: ground soil
hp	: heat pump
i	: inner
pile	: thermal pile
pipe	: spiral pipe
pipe,in	: pipe inlet
o	: outer
pipe,out	: Connector

pnl : “vertical” panel

s : ground soil

shell : “shell” section

sp : spiral

Reference

[1] M. De Carli, M. Tonon, A. Zarrella, and R. Zecchin, "A computational capacity resistance model (CaRM) for vertical ground-coupled heat exchangers," *Renew Energy*, vol. 35, no. 7, 2010, doi: 10.1016/j.renene.2009.11.034.

[2] A. Zarrella and M. De Carli, "Heat transfer analysis of short helical borehole heat exchangers," *Appl Energy*, vol. 102, 2013, doi: 10.1016/j.apenergy.2012.09.012.

[3] A. Kollmar, "Thermal Emission of Flat Heating Surfaces and Ceiling Heating Panels with Cylinderical Heat Sources (Wärmeabgabe von Plattenheizflächen und Heizdecken mit Zylindrischen Wärmequellen)," D.A. Sinclair (Tr. by), 37p, 1961.

[4] H. Ishino, "Research on calculation method of thermal design load in radiant heating and cooling systems," Sixth International IBPSA Conference (BS′ 99), 1999, pp. 885–892.

[5] A. N. Dravid, K. A. Smith, E. W. Merrill, and P. L. T. Brian, "Effect of secondary fluid motion on laminar flow heat transfer in helically coiled tubes," *AIChE Journal*, vol. 17, no. 5, 1971, doi: 10.1002/aic.690170517.

[6] V. Gnielinski, "New Equations for Heat and Mass Transfer in Turbulent Pipe and Channel Flow," *International Chemical Engineering*, vol. 16, no. 2, 1976.

[7] P. K. Namburu, D. K. Das, K. M. Tanguturi, and R. S. Vajjha, "Numerical study of turbulent flow and heat transfer characteristics of nanofluids considering variable properties," *International Journal of Thermal Sciences*, vol. 48, no. 2, 2009, doi: 10.1016/j.ijthermalsci.2008.01.001.

[8] T. Katsura, K. Nagano, Y. Sakata, and H. Wakayama, "A design and simulation tool for ground source heat pump system using energy piles with large diameter," *Int J Energy Res*, 2019, doi: 10.1002/ER.4372.

[9] "HC-10." Accessed: Nov. 17, 2022. [Online]. Available: https://www.eko-instruments.com/us/categories/products/thermal-analysis-instruments/hc-10

[10] B. Nordell, "Thermal Response Test (TRT) State-of-the Art 2011: IEA ECES," 2011 ANNEX 21.

[11] L.R. Ingersoll, H.J. Plass, "Theory of the ground pipe heat source for heat pump", ASHVE journal section, Heat. Pip. Air Cond. 119–122, 1948.

[12] T. Katsura, K. Nagano, Y. Nakamura, A study on design method for the ground heat exchanger's specification of ground source heat pump system, Nihon Kenchiku Gakkai Kankyokei Ronbunshu. 76 (2011) 59–66. https://doi.org/10.3130/aije.76.59.

[13] Q. Zhao, F. Liu, C. Liu, M. Tian, and B. Chen, "Influence of spiral pitch on the thermal behaviors of energy piles with spiral-tube heat exchanger," *Appl Therm Eng*, vol. 125, 2017, doi: 10.1016/j.applthermaleng.2017.07.099.

Chapter 4

Analyzing the Performance of Double Spiral Tube Ground Heat Exchangers in a Zero-Energy Building Using Measurement Data

4.1. Calculation of coefficient of heat extraction/injection

4.1.1. Heat injection/extraction of GSHP systems in summer and winter

Fig. 4.1 presents a schematic representation of the GSHP system examined in this study. This diagram highlights the critical components of the system, including the primary and secondary sides, the heat pump unit, the thermal pile, and the double spiral tube GHEs.

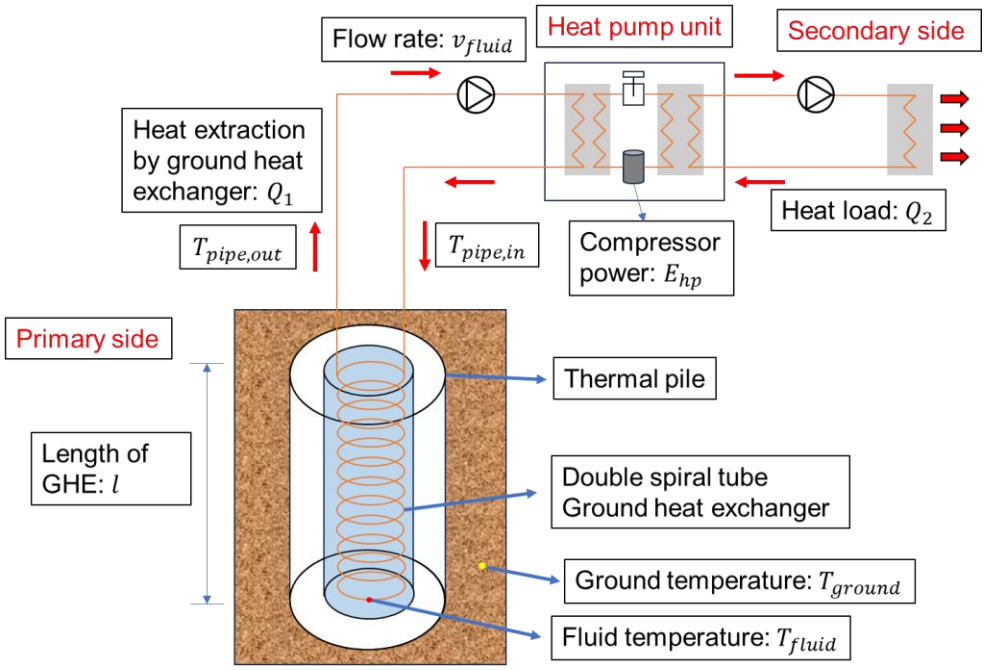

Fig. 4.1 Schematic of the ground-source heat pump (GSHP) system examined in this study.

In a GSHP system, GHEs are utilized for extracting or discharging heat to and from the ground [1]. In the summer, the transfer of heat (primary load Q_1) from the indoor environment to the ground (acting as a heat sink) was determined by using the temperature differential between the inlet and outlet of the pipe as follows.

$$Q_1 = \rho_{fluid} \cdot c_{fluid} \cdot v_{fluid} \cdot \left(T_{pipe,in} - T_{pipe,out}\right) \quad (4.1)$$

where ρ_{fluid}, c_{fluid} and v_{fluid} represent the density, specific heat capacity, and flow rate of the circulating fluid, respectively.

Subsequently, the heat removed from the indoor environment (secondary load Q_2) is equivalent to the amount remaining after subtracting the power consumption E_{hp}.

$$Q_2 = Q_1 - E_{hp} \quad (4.2)$$

In the winter, the process of extracting heat (primary load Q_1) from the ground (serving as the heat source) to

the indoor environment was determined by reversing the sequence as follows.

$$Q_1 = \rho_{fluid} \cdot c_{fluid} \cdot v_{fluid} \cdot \left(T_{pipe,out} - T_{pipe,in}\right) \quad (4.3)$$

The heat provided to the indoor environment (secondary load Q_2) was equal to the sum of the heat extracted and the power consumption E_{hp}.

$$Q_2 = Q_1 + E_{hp} \quad (4.4)$$

4.1.2. Coefficient of Heat Extraction/Injection

As detailed in **Chapter 2**, the performance of GHEs in both heat extraction and injection is influenced by multiple variables. These include the surrounding soil's composition, the GHEs' design and pipe materials, and the circulating fluid's flow rate. Among these factors, the temperature of the circulating fluid is of great importance. For example, in winter heat extraction scenarios, lowering the temperature of the circulating fluid, which is already considerably lower than the underground temperature, increases the temperature difference between the underground and the circulating fluid. This increment enhances heat extraction capability. However, it is crucial to avoid excessive alterations in the fluid's temperature to maintain its operational range. Deviating from this range can impair the heat pump's performance and trigger reliability concerns.

The efficiency of heat extraction or injection by GHEs can be quantified by calculating the heat extracted or injected per unit length and then dividing this value by the temperature difference between the undisturbed ground and the circulating fluid, as referenced in [2]. This calculation yields a ratio known as the coefficient of heat extraction/injection. This coefficient provides a more comprehensive metric for evaluating GHE performance than simply assessing heat transfer rates. It accounts for both the heat transfer per unit length and the temperature disparity between the ground and the fluid, thus offering a precise measure of different GHEs' capabilities in heat exchange under equivalent temperature differentials. Consequently, this coefficient serves as an effective tool for comparing and assessing various GHE configurations.

In this study, the circulating fluid temperature was determined by averaging the temperatures at the pipe inlet and outlet.

$$T_{fluid} = \frac{T_{pipe,in} + T_{pipe,out}}{2} \quad (4.5)$$

The coefficient of heat extraction/injection, expressed in watts per meter-kelvin (W/(m·K)), was calculated

using **Eq (4.6)** as follows.

$$q' = \frac{Q_1}{l \times \Delta T} = \frac{Q_1}{l \times \left(T_{ground} - T_{fluid}\right)} \tag{4.6}$$

where Q_1 represents the rate of heat extraction/injection, measured in watts (W), l is the underground depth of the GHEs in meters (m), and T_{ground} refers the undisturbed ground temperature in kelvin (K). Using the equations described above, an analysis of the measured data was conducted.

4.2. Measurement of a Zero Energy Building in Sapporo

4.2.1. Simplification of Large Quantities of Data

Continuing with the long-term measurement of the Zero Energy Building (ZEB), as detailed in **Chapter 3**, data was meticulously recorded at one-minute intervals. This process yielded an extensive dataset comprising over 880,000 entries in Excel. The measurement period spanned from 2021/08/27, to 2023/05/31. However, the effective analysis of this large dataset faced challenges due to the presence of invalid data, measurement errors, and null values. These issues primarily arose during periods when monitoring devices were not operational, such as holidays, rest days, and nighttime.

To mitigate the impact of erroneous data and enhance accuracy, a strategy of averaging the data over 60-minute intervals was adopted. This method effectively condensed the dataset to approximately 15,000 entries. For example, on 2022/01/19, between 16:00 and 17:00, the dataset includes 60 recordings per minute for variables like pipe inlet temperature, circulating fluid flow rate, energy consumption of the heat pump unit, and heat extraction rate of GSHP unit 1, determined using **Eq (4.3)**. Thus, the average value for each variable during this hour was computed and used to represent the data for that entire period, as depicted in **Fig. 4.2**.

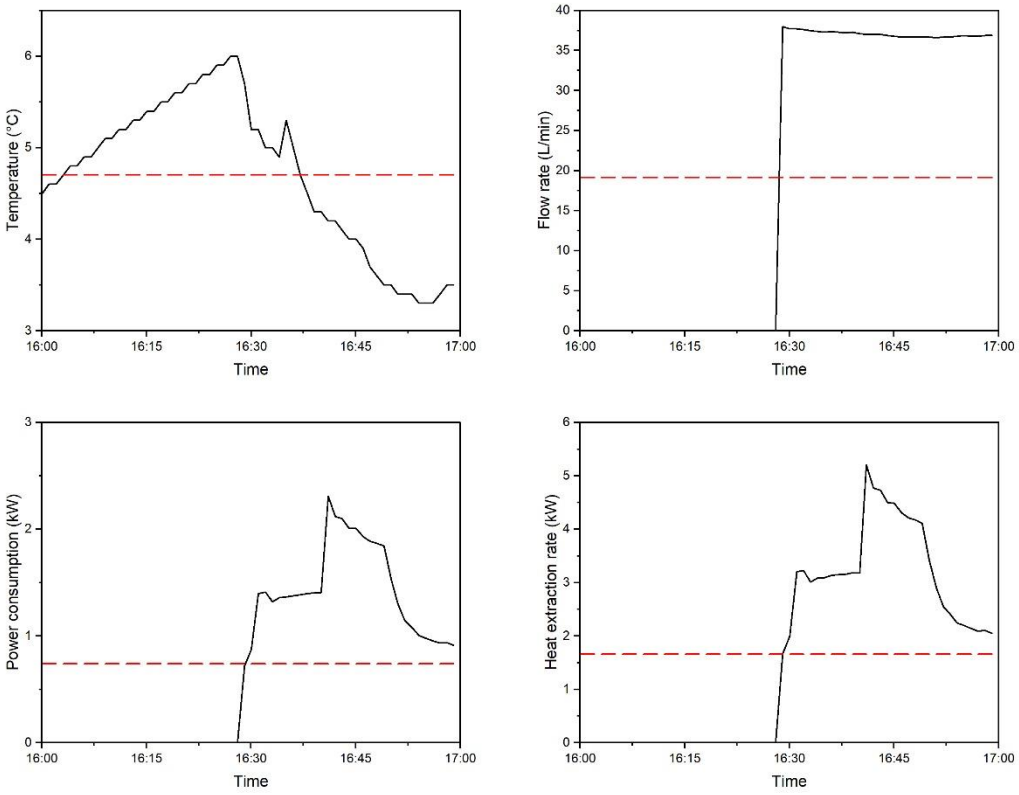

Fig. 4.2 Average values (red dotted line) of measured data from 16:00 to 17:00, 19 January 2022.

However, 15,000 datasets were still excessively large for precise analysis. To further reduce the volume of data, data from a specific hour were chosen to represent a full day's operation. This approach, focusing on periods of stable, uninterrupted system operation, was essential for ensuring data validity and representativeness.

The selection of the most representative hour was based on an analysis of hourly variations in the circulating fluid's flow rate over four distinct time periods, as depicted in **Fig. 4.3**. Regardless of whether it was a working day or holiday, the system typically began operations after 6:00 and shut down around 18:00, marked by a significant drop in flowrate that remained low until the next day's startup. Considering these operational patterns, the hour between 16:00 and 17:00 was identified as most representative of a typical day's operational conditions. This selection was made because the GSHP system was generally operating normally during this period. This approach helped avoid data distortion caused by zero flow rate periods when the system was not operational, which would render the recorded data invalid.

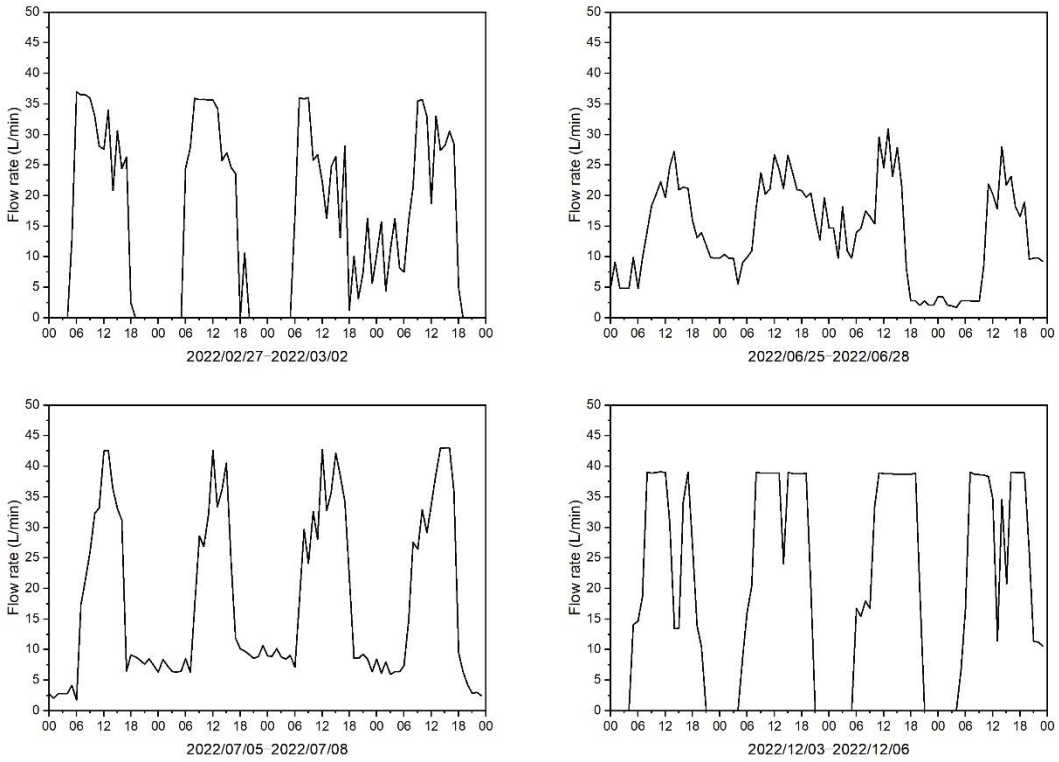

Fig. 4.3 Hourly fluctuations in the flow rate of the circulating fluid during four different periods.

4.2.2. Calculation of the Heat Extraction Rate and Fluid Temperature

The daily heat extraction rate was determined by summing the primary loads of the GSHP units over a 24-hour period. For example, the hourly heat extraction rate (in kilowatts, kW) for GSHP unit 1 on 2022/02/27, was calculated using Eq (4.3), as depicted in **Fig. 4.4**. Consequently, the total heat extraction for the day, quantified in kilowatt-hours per day (kWh/d), is calculated as follows.

$$U = \sum_{n=1}^{24} Q_1^n \times 1\,\mathrm{h} \tag{4.7}$$

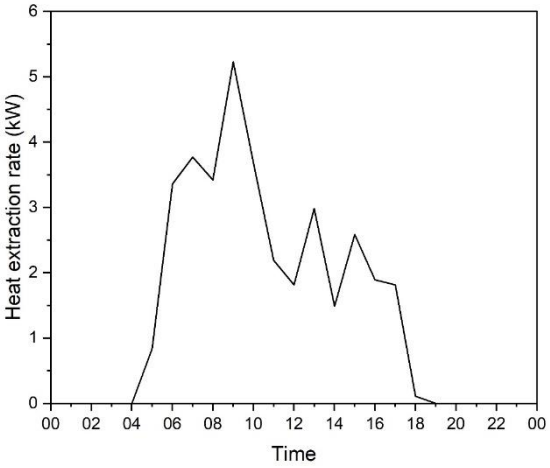

Fig. 4.4 Hourly variations in the heat extraction rate during the day.

The average daily temperature of the circulating fluid was calculated by averaging the temperature fluctuations of the fluid over a 24-hour period.

4.2.3. Data Visualization

Though the measured data can be condensed into 643 sets, corresponding to 643 days, the volume of data remained too extensive for intuitive analysis of underlying patterns. To address this, linear regression analysis and histograms are employed for visualizing the data.

For each GSHP unit, plot the temperature difference (ΔT) between undisturbed ground temperature and the average fluid temperatures at 16:00 and 17:00 daily on the x-axis. On the y-axis, plot the heat extraction rate (calculated using the average temperatures of pipe inlet and outlet at 16:00 and 17:00 daily) per unit length of the thermal pile Q_1/l, then the coefficient of heat extraction/injection can be determined using linear regression analysis.

Histograms were instrumental in visually representing the distribution of data points, aiding in the estimation of the coefficient of heat extraction/injection for the double spiral tube GHEs and in validating the linear regression analysis results. This methodology was applied to the coefficients of heat extraction/injection for GSHP units 1 and 2, analyzing a total of 15,418 hourly data sets. The data, ranging from 1.5 to 6.0 W/m·K, were categorized into 0.25 intervals to facilitate detailed analysis.

Considerable fluctuations were observed in the daily Coefficient of Performance (COP) calculations for the GSHP system, varying between workdays and holidays, influenced by operational durations. To reduce potential errors associated with long operational times, this study introduced a novel method. It involves summing the

hourly values (secondary load Q_2 and power consumption E_{hp}) over a long period to calculate seasonal COP. This method offers a more accurate reflection of real-life performance by assessing the efficiency of a heat pump unit over an entire cooling or heating season. The seasonal COP for a specific duration is obtained by summing up Q_2 over a heating/cooling season and then dividing it by the total power consumption E_{hp} for that period. This calculation was conducted as follows:

$$seasonal\ COP = \frac{\sum Q_2 \times 1\text{h}}{\sum E_{hp} \times 1\text{h}} \tag{4.8}$$

In this study, budget limitations restricted the extent of our measurements, impacting the ability to directly measure the power consumption of the GSHP system's circulation pump. According to the specifications, the GSHP system's circulation pump has a rated power of 0.4 kW and a rated flow rate of 40 L/min. During the measurement period, the power consumption of the circulating pump, denoted as E_{pump}, can be approximately determined based on fluctuations in the flow rate of the circulating fluid. Consequently, the evaluation of E_{pump} can be expressed through the following expression:

$$E_{pump} = 0.4\text{kW} \times \left(\frac{v_{fluid}}{40\text{L/min}}\right)^3 \tag{4.9}$$

By aggregating the electricity consumption of both the heat pump and circulation pump, the System's Coefficient of Performance (SCOP) can be calculated:

$$SCOP = \frac{\sum Q_2 \times 1\text{h}}{\sum (E_{hp} + E_{pump}) \times 1\text{h}} \tag{4.10}$$

It is important to note that due to the widespread shift to remote work and decreased office presence during the pandemic, up until the restrictions were relaxed in May 2022, the heat extraction/injection values prior to this date might not accurately reflect the true usage patterns of the GSHP systems. Therefore, to depict the annual operational conditions more accurately, data from June 2022 to May 2023 was utilized. **Fig. 4.5** delineates the methodology employed for the analysis of the collected data, which is crucial for evaluating the performance of the double spiral tube GHEs.

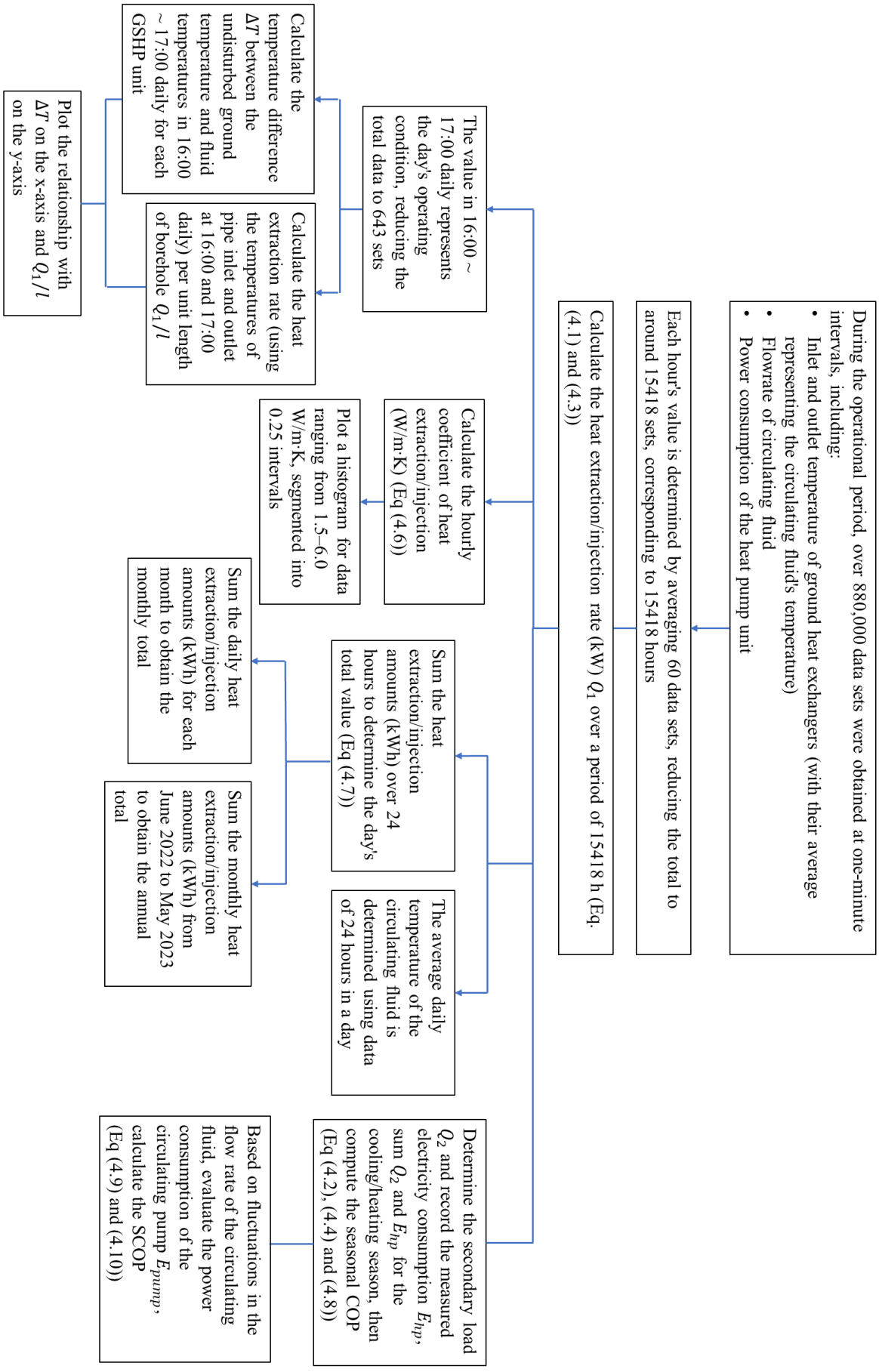

Fig. 4.5 Flow chart of data processing.

4.2.4. Uncertainty Analysis

The uncertainty associated with the coefficient of heat extraction/injection q' is a cumulative result arising from the propagation of individual uncertainties. This can be quantified using the following equation. Table 4.1 lists the experimentally measured parameters, x_i, and their respective uncertainties, $u(x_i)$.

$$u(q') = \sqrt{\sum_{i=1}^{n} \left(u(x_i) \frac{\partial q'}{\partial x_i} \right)^2} \tag{4.11}$$

Table 4.1 Experimental uncertainties.

Parameter	Unit	Uncertainty
Pipe inlet temperature $T_{pipe,in}$	°C	$(0.30 + 0.005\lvert T_{pipe,in} \rvert)$
Pipe outlet temperature $T_{pipe,out}$	°C	$(0.30 + 0.005\lvert T_{pipe,out} \rvert)$
Flowrate of circulating fluid v_{fluid}	L/min	$0.005 v_{fluid}$

4.3. Results

4.3.1. Monthly and Annual Heat Extraction/Injection Amount of the GHEs

Fig. 4.5-4.7 display the monthly heat extraction/injection amounts, along with the annual primary load, for the three GSHP units. These data spans from August 2021 to May 2023 and, separately, from June 2022 to May 2023. The transition from space heating to cooling operations occurred in October and May, leading to concurrent heat extraction and injection during these periods.

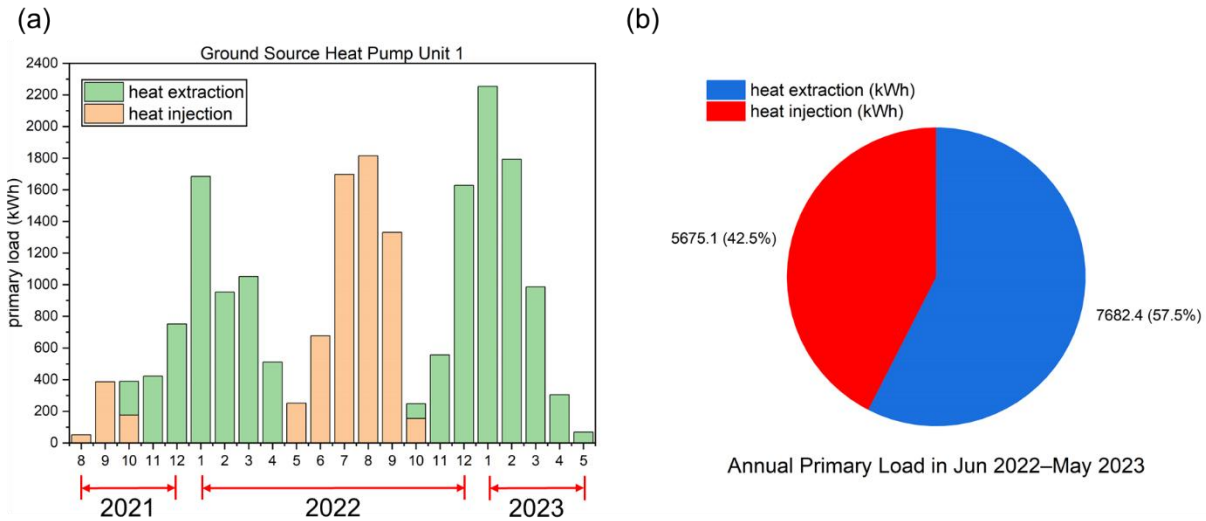

Fig.4.6 (a) Monthly heat extraction/injection amount and (b) the primary load of GSHP unit 1.

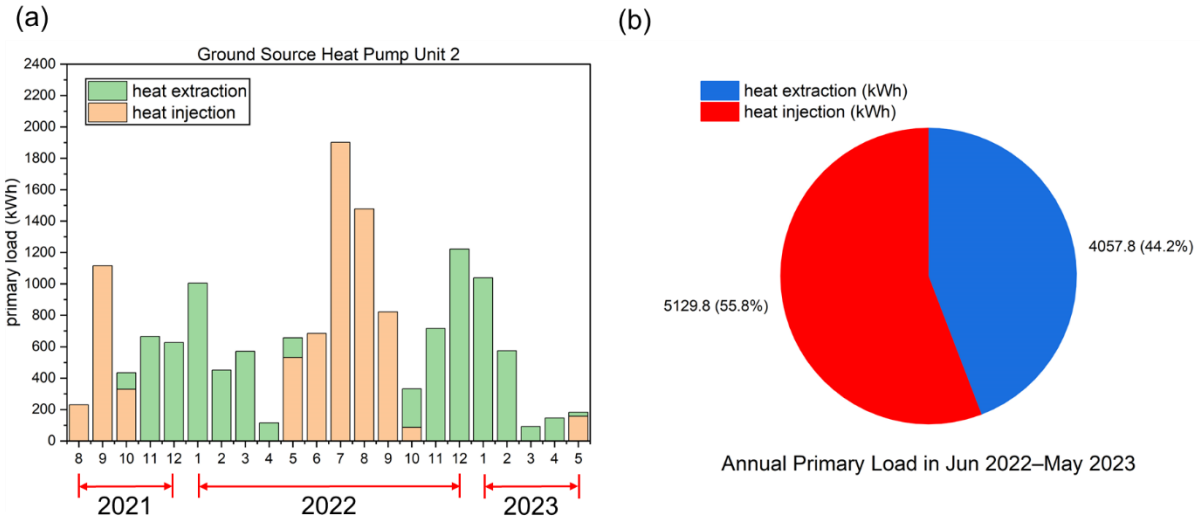

Fig.4.7 (a) Monthly heat extraction/injection amount and (b) the primary load of GSHP unit 2.

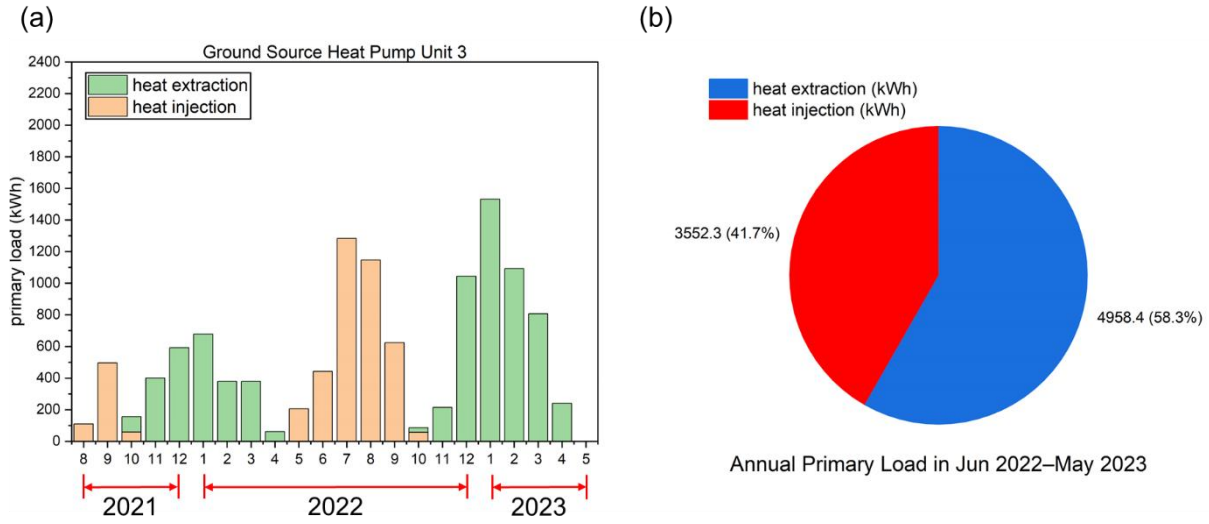

Fig.4.8 (a) Monthly heat extraction/injection amount and (b) the primary load of GSHP unit 3.

As depicted in **Fig.4.6**, the first floor of the building, hosting stores and a central control room, experiences the highest occupancy rates, showing nearly constant utilization throughout the year with the longest operating time. This constant occupancy led to relatively balanced heating and cooling demands. Analyzing the period from June 2022 to May 2023, it's evident that the heat extraction from the ground surpassed the heat reintroduction. This trend is typical in colder regions, where heating needs substantially outweigh cooling requirements.

Fig.4.7 illustrates that the second floor, primarily occupied by offices, necessitates space heating and cooling

exclusively during working days. Due to the building's superior airtightness, heating demands in winter were not excessively high. However, the recent trend of escalating summer temperatures led to a notably higher demand for space cooling in the summer of 2022, substantially surpassing winter's heating requirements. In the same period, from June 2022 to May 2023, the heat discharged into the ground was greater than that extracted.

As shown in **Fig.4.8**, the third floor, which accommodates conference rooms, requires heating and cooling only during meetings, thus having the least operational time. Consequently, its heating and cooling demands are similar to those of the first floor, with winter heating requirements exceeding those for summer cooling.

4.3.2. Daily Heat Extraction/Injection Rate of the GHEs and the Average Temperature of the Circulating fluid

Fig. 4.9 (a) shows the daily variation in the heat extraction rate for the double spiral tube GHEs of GSHP unit 1, monitored over a period of 643 days. Meanwhile, **Fig. 4.9 (b)** depicts the fluctuation in the daily average temperature of the circulating fluid within double spiral tube GHE, spanning from June 2022 to May 2023. It should be noted that data points representing days with zero heat extraction or injection were excluded from this analysis. Notably, the heat extraction rate exhibited negative values during the summer cooling period (indicating heat injection into the ground) and positive values throughout the winter heating period.

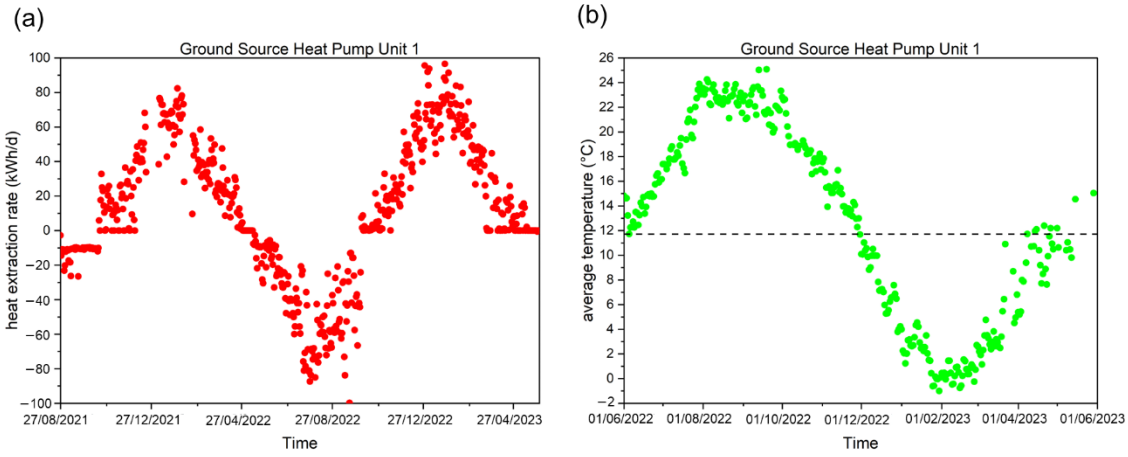

Fig.4.9 Daily variations in the (a) heat extraction amount and (b) daily average temperature of the circulating fluid for the double spiral tube GHEs of GSHP unit 1.

The first floor of the building, which accommodates the stores and the central control rooms of the system, experiences high occupancy rates. This situation necessitates considerable heating and cooling to maintain a comfortable environment. As illustrated in **Fig.4.10(a)**, the heat extraction amount for GSHP unit 1 peaked

during the December 2021–February 2022 and December 2022–February 2023 heating seasons. Concurrently, the circulating fluid's temperature decreased notably from December 2022 to February 2023.

Throughout these winter heating periods, the heat extraction rate consistently exceeded 60 kWh/day, peaking at over 80 at the start of 2022 and exceeding 100 kWh/day in early 2023. This intense activity reduced the fluid temperature to below 0 °C, though it remained above −2 °C. In contrast, during the summer cooling period from July 2022 to September 2022, the heat discharged into the ground consistently exceeded 60 kWh/day, while the circulating fluid's temperature was maintained below 26 °C, ensuring optimal operational conditions.

Fig. 4.10 and **Fig. 4.11** demonstrate the operational conditions for GSHP units 2 and 3. The second and third floors, utilized mainly on workdays and for meetings, have lower occupancy and, consequently, reduced heating demands in winter compared to the ground floor. The maximum winter heat injection for these floors barely surpassed 60 kWh/day. Over a year, the fluid temperature fluctuated between 8 and 24 °C. highlighting a substantial requirement for space cooling, even in colder regions. For instance, Hokkaido experienced an unusually warm summer in 2021.

Given the anticipated ongoing imbalance between heat injection and extraction across the years, it is crucial to address not only the anti-freeze properties of the circulating fluid during winter but also the potential increase in fluid temperature during the summer cooling periods.

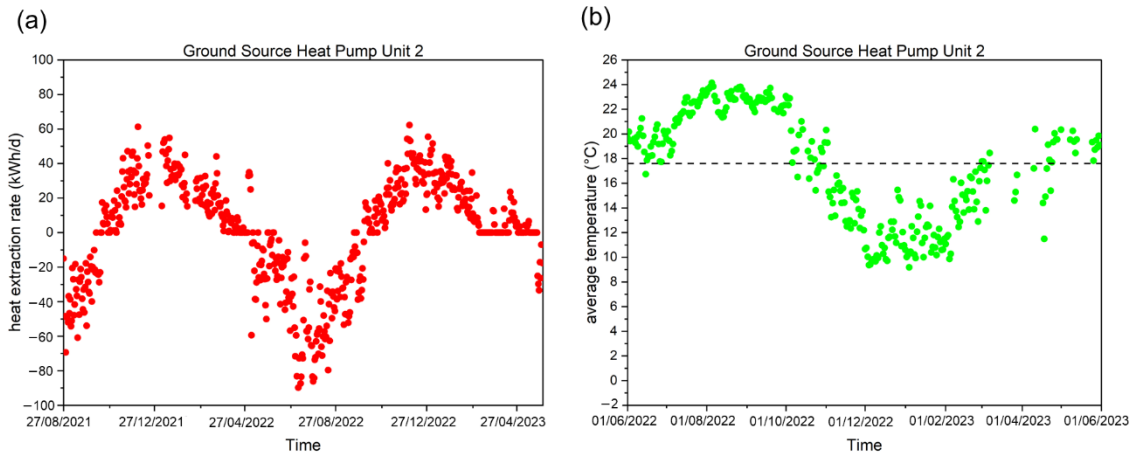

Fig.4.10 Daily variations in the (a) heat extraction amount and (b) daily average temperature of the circulating fluid for the double spiral tube GHEs of GSHP unit 2.

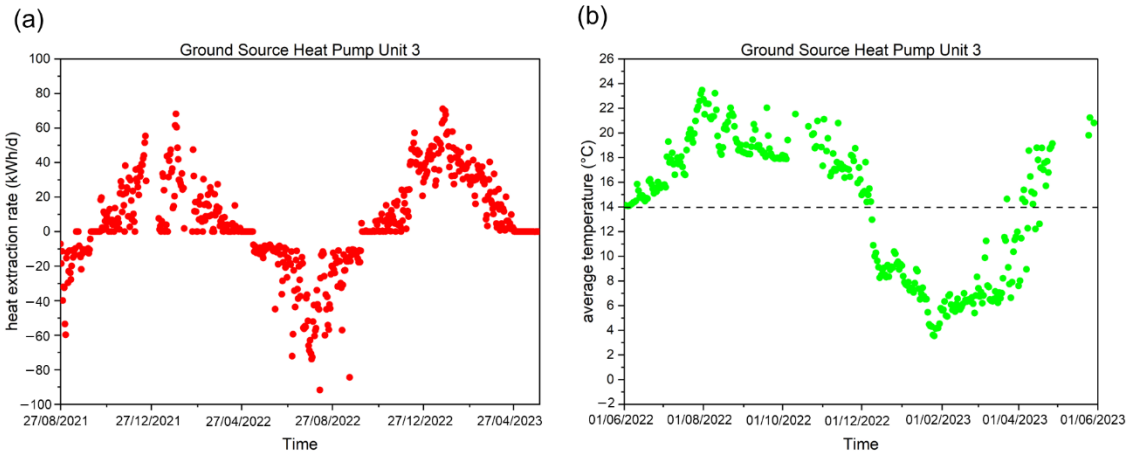

Fig.4.11 Daily variations in the (a) heat extraction amount and (b) daily average temperature of the circulating fluid for the double spiral tube GHEs of GSHP unit 3.

Theoretically, long-term operation may lead to a continuous increase in ground temperature, which could impact the system's efficiency. Nonetheless, the temperature of the circulating fluid in the 3 GSHP systems examined in this study remained within the operational range, showcasing the system's robust adaptability.

4.3.3. Calculation and Comparison of the Coefficient of Heat Extraction/Injection of the GHEs

Fig.4.12–14 depict the data points (red) representing the temperature difference ΔT between the undisturbed ground temperature and the fluid temperatures, alongside the heat extraction rate per unit length for thermal piles of 80 m and 120 m of GSHP units 1 and 3, and unit 2, respectively.

These figures employ linear regression analysis for data visualization. Analysis of the regression line's slope (blue) indicates that the coefficient of heat extraction/injection for double spiral tube GHEs surpasses 3.4 W/m·K, with values even exceeding 4.3 W/m·K.

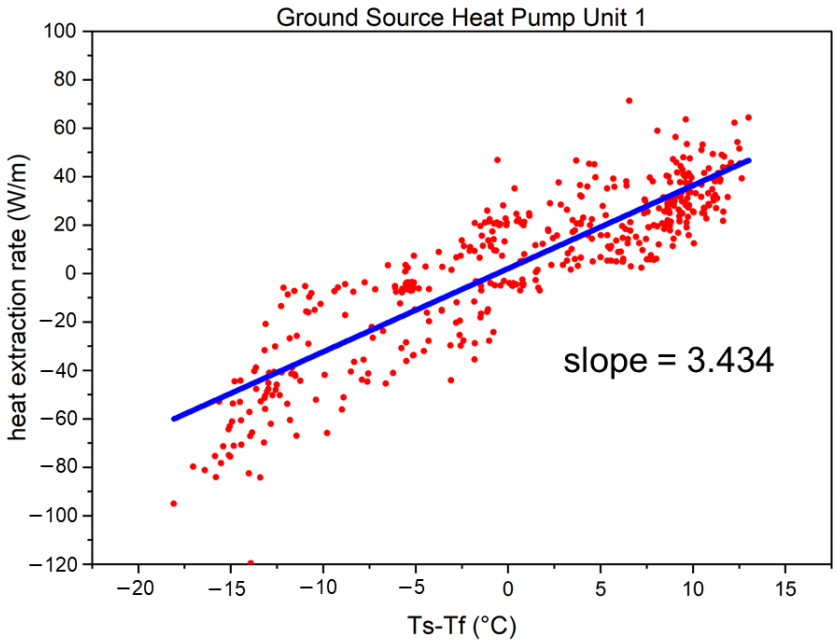

Fig.4.12 The relationship between the heat extraction rate per length and temperature difference between the undisturbed ground temperature and fluid temperatures for GSHP unit 1 (red dots) and regression line (blue).

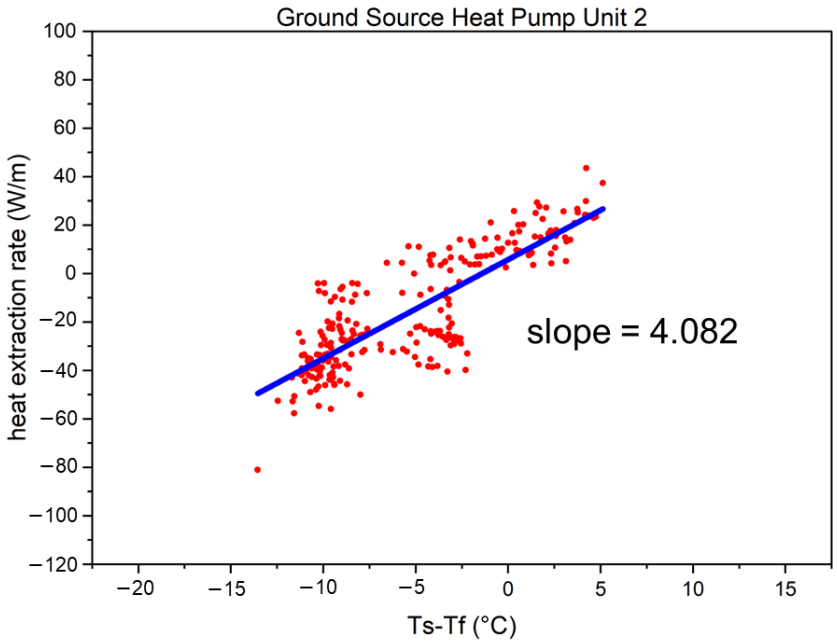

Fig.4.13 The relationship between the heat extraction rate per length and temperature difference between the undisturbed ground temperature and fluid temperatures for GSHP unit 2 (red dots) and regression line (blue).

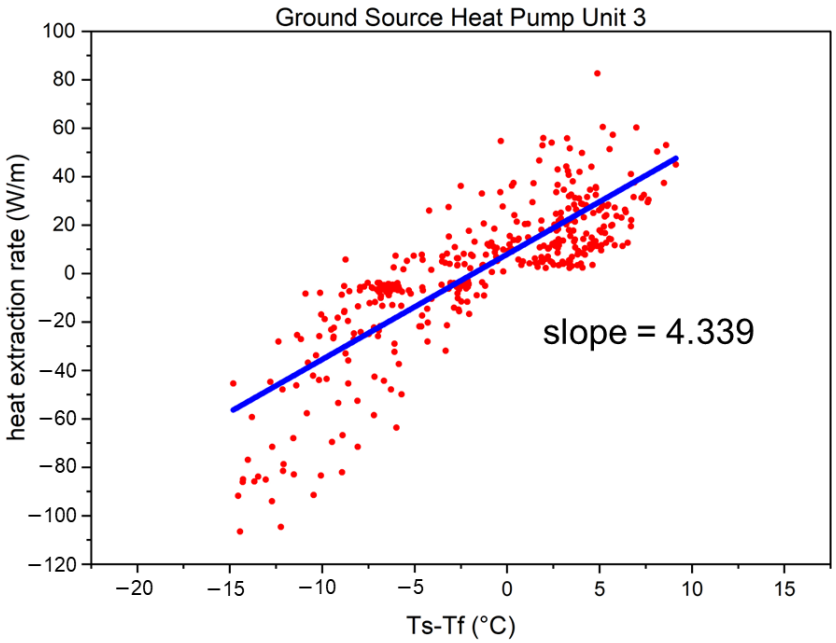

Fig.4.14 The relationship between the heat extraction rate per length and temperature difference between the undisturbed ground temperature and fluid temperatures for GSHP unit 3 (red dots) and regression line (blue).

Additionally, **Fig.4.15** and **Fig.4.16**, utilize histograms to showcase the calculated coefficients of heat extraction/injection on an hourly basis. Frequency analysis indicates that the commonly observed coefficients of double spiral tube GHEs of GSHP unit 1 fall within 3.5–4.0 W/m·K, whereas for double spiral tube GHEs of GSHP unit 2, these coefficients vary from 3.75 to 5.0 W/m·K. This latter range is less distinct, potentially due to the large heat capacity of the thermal pile causing deviations and insufficient operation time. These findings align with the slopes of the regression lines observed earlier.

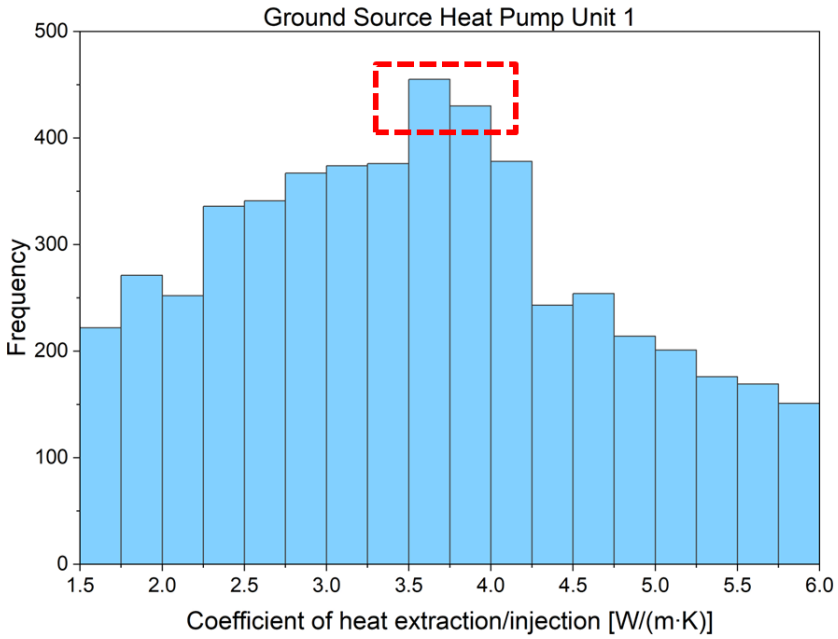

Fig.4.15 Distribution of hourly coefficient of extraction/injection for GSHP unit 1 (red box highlights the value with the highest frequency).

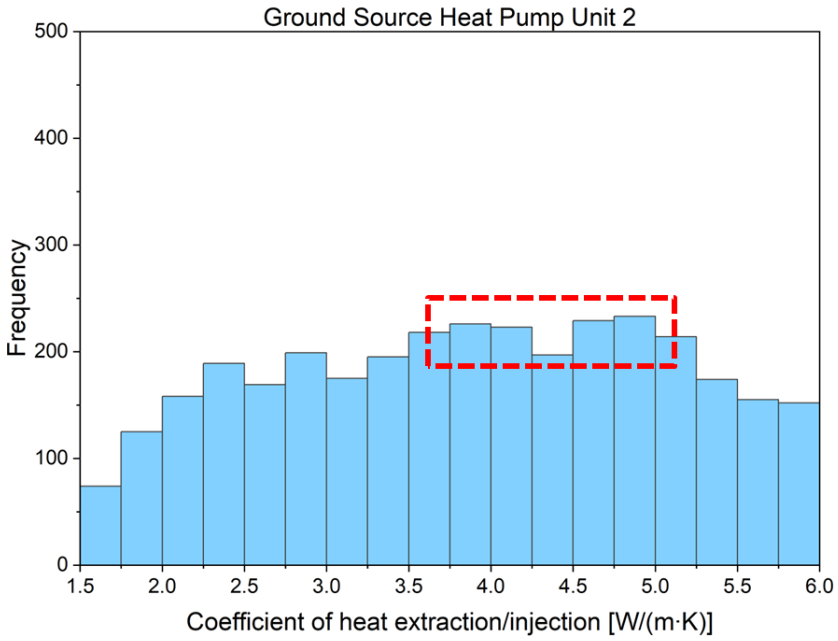

Fig.4.16 Distribution of hourly coefficient of extraction/injection for GSHP unit 2 (red box highlights the value with the highest frequency).

4.3.4. Performance Evaluation of the GSHP System

Based on the measured data, two periods of space cooling were identified in the summer months: 2021/08/27–2021/10/18 and 2022/05/06–2022/10/05. Correspondingly, two space heating periods were observed during the

winter season: 18 October–6 May 2022 and 5 October–25 May 2023. The seasonal COP for each of these periods is depicted in **Fig.4.17**.

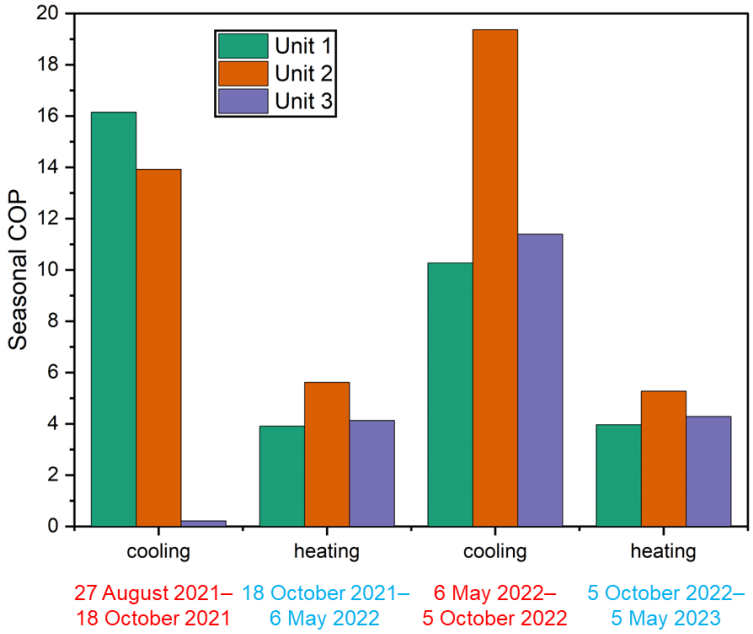

Fig.4.17 Seasonal COP of three GSHP units during four periods (red: summer cooling; blue: winter heating).

Except for the first cooling period of GSHP unit 3, the seasonal COP of all GSHP units exceeded 10 in the summers of both 2021 and 2022, with unit 2 achieving a remarkable seasonal SCOP of 20 in summer 2022. This high performance is primarily due to two factors. Firstly, the ambient temperature in colder regions like Sapporo, Japan, typically remains below 30 °C, significantly lower than many other places. This leads to a smaller temperature differential between the indoor setting (26 °C) and the outdoor temperatures, thereby reducing the need for extensive space cooling and easing the operational demand on the GSHP system. Secondly, the building employs a free cooling strategy, utilizing naturally cool air or water instead of mechanical refrigeration. When external temperatures are low, this method effectively cools the interior with minimal energy consumption, considerably enhancing the COP.

During the winters of 2022 and 2023, all GSHP units maintained a COP above four, which is notable given Sapporo's harsh winter conditions, where temperatures frequently drop below 0 °C, creating a significant temperature differential with the indoor setting of 22 °C. This performance is particularly impressive compared to traditional air source heat pumps with a COP of around 2, and conventional GSHP systems with borehole GHEs, which typically have a COP of about 3. The studied building's GSHP systems, equipped with thermal

piles and double spiral tube GHEs, demonstrated exceptional efficiency.

Section 4.2.3 provides a thorough discussion on calculating SCOP. Considering the electricity used by the GSHP system's circulation pump, results were obtained using **Eq (4.10)**. The calculated SCOP for each GSHP unit is depicted in **Fig.4.18**. When compared to the seasonal COP shown in **Fig.4.17**, a noticeable reduction in SCOP is observed for each unit, particularly during the summer cooling period. Despite the use of free cooling, the energy required for fluid movement in the circulation pumps leads to a substantial decrease in SCOP. In winter, the SCOP does decline, but to a lesser extent, aligning with the design specifications of the GSHP unit and underscoring the system's exceptional thermal efficiency.

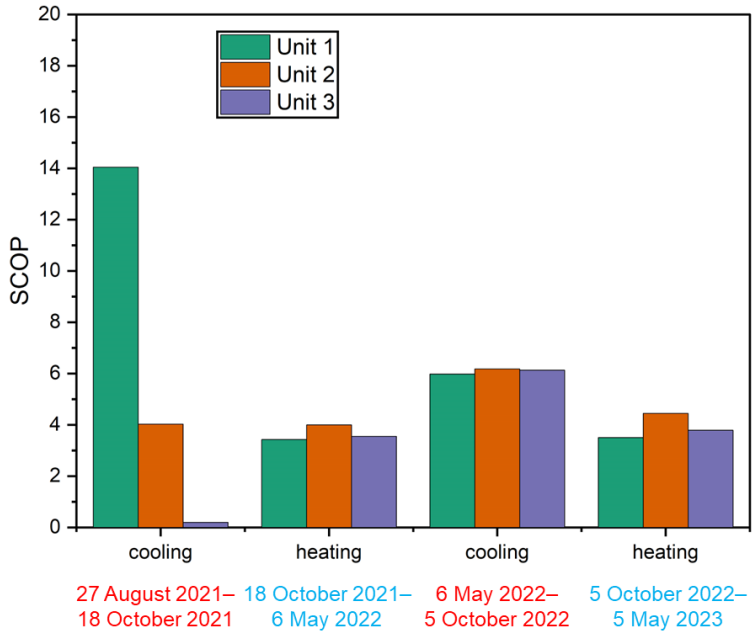

Fig.4.18 SCOP of three GSHP units during four periods (red: summer cooling; blue: winter heating).

4.3.5. Uncertainty Analysis

To analyze the uncertainty of the coefficient of heat extraction/injection q', a detailed review was conducted on a four-hour operational dataset from GSHP unit 1, recorded on 2022/07/31 was examined. This dataset included minute-by-minute records of pipe inlet and outlet temperatures, along with flow rates. Utilizing this dataset, q' was calculated for each minute. **Table 4.2** presents the hourly mean values derived from these calculations. The uncertainty of q' for each hour was determined using **Eq (4.11)**. The analysis indicates that a slightly higher error rate in the experimental temperature measurement equipment leads to increased cumulative uncertainty. However, the uncertainty $u(q')$ remains within an acceptable range. Moreover, during continuous operation of the GSHP system, the short-term values of q' are approximately around 4, which is consistent with

the findings from Section 4.3.3. Similarly, values estimated using the approximate linear method are also around 4.

Table 4.2 Pipe inlet/out temperature, fluid flowrate, coefficient q' and its uncertainty $u(q')$ during a 4 h operational period.

No.	Period	Pipe Inlet Temperature	Pipe Outlet Temperature	Fluid Flowrate	q'	$u(q')$
1	15:00–16:00	26.15 °C	24.49 °C	43.86 L/min	4.140	0.756
2	16:00–17:00	25.98 °C	24.31 °C	43.84 L/min	4.253	0.764
3	17:00–18:00	25.87 °C	24.23 °C	43.82 L/min	4.175	0.769
4	18:00–19:00	25.72 °C	24.15 °C	43.81 L/min	4.039	0.774

4.4. Discussion

4.4.1. Comparison with Traditional U-Tube GHEs

U-tube GHEs have been used in GSHP systems for decades and are frequently found in energy-efficient homes. However, this study found that thermal piles and double-spiral tube GHEs, due to their larger diameters and heat capacity, provided superior heat exchange capabilities, resulting in enhanced thermal performance compared to U-tube GHEs.

A residential house in Sapporo, Japan, adopting conventional U-tube GHEs, has been under continuous observation since 2005. Detailed specifications of this house are presented in **Table 4.3**.

Table 4.3 Basic information on the residential house in Sapporo, Japan.

Description	Value
Location	Sapporo, Japan
Measurement period	October 2005–May 2008
Type of ground heat exchanger	Borehole single U-tube
Borehole vertical length	100 m
Circulating fluid	40% ethylene glycol solution
Rated heat extraction	4.5 kW
Rated heating output	6.2 kW

Rated power consumption	1.7 kW
Temperature of undisturbed layer	10.4 °C

The GSHP system in the abovementioned house is exclusively utilized for space heating. Over the period from October 2006 to May 2007, amounting to 4714 hours, the coefficient of heat extraction was determined on an hourly basis using collected data. This analysis is illustrated in **Fig.4.19**, where the majority of data points fall within the range of 1.8–2.2 W/m·K. This suggests that the typical heat extraction/injection coefficient for U-tube GHEs is approximately 2 W/m·K. In contrast, the double-spiral tube GHEs demonstrated significantly higher values, typically between 3.5–4.5 W/m·K, underscoring superior efficiency.

Additionally, the outcomes from the simulation tool described in **Chapter 3**, which forecasts the long-term thermal efficiency of GHEs, support these observations. The simulated coefficient for heat extraction/injection for the double-spiral tube GHE was approximately 4 W/m·K, compared to around 2 W/m·K for the standard U-tube GHE. This comparison not only substantiates the accuracy of the simulation model but also emphasizes the superior performance of double-spiral tube GHEs relative to traditional U-tube designs.

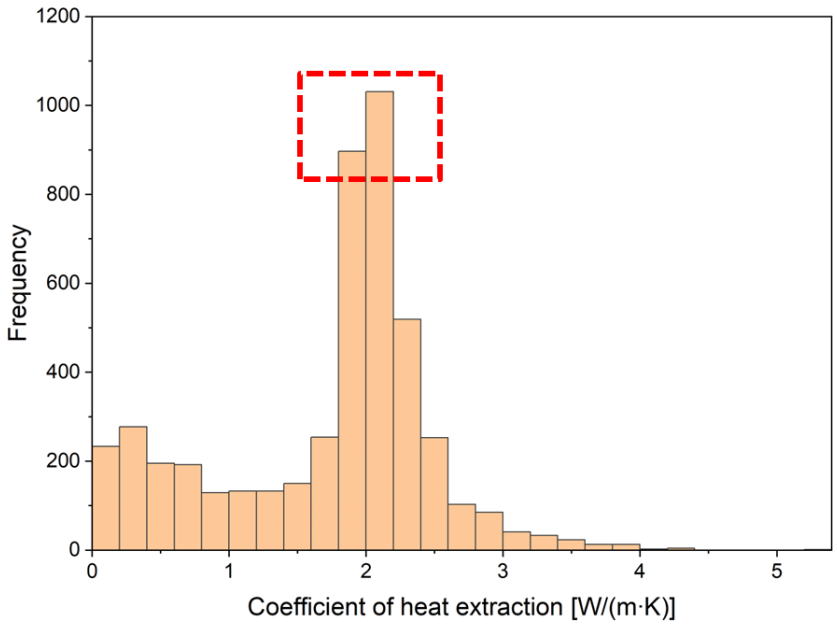

Fig.4.19 Distribution of the hourly coefficient of extraction for the residential house using U-tube GHEs (red box highlights the value with the highest frequency).

4.4.2. Cooling Demands of Places in Cold Region

Sapporo, Hokkaido's capital in Japan, is predominantly known for its cold climate, primarily characterized by

harsh winters and significant snowfall. However, the research results presented in Section 4.3.4 reveals a surprising observation: Sapporo exhibits a notably high Seasonal Coefficient of Performance (COP) during summer months. This phenomenon can be linked to its relatively mild summer weather, marked by fewer hot days and significantly lower temperatures compared to other regions in Japan. Consequently, the smaller temperature differential between indoor and outdoor settings substantially enhances the GSHP system's efficiency, particularly in terms of space cooling.

This study uncovers an unexpected result: Despite Sapporo's cold climate and its general classification as a heating-dominant region, the cooling demand during summer was higher than the heating demand during winter in some office buildings. This is attributed to the growing need for cooling in traditionally colder areas, a trend amplified by the gradual increase in summer temperatures due to global warming. Over time, these alterations may lead to sustained thermal imbalances in the soil. Addressing this emerging challenge necessitates the implementation of various strategies, such as installing cooling towers.

4.5. Conclusion

In this chapter, the thermal performance of thermal piles equipped with double spiral tube GHEs is explored, using actual measured data of GSHP systems installed in a ZEB. The key findings are as follows:

1) In GSHP unit 1, which has the longest operational duration, the circulating fluid temperature consistently remained above −2 °C in winter and did not exceed 26 °C in summer. In comparison, other GSHP units exhibited circulating fluid temperature ranges from 4 to 24 °C. Notably, the heat extraction/injection coefficient of double spiral tube GHEs of GSHP unit 1 exceeded 3.4 W/m·K, with GSHP unit 3 surpassing 4.3 W/m·K. Histogram analysis further support to these findings.
2) There was a noticeable imbalance between heat extraction and injection in the GSHP units catering to the energy needs of the second and third floors. This could potentially lead to long-term soil thermal imbalance. Despite this, the circulating fluid's temperature stayed within a suitable range for approximately two years, affirming the system's feasibility of long-term operation and resilience to climatic change.
3) Seasonal COP calculations indicated a high operational efficiency of the GSHP units, exceeding 10 in summer cooling and 4 in winter heating. These results underscore the benefits of using thermal piles equipped with double spiral tube GHEs. Additionally, after evaluating the power consumption of the circulation pump, the SCOP was calculated, which, although lower than COP, aligns with the heating COP of the GSHP system presented in **Chapter 3**.

4) In cold regions, many ZEBs without GSHP systems rely mainly on kerosene or gas for winter heating, often neglecting summer cooling. This research indicates that GSHP systems, offering both efficient heating and cooling, represent a promising and sustainable option for widespread future use.

NOMENCLATURE

c	: specific heat capacity [J/(kg·K)]
E	: power consumption [kW]
l	: length/depth [g]
q'	: coefficient of heat extraction/injection [W/m·K]
Q	: heating/cooling load [kW]
T	: temperature [°C]
U	: daily primary load [kWh]
u	: uncertainty [-]
v	: flow rate [m^3/s]
ρ	: density [kg/m^3]

ABBREVIATIONS

BHE	: borehole heat exchanger
COP	: coefficient of performance
GHE	: ground heat exchanger
GSHP	: ground source heat pump
PHC	: precast high-strength concrete
SCOP	: system coefficient of performance
ZEB	: zero energy building

SUBSCRIPTS

1	: primary side
2	: secondary side
b	: borehole of energy pile
fluid	: circulating fluid
hp	: heat pump
pump	: circulation pump
pipe,in	: pipe inlet
pipe,out	: pipe outlet
ground	: ground soil

Reference

[1] T. Katsura, K. Nagano, and Y. Nakamura, "A study on design method for the ground heat exchanger's specification of ground source heat pump system," *Journal of Environmental Engineering*, vol. 76, no. 659, 2011, doi: 10.3130/aije.76.59.

[2] K. Yang, T. Katsura, S. Nagasaka, and K. Nagano, "Development and application of a new calculation method for double spiral ground heat exchangers," *Energy Build*, vol. 291, p. 113144, Jul. 2023, doi: 10.1016/J.ENBUILD.2023.113144.

Chapter 5

Optimizing Thermal Pile and Double Spiral Tube Ground Heat Exchanger for Ground Source Heat Pump System Using New Metric and Simulation Software

5.1. Methodology

In **Chapter 4**, a novel evaluation metric, designated as the coefficient of heat extraction/injection q', is introduced to assess the thermal efficiency of GHEs. This parameter has been incorporated into GroundClub, a simulation program for GSHP system systems, facilitating a specialized tool for determining the heat exchange capacity of double spiral tube GHEs. By modifying variables such as the spiral pitch length, daily operational duration, and underground soil conductivity, an approximation curve was formulated for use in further simulations. These simulations can provide recommendations for the optimal spiral length, the number of thermal piles required, and the overall cost of thermal piles for buildings with distinct heating and cooling demands situated in zones with diverse undisturbed ground temperatures.

5.1.1. Integration with GroundClub and calculation procedure

Prior to introducing the methodology in this Chapter, the concepts of the coefficient of heat extraction/injection and GroundClub was introduce again at the beginning. Ground Heat Exchangers (GHEs), as critical components of Ground Source Heat Pump (GSHP) systems, are instrumental in either extracting or discharging heat to or from the ground. The precise estimation of GHE thermal efficiency is therefore crucial in the design stage.

Previous studies [1][2][3] have demonstrated that GHE performance is affected by several factors including the surrounding soil composition, the design and pipe materials of the GHEs, and the circulating fluid's flow rate. Further studies [4][5][6] underscored the significant impact of the undisturbed ground temperature and circulating fluid temperatures on GHE thermal efficiency.

Some researchers [7] have empirically assessed the heat extraction/injection capabilities of GHEs, using parameters like heat extraction/injection per unit length of GHE and the temperature differential between the ground and circulating fluid. This has led to the formulation of the "coefficient of heat extraction/injection." This coefficient offers a more comprehensive evaluation of GHE performance compared to the commonly used Heat Transfer Rate (HTR). It incorporates both the heat extraction/injection per unit length of GHE and the associated temperature difference, providing a more complete understanding of a GHE's heat exchange capacity under consistent temperature variations. Therefore, this innovative metric is versatile and applicable to various GHE configurations.

Hokkaido University's Environmental System Research Laboratory developed GroundClub [8], a GSHP

system simulation program. GroundClub utilizes a combination of Infinite Line Source (ILS) and Infinite Cylindrical Source (ICS) models to simulate temperature changes at the pipe inlet/outlet and in the surrounding ground.

5.1.2. Calculating the coefficient of heat extraction/injection

In **Chapter 2**, a novel calculation method for assessing the heat transfer in double spiral tube GHEs within thermal piles is proposed. This method employs the concept of fin efficiency by drawing a parallel between vertically buried double spiral tube GHEs and horizontally placed hot water pipes in radiant heating panels. This analogy enables straightforward and accurate assessment of temperature variations. Subsequently, this method is integrated with the GroundClub, making a new tool suitable for conducting long-term simulations. It is versatile, suitable for GSHP systems with thermal piles of various diameters and underground depths and can accommodate double spiral tube GHEs differing in diameter and pitch length. Furthermore, it can consider distinct geographical factors, including specific soil conductivities, unique undisturbed ground temperatures, and designated intermittent operation modes (daily operational duration) [9].

In **Chapter 4**, long-term measurements were taken at a zero-energy building in Sapporo, Japan, equipped with thermal piles and double spiral tube GHEs. This intensive monitoring aimed to gather essential data for the design of double spiral tube GHEs. Unlike many prior studies that relied hypothetical values in the design of GHEs, using assumed building loads, working temperature ranges and flowrates for circulating fluid. These approaches cannot guarantee the effectiveness of the designed GHEs and may result in failure under extreme conditions. In this research, long-term measurement data was analyzed to determine the circulating fluid flowrate, circulating fluid operating temperature range, and the heat transfer rates of the GHEs as inputs for subsequent simulations.

To verify the efficacy of the designed GSHP systems, it is essential to confirm that the GHEs can maintain effective functioning at the maximum allowable circulating fluid flowrate and heat transfer rate, while remaining within its operational temperature limits. In this study, measured peak values were used as the design constraint to determine the optimal design length of GHEs. This method guarantees that the GHEs are adequately sized to operate under diverse extreme conditions. Based on measurements from 21 months and a specific week from 2022/07/01 to 2022/07/08, the data analysis revealed that at a 20 m depth, the double spiral tube GHEs exhibited peak heat transfer rates of around 150 W/m and circulating fluid flow rates of 15 L/min, as depicted in **Fig.5.1**. Notably, the heat transfer rate during the summer (cooling period) is negative, indicating heat injection into the ground, and positive throughout the winter (heating period).

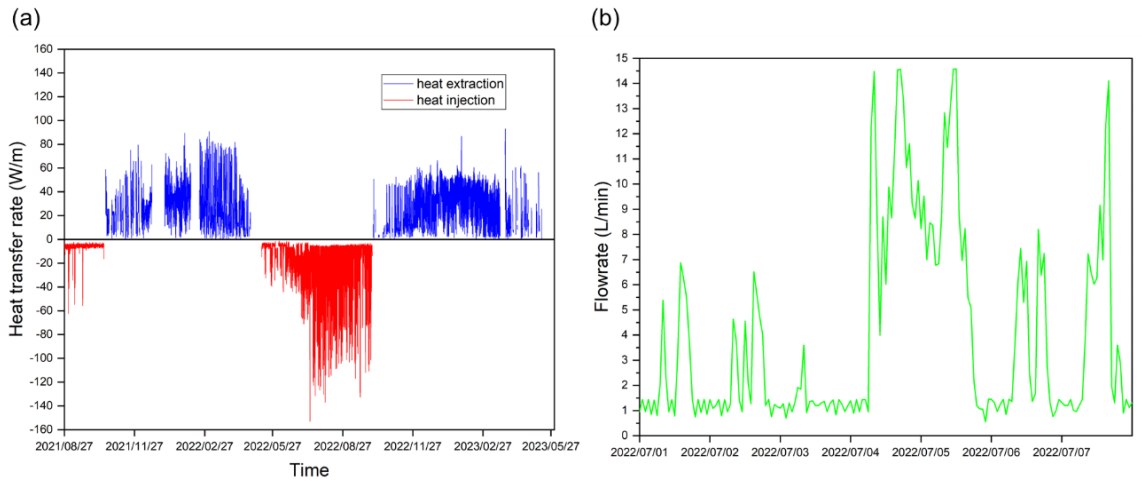

Fig .5.1 (a) Heat transfer rate over the monitoring period obtained from long-term measurement data and (b) circulating fluid flowrate across one week of a 20 m depth thermal pile with double spiral tube GHEs.

Based on the measured data, the maximum heat exchange capacity of double spiral tube GHE with an underground depth of 20 m was determined to be 150 W/m. The maximum flow rate of the circulating fluid was set at 15 L/min. In the subsequent simulations conducted using GroundClub, the heat load was configured at 3 kW, consistent with a capacity of 150 W/m, and maintained the circulating fluid's flow rate at 15 L/min.

These simulations mirrored the Thermal Response Test (TRT) procedures, as depicted in **Fig. 5.2**. In this process, the circulating fluid, after emerging from underground, is heated by a predetermined heat load before being recirculated to dissipate heat into the surrounding soil. The thermal conductivity of the soil was set at 2 W/m·K, ensuring that all other parameters conformed to the specifications of the location of reference building delineated in Chapter 3. The objective was to ascertain the temperature variations at the pipe inlet ($T_{pipe,in}$) and outlet ($T_{pipe,out}$) after long-term operation under a constant heat load and flow rate. A simulation (over one year, equivalent to 8760 h) was conducted using GroundClub, the results are shown in **Fig. 5.3**.

Utilizing the long-term temperature data in **Fig. 5.3**, the coefficient of heat extraction/injection corresponding to the hourly temperature changes was calculated. This calculation, based on the methods detailed in **Chapter 4**, yielded results illustrated in **Fig. 5.4**. As **Fig. 5.4** indicates, the calculated coefficient (q') reached stability after one year of continuous operation. The coefficient after 8760 h of operation (3.11 W/(m·K)) can be regarded as the inherent heat exchange capacity of the double spiral tube GHE with a pitch length of 250 mm. In subsequent calculations, this value can be treated as a constant physical property that is similar to density and thermal conductivity.

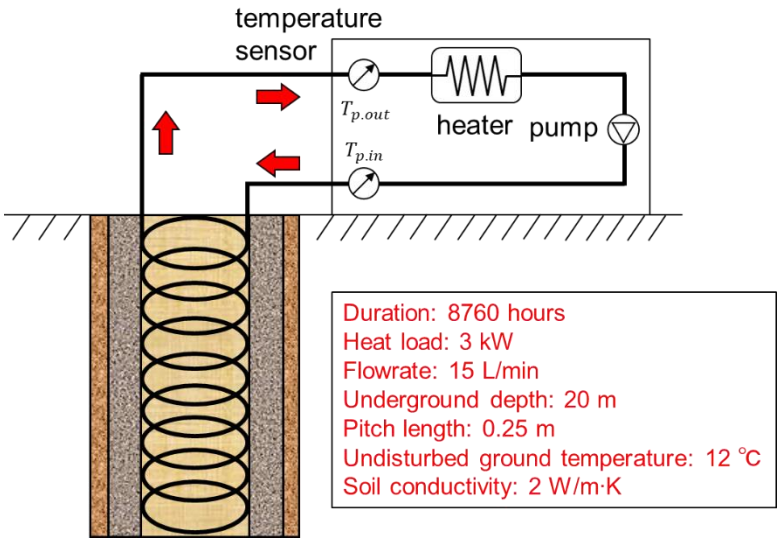

Fig. 5.2 Schematic diagram of thermal response test (TRT).

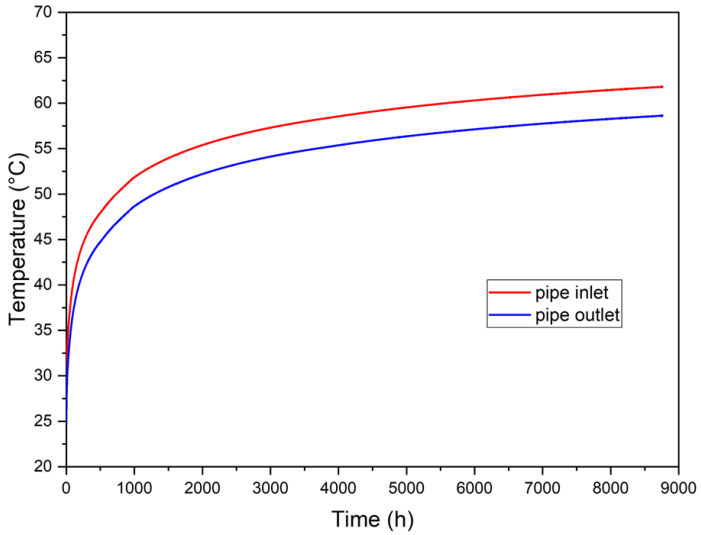

Fig. 5.3 Change of inlet and outlet temperatures of double spiral tube GHE over 8760 h.

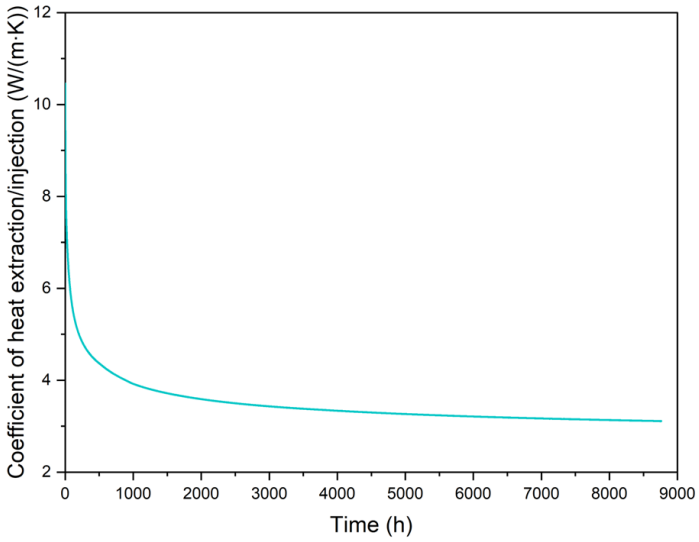

Fig. 5.4 Calculated coefficient of heat extraction/injection for double spiral tube GHE.

5.1.3. Data analysis utilizing approximation functions

Using the calculation approach described in **Section 5.1.2**, a series of simulations were executed to calculate the coefficient q' of double spiral tube GHEs with various pitch lengths under the same conditions. The results are shown in **Fig. 5.5**.

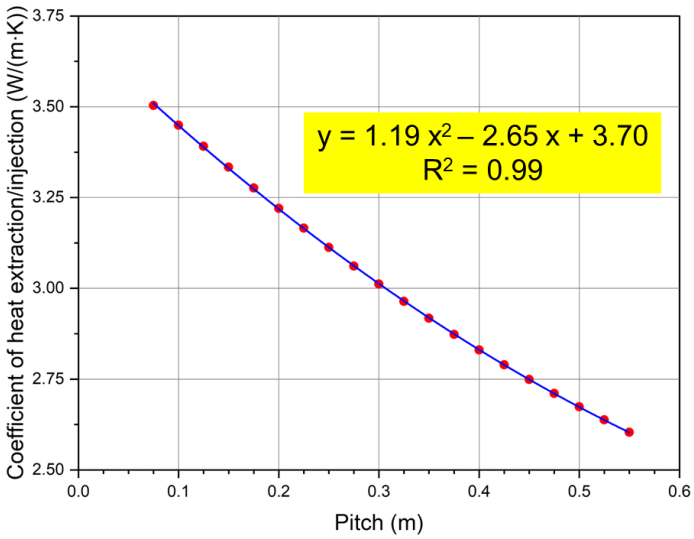

Fig. 5.5 Coefficient of double spiral tube GHEs with 20 different pitch lengths (red dots) and approximation function (blue line).

The coefficient of heat extraction/injection for double spiral tube GHEs, under constant undisturbed ground temperature and soil thermal conductivity, is evidently influenced by the pitch length. A highly accurate quadratic function (R^2 = 0.99) was derived to represent this relationship. To establish this predictive model, GroundClub was exclusively utilized to develop an approximation function correlating the pitch length with the coefficient of heat extraction/injection. Following this, the derived equation was applied in further simulations to compute the corresponding coefficients for each pitch length of the double spiral tube GHE.

5.1.4. Calculating construction cost of thermal piles

Previous studies predominantly concentrated on the design and modeling of spiral GHEs, and limited attention was given to calculating the required length and number of spiral GHEs or the associated construction

costs of building GSHP systems using spiral GHEs. This research employs simplified calculation method [10] to estimate the construction costs of constructing double spiral tube GHEs.

The design of thermal piles primarily revolves around their thermal performance in relation to the anticipated heating and cooling load profiles. Essentially, the thermal design problem involves maintaining fluid temperatures within acceptable limits to meet the varying heating and cooling demands of the pile heat exchange system. Building on the previous computational example, this study examines a building with defined cooling and heating loads of $Q_C = 70\ kW$ and $Q_H = 70\ kW$, respectively. The Coefficients of Performance (COP) were given by $COP_C = 5$ for cooling and $COP_H = 4$ for heating, based on assumptions within a reasonable range. The operating temperature range of the circulating fluid, T_f, was also determined from 21 months of fluid temperature data gathered from long-term measurements, as detailed in Section 5.1.2. As depicted in **Fig. 5.6**, the viable temperature range for the circulating fluid was established between -5 °C and 30 °C.

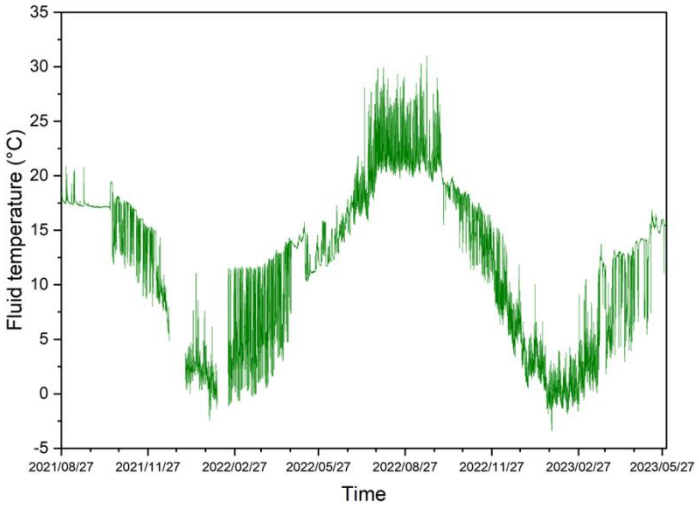

Fig. 5.6 Temperature change in circulating fluid (obtained from long-term measurement data).

Utilizing the approximation equation derived in Section 5.1.3, the coefficient of heat extraction/injection can be determined for a double spiral tube GHE with any specified pitch. The coefficient, denoted as q', is measured in W/(m·K). By applying the defined temperature range for the circulating fluid, the heat extraction or injection capacity (expressed in W/m) for a double spiral tube GHE is calculated as follows:

$$q_{Extraction} = q' \times \left(T_{ground} - T_{fluid,min}\right); q_{Injection} = q' \times \left(T_{fluid,max} - T_{ground}\right) \quad (5.1)$$

where T_{ground} signifies the undisturbed ground temperature, q' represents the coefficient of heat extraction/injection of a double spiral tube GHE at a particular pitch, and $T_{fluid,min}$ and $T_{fluid,max}$ are the lower and upper bounds of the working temperature of the circulating fluid, respectively.

The necessary quantity n of thermal piles equipped with double spiral tube GHEs can then be calculated as follows,

$$n = \max\left(Q_H \times \frac{COP_H - 1}{COP_H} \div (q_{Extraction} \times l), Q_C \times \frac{COP_C + 1}{COP_C} \div \left(q_{Injection} \times l\right) \right) \tag{5.2}$$

where l represents the vertical underground length of the thermal piles, assumed to be 20 meters in this calculation example.

The total length of pipe required for all double spiral tube GHEs is subsequently calculated. As detailed in **Chapter 3**, the thermal pile has an external and internal diameter of 0.6 m and 0.4 m, respectively. With the pipe's external diameter being 0.032 m, the distances from the outermost and innermost sides of the spiral pipe to the center are 0.2 m and 0.168 m, respectively. Given these dimensions, the total pipe length can be determined using the following equation:

$$l_{sp} = n * \left(\frac{l}{l_{pitch}}\right) * \sqrt{\left(l_{pitch}^2 + \left(\pi * \left(r_{sp,i} + r_{sp,o}\right)\right)^2\right)} \tag{5.3}$$

where $r_{sp,o}$ and $r_{sp,i}$ represent the distances from the outermost and innermost sides of the spiral pipe to the center, respectively. l_{pitch} is set at 0.25 m in this calculation example.

Before construction begins, it is necessary to insert thermal pipes into the foundation piles for the installation of GHEs. The associated costs have been estimated as follows:

- Cost of spiral pipe: The cost is calculated at 500 Japanese Yen per meter. This rate is a revision from the previously cited cost of 1,864 Yen per meter, reflecting technological advancements that are expected to

lower prices over time. This updated cost estimate is used to enhance the accuracy of simulation results.

- Integration cost of GHE into thermal pile: The expense for incorporating GHE into each thermal pile is 30, 000 Yen.
- Cost for lateral piping: For each set of thermal piles, the lateral piping costs amount to 90,000 Yen.

With these unit costs established, the total investment required for the installation of double spiral tube GHEs and N sets of thermal piles can be accurately calculated.

$$cost = 500 * l_{sp} + 30000 * n + 90000 * n \quad (5.4)$$

The pitch lengths were adjusted from 0.05 m to 0.55 m in 0.005 m increments to assess the corresponding construction costs for double spiral tube GHEs corresponding to each pitch length. This process generated 100 datasets, as illustrated in **Fig. 5.7**.

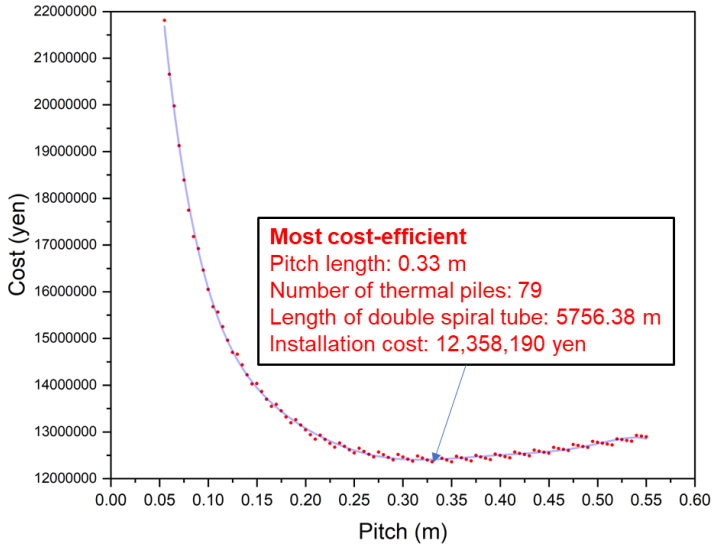

Fig. 5.7 Total cost of installing thermal piles and applying double spiral tube GHEs of different pitch length (red dots).

Analysis of the data points and the trend line **Fig. 5.7** reveals that the installation cost of double spiral tube GHEs varies with pitch length. Initially, as the pitch length increases from 0.05 m to 0.55 m, the cost decreases. However, beyond a certain point, marked by a minimum value, the cost begins to rise again. The most cost-effective installation occurs at a pitch length of 0.33 m. This configuration requires 79 thermal piles, with the spiral pipe extending 5756.38 meters, culminating in a total installation expense of 12,358,190 yen. These findings suggest that for buildings in colder regions that require the continuous operation of GSHP systems, an

optimal configuration approximates 1.1 thermal piles (underground depth of 20 m) per 1 kW of load demand.

5.1.5. Calculation flow

Sections 5.1.3 and **5.1.4** present examples cost calculations for designing double spiral tube GHEs in a building located in Sapporo. The building was designed with a cooling load of 70 kW, coefficient of performance (COP) of 5, along with a heating load of 70 kW with a COP of 4. The annual temperature of the undisturbed layer in this region remains a consistent 12°C. The thermal conductivity of the underground soil was taken as 1.4 W/(m·K). This study aims to determine the required number of 20-m-depth thermal piles equipped with double spiral tube GHEs and to estimate the total installation cost.

A critical aspect of this computational method is optimizing the pitch length of the double spiral tube GHEs, as this affects the installation cost. Reducing the pitch length can increase total pipe length, leading to an increase in the coefficient of heat extraction/injection. This, in turn, improves the heat exchange efficiency between the circulating fluid and the ground. However, there is a limit to how much the spiral pitch can be decreased. It is crucial to optimize this pitch by balancing both the total length of the pipes and the overall installation costs.

The optimal design of double spiral tube GHE for GSHP system in a building involves a systematic four-step approach:

1. Site preparation:
    - Determine the precise location for the GSHP system within the building.
    - Obtain the undisturbed ground temperature and soil thermal conductivity.
    - Establish necessary underground specifications, including underground depth, outer and inner diameters of both thermal piles and spiral pipe.
    - Gather data on thermal properties of the pile, grout, soil, and pipe.
2. Simulation via GroundClub:
    - Input all predetermined data into GroundClub.
    - Initiate simulation runs starting at a pitch length of 0.05 m, increasing in increments of 0.025 m up to 0.55 m. A set of 20 data sets is sufficient for efficient approximation.
    - Determine the maximum flow rate of the circulating fluid and the maximum heat exchange capacity of the GHE by referencing historical measured data.
    - Simulate the double spiral tube GHE over a full year (8,760 hours) under conditions of maximum thermal load and specified operation mode to record the temperature variations at the inlet and outlet.

- Use temperatures after 8,760 hours to determine the coefficient of heat extraction/injection for the double spiral tube GHEs of each pitch length.
- Derive a functional approximation correlating the pitch length of the double spiral tube GHE to its heat exchange capacity, q'.

3. Heat Exchange Capacity Analysis:
   - Identify key parameters: maximum flow rate and operational temperature range of the circulating fluid, GHE's maximum heat exchange capacity, building's heating and cooling demands, and expected COP.
   - Start with a base pitch length of 0.05 m, incrementally increasing to 0.55 m, and adjust increments as needed to refine simulation outcomes.
   - Use the approximation equation obtained from Step 2 to estimate the double spiral tube GHE's heat exchange capacity, q', in W/(m·K), and calculate peak heat extraction and injection (W/m). This determines the required number of thermal piles and total length of spiral pipe to meet building load demands.
4. Cost Analysis:
   - Apply regional manufacturing and installation cost data to calculate total investment for installing thermal piles equipped with double spiral tube GHEs.
   - Evaluate 100 datasets reflecting costs for each spiral pitch length to identify the most cost-effective option.
   - Select the pitch length with the lowest associated cost as optimal, representing the most efficient double spiral tube GHE arrangement for building applications.

The computational process was completed in about seven minutes using MATLAB. Alternative simulation software may be used to expedite computation, focusing primarily on determining temperatures at the pipe inlet and outlet. A flowchart of this computational process is illustrated in **Fig. 5.8**.

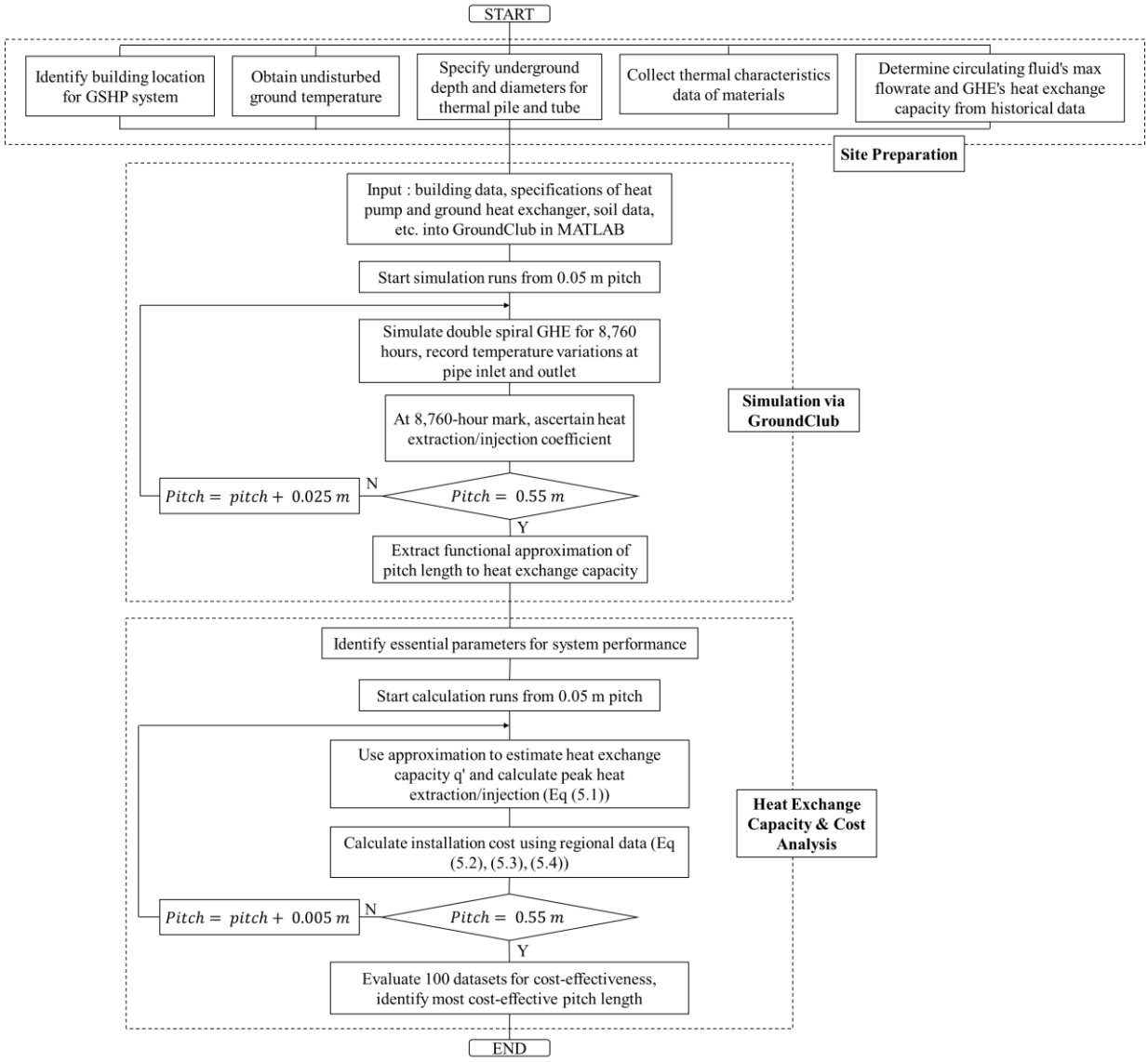

Fig. 5.8 Calculation flow of the design method.

5.2. Result

Employing the computational methods detailed above, a range of parameters was modified in simulations to generate a comprehensive spectrum of results across various scenarios. This was followed by a thorough examination of simulation results to assess the impact of each individual parameter on the system's performance.

5.2.1. Variations in operational duration

The results analyzed in **Chapter 4** have indicated that the daily operational duration has a substantial impact on the thermal efficiency of GHEs. Considering this, the following simulations were conducted:

- The settings used were the same as those employed in the calculation example: building cooling load $Q_C = 70\,kW$ with $COP_C = 5$, heating load $Q_H = 70\,kW$ with $COP_H = 4$. Undisturbed ground temperature $T_s = 12$ ℃; thermal conductivity of the underground soil $T_s = 2\,W/(m \cdot K)$; thermal pile's underground depth $l = 20\,m$ and outer/inner diameter $d_{pile,o} = 0.6\,m$, $d_{pile,i} = 0.4\,m$. Pitch length is available from $l_{pitch} = 0.05\,m$ to $l_{pitch} = 0.5\,m$. To derive the coefficient of heat extraction/injection for double spiral tube GHE, the heat load was set as $Q = 3\,kW$ and the circulating fluid flowrate was $v_{fluid} = 15\,L/min$.
- In the initial design phase of a GSHP system, it is critical to establish the daily operational duration of the system, especially since GSHP systems in most buildings do not necessitate continuous operation. For example, commercial buildings such as offices typically operate only during business hours, while residential buildings tend to be more active in the evening when occupants are home. In this study, daily operational durations are categorized into four groups: 24 hours per day (24 h/d), 18 hours per day (18 h/d), 12 hours per day (12 h/d), and 6 hours per day (6 h/d). By keeping the other variables constant, the daily operational duration is adjusted to match to the varying heating and cooling demands of different building types. The heat discharge from the GHEs to the ground across the specified durations during the summer cooling period is shown in **Fig.5.9**.
-

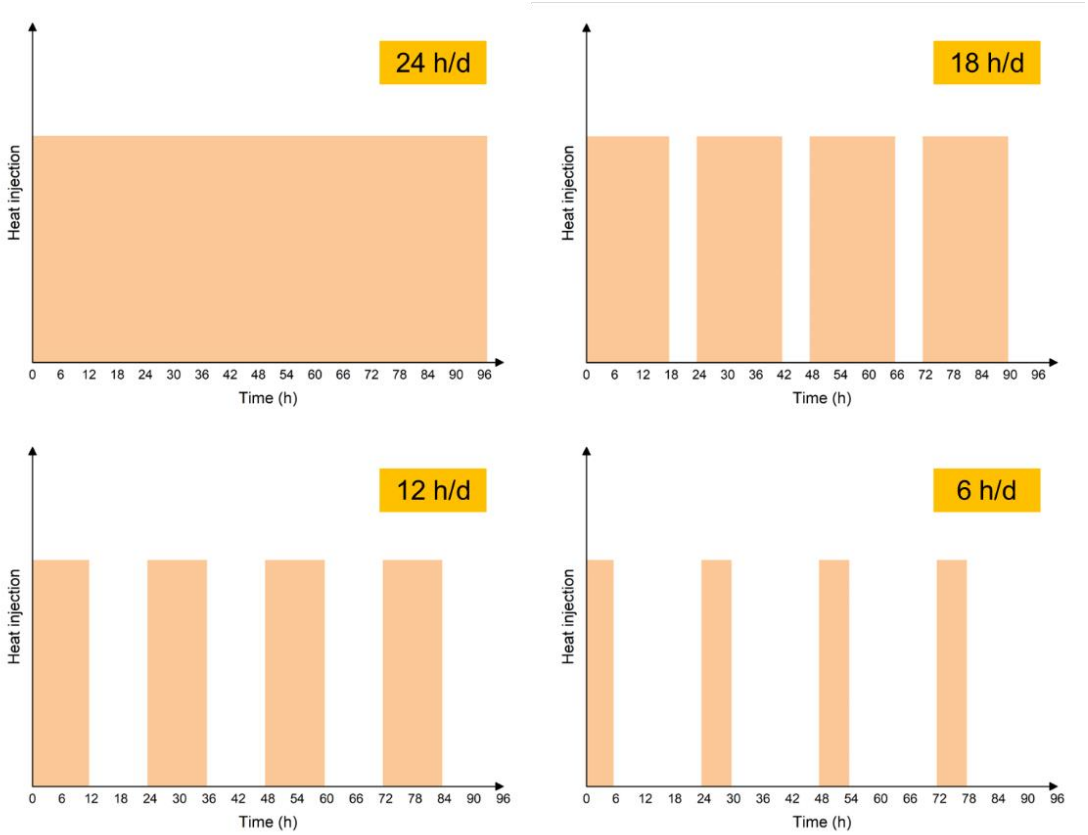

Fig. 5.9 Heat injection rate over different daily operational durations.

- The coefficient q' for double spiral tube GHEs with a pitch length of 0.1 m, 0.2 m, 0.3 m, 0.4 m, 0.5 m, the optimal pitch length and corresponding installation cost, and the quantities of thermal piles required for each operational mode are presented in **Fig.5.10 (a)** and **(b)**.

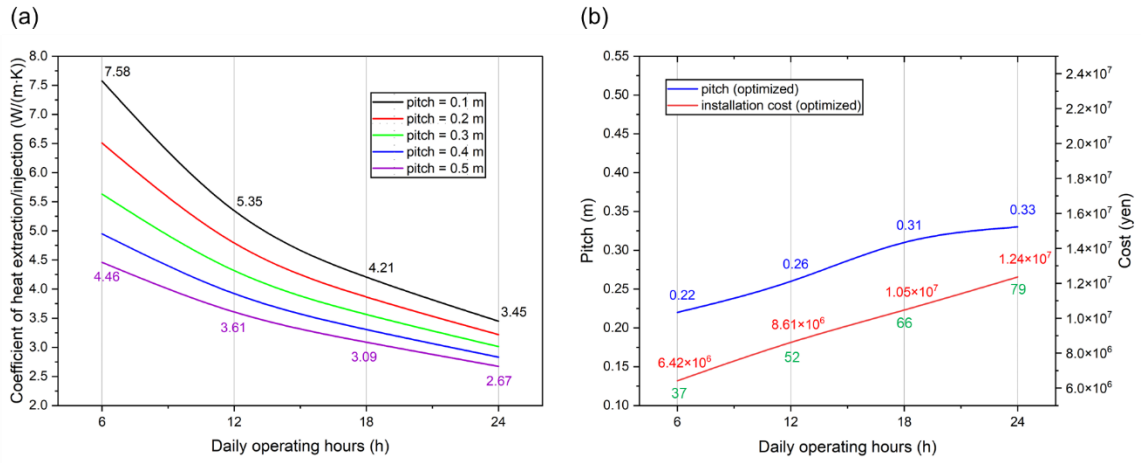

Fig. 5.10 (a) Coefficient of heat extraction/injection for double spiral tube GHEs with different pitch lengths and (b) the most cost-efficient pitch length (blue), total cost (red), and quantities of thermal piles required (green) in four operating modes.

As shown in **Fig.5.10**, the thermal efficiency of the double spiral tube GHEs not only diminishes with an increase in pitch length, but also undergoes a marked decrease as the duration of daily operation extends. Additionally, as illustrated in **Fig.5.10 (b)**, there is a noticeable increase in both the optimized pitch length and the total installation costs of the thermal piles, correlating with the extension of the daily operational time required to meet the building's load demands.

5.2.2. Variation in undisturbed ground temperature

Like many other countries, Japan experiences significant regional variations in undisturbed ground temperatures. For example, the underground temperature in Sapporo is approximately 12 °C, while in Tokyo, it's approximately 17 °C. Utilizing the same simulation settings outlined in Section 5.2.1 and setting the daily operation duration of the GSHP system to 24 h, this study modeled underground soil temperatures at 10 °C, 12 °C, 14 °C, 16 °C, 18 °C, and 20 °C. This range effectively represents the range of underground temperature profiles across different Japanese regions. The simulation results, as depicted in **Fig.5.11**, illustrate how the heat

exchange coefficient q' for double spiral tube GHEs varies with changing pitch lengths. From these results, it was possible to determine the optimal pitch length and the associated installation costs for each of the six varying conditions.

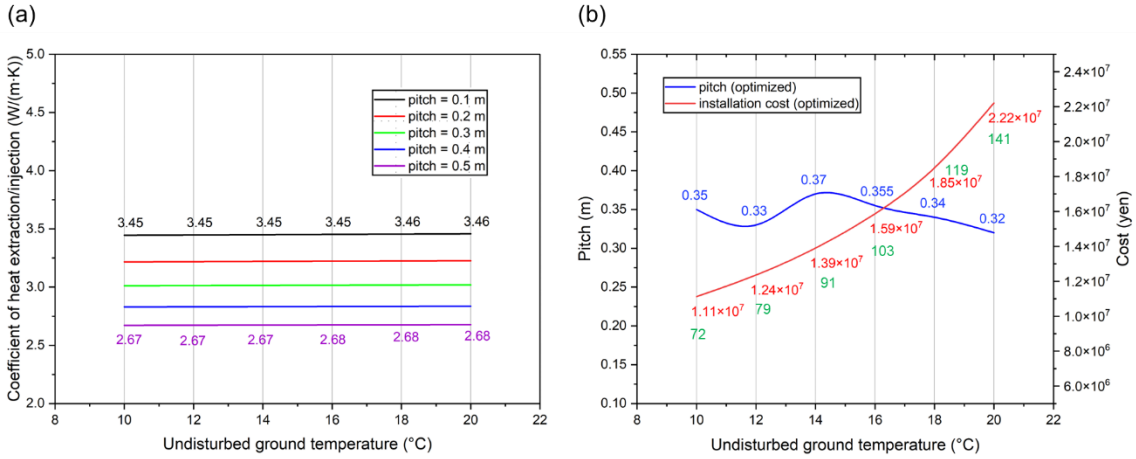

Fig. 5.11 (a) Coefficient of heat extraction/injection for double spiral tube GHEs with different pitch length and (b) most cost-efficient pitch length (blue), total cost (red), and quantities of thermal piles (green) required under six underground temperatures.

It is evident from **Fig. 5.11 (a)** that the coefficient q' for the double spiral tube GHEs diminishes with increasing pitch length. However, the impact of variations in underground soil temperature on the thermal efficiency of double spiral tube GHEs seems to be minimal. Furthermore, **Fig. 5.11 (b)** demonstrates that the construction costs for thermal piles escalate sharply in regions with higher underground temperatures.

5.2.3. Variation in underground soil conductivity

The temperature of underground soil varies, and it also possesses thermal conductivities that vary considerably across different regions and affect the heat transfer performance of GHEs. These variations are predominantly due to the distinct material composition and structural characteristics of the soil in various regions. Employing the same simulation parameters as those described in **Section 5.2.2** and setting the undisturbed ground temperature at 12 °C, this study modeled the thermal conductivity of underground soil at 2.0, 2.2, 2.4, 2.6, 2.8, and 3.0 W/(m·K). This approach was adopted to thoroughly evaluate how soil properties affect the thermal performance of GHEs. The simulation results are shown in **Fig.5.12 (a)**, with the variation in q' for the double spiral tube GHEs at different pitch lengths. The optimal pitch length for each thermal conductivity scenario is shown in **Fig.5.12 (b)** and the correlation with the associated installation costs.

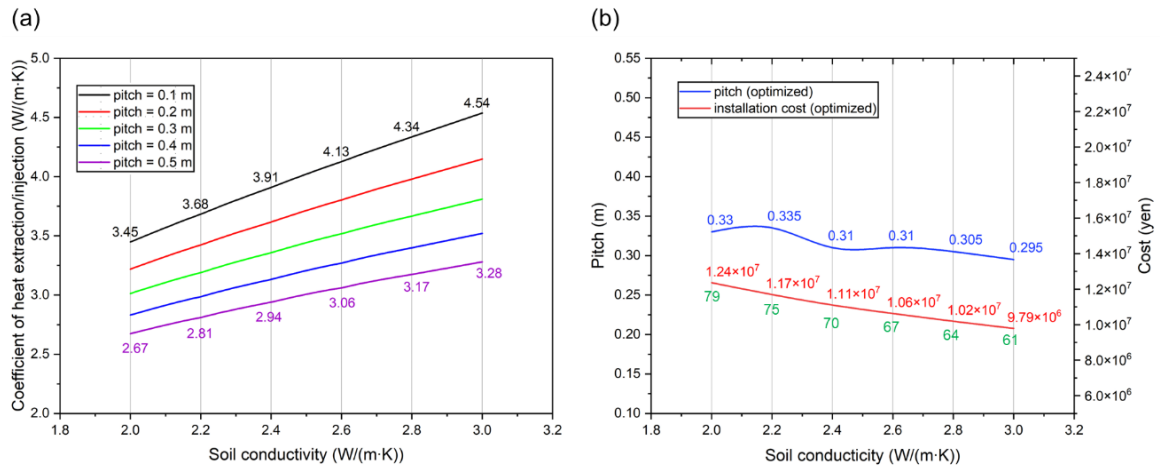

Fig. 5.12 (a) Coefficient of heat extraction/injection for double spiral tube GHEs with different pitch length and (b) most cost-efficient pitch length (blue), total cost (red), and required quantities of thermal piles (green) at sites with six different soil conductivity values.

As shown in **Fig. 5.12 (a)**, there is a noticeable decline in the q' of the double spiral tube GHEs as the pitch length increases. Conversely, the coefficient increases in correspondence with the rising thermal conductivity of the underground soil. As shown in **Fig. 5.12 (b)**, the construction costs for thermal piles are consistently reduced in areas with higher soil thermal conductivity. This reduction in costs is primarily due to the diminished underground thermal resistance that accompanies an increase in soil conductivity, consequently improving the heat transfer efficiency of the GHEs.

5.2.4. Variation in underground depth

In this study, the impact of varying the underground depth of thermal piles is explored on the heat transfer performance of the GHEs. Given the stabilization of shallow underground temperatures beyond a depth of 10 m, the simulation parameters detailed in **Section 5.2.3** was used and set the soil conductivity at 2.0 W/(m·K) to model the thermal pile at depths of 15 m, 20 m, 25 m, and 30 m. To maintain a consistent GHE heat transfer rate of 150 W/m, the corresponding heat loads were adjusted to 2.25 kW, 3 kW, 3.75 kW, and 4.5 kW. The simulation results are shown in **Fig. 5.13 (a)** with the variation in q' for the double spiral tube GHEs across different pitch lengths. The optimal pitch length for each underground depth of thermal pile is shown in **Fig. 5.13 (b)**, along with the corresponding installation costs.

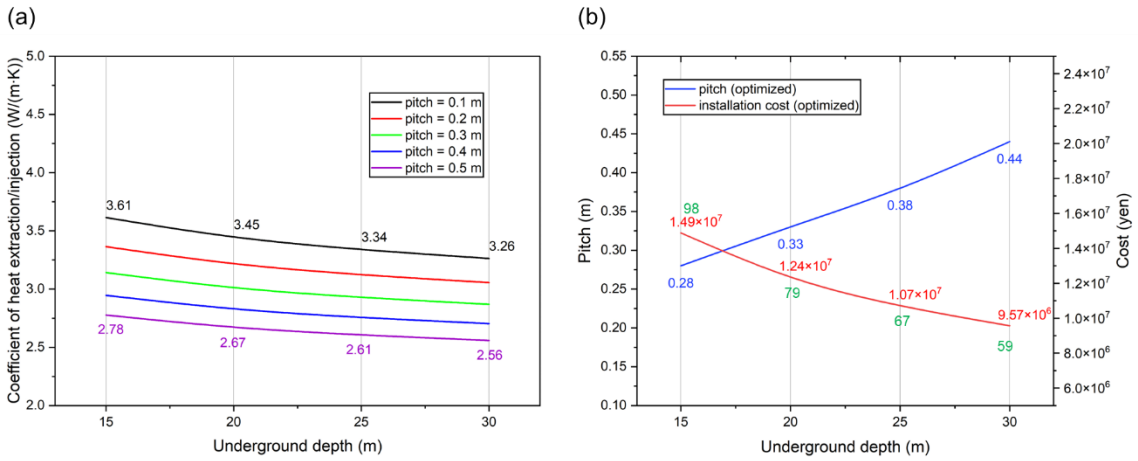

Fig. 5.13 (a) Coefficient of heat extraction/injection for double spiral tube GHEs with different pitch length and (b) most cost-efficient pitch length (blue), total cost (red), and required quantities of thermal piles (green) at sites with six different soil conductivity values.

As illustrated in **Fig. 5.13 (a)**, the coefficient q' for the double spiral tube GHEs exhibits a decreasing trend with an increase in pitch length. This decrease continued with an increase in the underground depth. The underlying cause of this pattern is the greater influence of ambient ground surface temperatures at shallower depths, which marginally boosts heat transfer efficiency. Furthermore, **Fig. 5.13 (b)** demonstrates that deeper underground installation significantly reduces both the quantities of thermal piles required and the associated costs of integrating GHEs. Moreover, the optimized pitch length appears to increase for installations at greater depths. This can be attributed to the requirement for larger pitch lengths to maintain the equivalent lengths of the spiral pipes at increased underground depths.

5.2.5. Variation in pile diameter

The thermal pile represents a novel type of GHE, distinguished by its significantly larger diameter compared to the standard borehole sizes found in conventional GHEs. By employing the simulation parameters outlined in Section 5.2.4, this study establishes an underground depth of 20 meters and explores a range of thermal pile diameters, including 0.5 m, 0.6 m, 0.7 m, 0.8 m, and 0.9 m. Concurrently, the pile thickness was consistently maintained at 0.1 m, resulting in corresponding inner diameters of 0.3 m, 0.4 m, 0.5 m, 0.6 m, and 0.7 m.

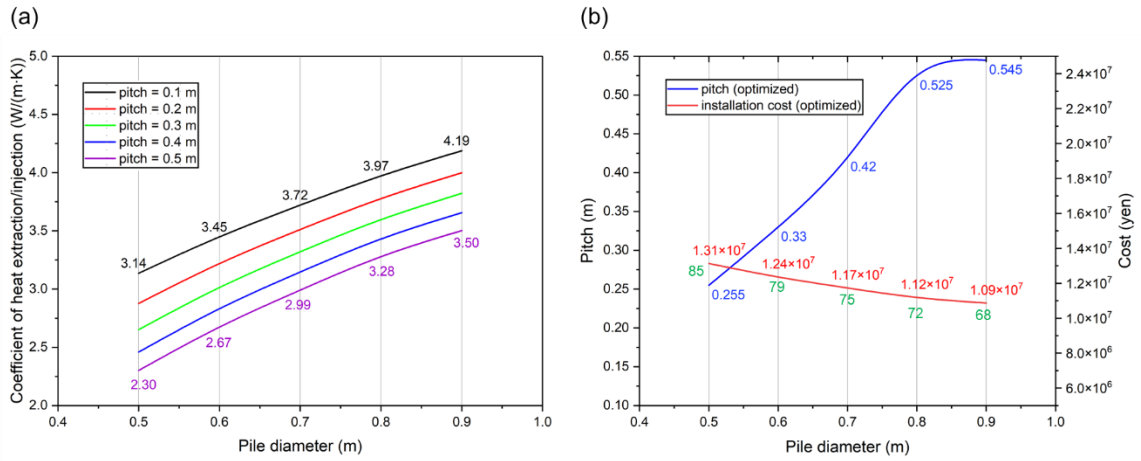

Fig. 5.14 (a) Coefficient of heat extraction/injection for double spiral tube GHEs with different pitch length and (b) most cost-efficient pitch length (blue), total cost (red), and required quantities of thermal piles (green) at sites with six different soil conductivity values.

As illustrated in **Fig. 5.14** (a), the q' of the double spiral tube GHEs demonstrates a declining trend as the pitch length increases. In contrast, it increases with an increase in pile diameter. This pattern aligns with the trends observed for increasing soil thermal conductivity, as discussed in **Section 5.2.3**. Correspondingly, as shown in **Fig. 5.14** (b), a larger pile diameter substantially lowers installation costs. Moreover, the optimized pitch length was found to increase markedly with an increase in pile diameter.

5.3. Discussion

5.3.1. Design strategies for thermal piles with double spiral tube GHEs

The simulation results presented in Section 2 highlight several important points that need to be addressed when designing GSHP systems employing thermal piles with double spiral tube GHEs.

The simulation results presented in Section 5.2.1 agree with findings in **Chapter 4**, which evaluate GSHP units with double spiral tube GHEs for providing heating and cooling in three distinct room types: retail stores with extended operating hours, office spaces requiring climatic control only during work hours, and conference rooms used intermittently. The data analysis conducted in **Chapter 4** revealed that the coefficient of heat extraction/injection was the highest for double spiral tube GHEs applied to conference rooms (4.339 W/(m·K)), followed by offices (4.082 W/(m·K)) and then retail stores (3.434 W/(m·K)). These analytical findings align closely with the simulation results of **Section 5.2.1**, reinforcing the notion that shorter operational durations amplify the thermal efficiency of GHEs.

In Section 5.2.2, the impact of undisturbed ground temperature variations on installation costs was examined.

The simulation results suggested that higher underground temperatures were correlated with increased installation costs. However, this trend was primarily linked to the predefined operational temperature range of the circulating fluid. When altering the maximum permissible temperature of this fluid from 30 °C to 50 °C, a different trend was noted. As shown in **Fig. 5.15**, the minimal installation expense corresponds to an undisturbed ground temperature of 16 °C. This finding highlights the substantial impact of optimal circulating fluid type and its temperature range on the efficiency and cost-effectiveness of GSHP systems. Moreover, integrating these insights with the findings from **Section 5.2.3**, which showed the drastic variations in installation costs owing to differences in soil conductivities, it becomes evident that it is critical to comprehensively analyze the underground soil property in the planning stages when designing a GSHP system.

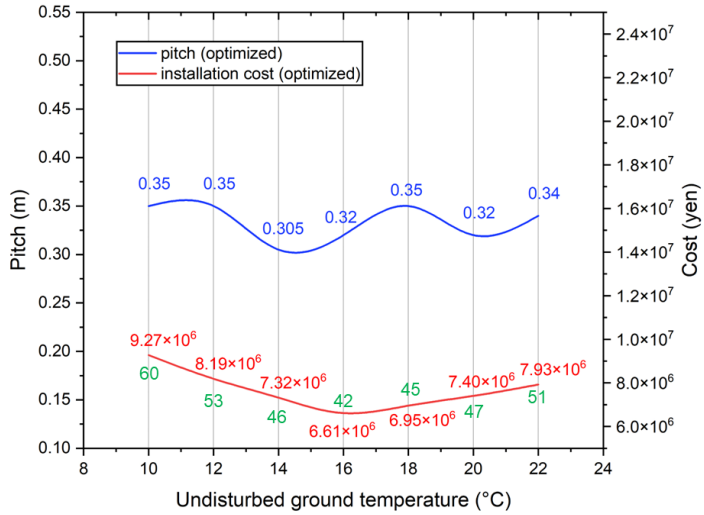

Fig. 5.15 The most cost-efficient pitch length (blue), total cost (red), and required number of thermal piles (green) using thermal piles under seven underground temperatures with a permissible circulating fluid temperature range of -5 °C to 50 °C.

5.3.2. Optimal pitch length for most thermal piles with double spiral tube GHEs

Based on the simulation results presented in **Section 2**, a set of design guidelines was established for thermal piles equipped with double spiral tube GHEs. These guidelines highlight the relationship between the diameter of the pile and the ideal pitch length for double spiral tube GHEs, applicable to thermal piles at underground depths ranging from 10 m to 30 m. The determined correlations are as follows:

- For thermal piles with a pile diameter of 0.5 m, the optimal pitch length ranges from approximately 0.2 m to 0.3 m. This range not only minimizes installation costs, but also ensures optimal thermal efficiency.
- With a pile diameter of 0.6 m, the ideal pitch length extends from roughly 0.25 m to 0.35 m.
- For a pile diameter of 0.7 m, the most suitable pitch length lies between 0.35 m and 0.45 m.

- When the pile diameter exceeds 0.8 m, the optimal pitch length for the double spiral tube GHEs is approximately 0.5 m.
- In most scenarios, 60–80 sets of thermal piles are required to support a building with a load demand of 70 kW. Therefore, for buildings requiring continuous operation of GSHP systems, an optimal configuration is estimated at about 0.9 to 1.1 thermal piles, each with a depth of 20 m, per 1 kW of load demand.

5.4. Conclusion

This chapter introduces an optimal design method for large-diameter vertical GHEs employed in GSHP systems. This approach enables the rapid calculation of the optimal pitch length for double spiral tube GHEs and estimates installation costs for thermal piles. A unique thermal efficiency evaluation index enhances this method, offering a more precise and practical design approach for thermal piles with double spiral tube GHEs. Key insights from our study include:

1) Design Methodology: this study proposes a method for calculating the specifications of thermal piles equipped with double spiral tube GHEs. This method optimizes pile diameter and pitch length, leading to an efficient, cost-effective GSHP system design.
2) Impact of pitch length and operation duration: the thermal efficiency of double spiral tube GHEs decreases with increasing pitch length and longer daily operations. This underlines the importance of carefully selecting pitch length and operating hours in the design of GSHP systems to maximize thermal efficiency.
3) Impact of soil properties and construction costs: the result of this study shows how soil properties, specifically thermal conductivity and temperature of the undisturbed layer, affect the thermal efficiency and construction costs of GHEs.
4) Effects of underground depth and pile diameter: the results reveal the influence of underground depth and pile diameter on double spiral tube GHE performance. Shallower depths slightly improve thermal efficiency, while a larger pile diameter enhances efficiency and reduces installation costs.

The developed simulation tool and design guidelines provide a comprehensive methodology for optimizing thermal pile and double spiral tube GHE design, especially useful for adapting GSHP systems across various geographical and soil conditions.

This study's novelty lies in its integration of a new heat transfer calculation method for spiral GHEs and the introduction of new thermal efficiency metrics, distinguishing it from most existing research which focuses primarily on heat transfer modeling and analysis. This research provides a clear design methodology and a strategy for identifying optimal solutions.

NOMENCLATURE

c	: specific heat capacity [J/(kg·K)]
d	: diameter [m]
l	: length/depth [m]
n	: quantities of thermal piles [-]
Q	: thermal load [kW]
q	: thermal load per unit length [W/m]
q'	: coefficient of heat extraction/injection [W/m·K]
r	: radius [m]
T	: temperature [℃]
v	: flow rate [m^3/s]
ρ	: density [kg/m^3]

ABBREVIATIONS

CaRM	: capacity and resistance model
COP	: coefficient of performance
GHE	: ground heat exchanger
GSHP	: ground source heat pump
HTR	: heat transfer rate
ICS	: infinite cylinder source
ILS	: infinite line source
TRT	: thermal response test

SUBSCRIPTS

1	: primary side of ground source heat pump system
2	: secondary side of ground source heat pump system
C	: cooling period
Extraction	: heat extraction from ground
H	: heating period
Injection	: heat injection into ground
fluid	: circulating fluid

fluid,max	: maximum value of fluid operational temperature
fluid,min	: minimum value of fluid operational temperature
ground	: ground soil
i	: inner of thermal pile
o	: outer of thermal pile
pipe,in	: pipe inlet
pipe,i	: inner of spiral tube
pipe,o	: outer of spiral tube
pipe,out	: pipe outlet
sp	: spiral pipe
sp,i	: inner side of spiral tube
sp,o	: outer side of spiral tube

Reference

[1] F. Tang and H. Nowamooz, “Factors influencing the performance of shallow Borehole Heat Exchanger,” *Energy Convers Manag*, vol. 181, 2019, doi: 10.1016/j.enconman.2018.12.044.

[2] A. Jahanbin, “Thermal performance of the vertical ground heat exchanger with a novel elliptical single U-tube,” *Geothermics*, vol. 86, 2020, doi: 10.1016/j.geothermics.2020.101804.

[3] X. Li, Y. Chen, Z. Chen, and J. Zhao, “Thermal performances of different types of underground heat exchangers,” *Energy Build*, vol. 38, no. 5, 2006, doi: 10.1016/j.enbuild.2005.09.002.

[4] G. Zhang, Z. Cao, Y. Liu, and J. Chen, “Field test and numerical simulation on the long-term thermal response of phc energy pile in layered foundation,” *Sensors*, vol. 21, no. 11, 2021, doi: 10.3390/s21113873.

[5] Jalaluddin, A. Miyara, R. Tarakka, A. A. Mochtar, and I. R. Muhammad Anis, “Thermal performance of shallow spiral-tube ground heat exchanger for ground-source cooling system,” in *IOP Conference Series: Materials Science and Engineering*, 2019. doi: 10.1088/1757-899X/619/1/012012.

[6] X. Huang, Z. Yao, H. Cai, X. Li, and H. Chen, “Performance evaluation of coaxial borehole heat exchangers considering ground non-uniformity based on analytical solutions,” *International Journal of Thermal Sciences*, vol. 170, 2021, doi: 10.1016/j.ijthermalsci.2021.107162.

[7] T. Katsura, K. Nagano, and Y. Nakamura, “A study on design method for the ground heat exchanger’s specification of ground source heat pump system,” *Journal of Environmental Engineering*, vol. 76, no. 659, 2011, doi: 10.3130/aije.76.59.

[8] T. Katsura, K. Nagano, Y. Sakata, and H. Wakayama, “A design and simulation tool for ground source heat pump system using energy piles with large diameter,” *Int J Energy Res*, 2019, doi: 10.1002/ER.4372.

[9] K. Yang, T. Katsura, S. Nagasaka, and K. Nagano, “Development and application of a new calculation method for double spiral tube ground heat exchangers,” *Energy Build*, vol. 291, p. 113144, Jul. 2023, doi: 10.1016/J.ENBUILD.2023.113144.

[10] S. Kavanaugh and K. Rafferty, *Geothermal heating and cooling : design of ground-source heat pump systems*, vol. 1. 2015.

Chapter 6

Conclusion and Future Study

6.1. Conclusion

Thermal piles, as an emerging type of vertical Ground Heat Exchanger (GHE), demonstrate a high heat exchange capability due to their large diameter and high thermal capacity. This allows for the incorporation of complex heat exchange pipes, further enhancing their thermal performance. The primary advantage of thermal piles is that they do not require additional land for installation, as they are integrated directly beneath buildings. This utilization leverages the high thermal capacity of foundation piles, thereby improving the heat exchange efficiency with the underground.

This thesis, encompassing 5 chapters, delves into innovative methodologies for the design and performance evaluation of thermal piles. It summarizes the main achievements of each chapter as follows:

Chapter 1 sets the stage for this research by outlining the context and significance of the study. It emphasizes the escalating global demand for energy and the intensifying impacts of climate change, highlighting the imperative shift towards renewable energy sources, with a specific focus on reducing CO2 emissions. In the realm of geothermal energy, Ground Source Heat Pump (GSHP) systems emerge as the predominant technology. However, the high installation and drilling costs associated with conventional GHEs have hindered the widespread adoption of GSHP systems. While thermal piles offer a promising alternative, enabling both land conservation and significant reduction in required underground depth, they warrant further research due to their distinct thermal behavior compared to traditional GHEs. This study explores the use of a double spiral pipe configuration for heat exchange in thermal piles, a sophisticated system that necessitates comprehensive analysis of heat transfer dynamics. The chapter delineates the research objectives, aimed at devising innovative methods for the design and performance evaluation of thermal piles, thereby bridging the identified gaps in existing literature.

Chapter 2 provides a thorough review of the existing literature on spiral tube GHEs and their integration into thermal piles. It emphasizes the simplicity and computational accuracy of the Capacity and Resistance Model (CaRM) over conventional models. This emphasis is crucial as it highlights the need for precise metrics to evaluate the thermal efficiency of GHEs. As essential components of GSHP systems, GHEs play a critical role in extracting or discharging heat to or from the ground. Consequently, accurately estimating the thermal efficiency of GHEs is of great importance during the design phase. This necessity arises from the GHE performance being sensitive to various influencing factors, such as underground depth, soil properties, and undisturbed temperature. Although previous studies have developed several efficient methods for examining

spiral tube GHEs, these techniques often encounter various limitations and flaws. This chapter lays the groundwork for the development of innovative design and evaluation methods proposed in this thesis, aimed at addressing these identified deficiencies.

Chapter 3 presents an innovative calculation method for double spiral tube GHEs, designed to enhance the precision and efficiency of heat transfer calculation. This method utilizes the CaRM approach, providing an in-depth analysis of the heat transfer process within thermal piles. A key innovation is the incorporation of fin efficiency, which significantly streamlines heat transfer calculations for spiral pipes. The chapter also offers a detailed introduction to a Zero-Energy Building (ZEB) located in Sapporo, which is utilized as the data collection site for method validation. This new calculation method has been incorporated into the GroundClub and rigorously validated within a GSHP system for winter heating and summer cooling applications. Simulation results closely align with actual measured data, exhibiting a low Root Mean Squared Error (RMSE) and very accurate fluid temperature changes. This method's superiority in precision and applicability is further evidenced by comparing it with another model used for studying spiral tube GHEs. The comparison shows that due to the application of fin efficiency for simplified heat transfer in this model, the calculated results are more accurate.

Chapter 4 presents an empirical analysis of the performance of double spiral tube GHEs in the ZEB, drawing on nearly two years of operational data. This study advances prior research by introducing a novel, comprehensive metric: the coefficient of heat extraction/injection q', for a more precise evaluation of GHE performance. The chapter describes the methodology employed to calculate this metric, focusing on assessing the thermal efficiency of GHEs. A thorough analysis of extensive measurement data is conducted, involving data simplification through linear regression and histograms for clearer visualization. This approach identifies an efficiency rate for thermal piles with double spiral tube GHEs at approximately 4 W/m·K, a figure substantially higher than that of conventional U-tube GHEs. These findings highlight the efficacy of the newly introduced evaluation metric, confirming its practical relevance.

Additionally, the chapter evaluates the performance of the Ground Source Heat Pump (GSHP) system. This includes calculating the System Coefficient of Performance (SCOP), Seasonal COP, and the annual heat extraction/injection rates of GHEs using measured data. The study reveals that climate warming, marked by rising summer temperatures in colder regions, leads to a notable increase in cooling demand, occasionally exceeding winter heating requirements. This persistent imbalance in heat extraction and injection results in underground temperature fluctuations, which impact the efficiency of heat pumps. These insights underscore the

importance of considering these climatic factors in the design and implementation of future GSHP systems.

Chapter 5 integrates the computational methods for double spiral tube GHE, introduced in **Chapter 3** with the performance evaluation metrics for GHEs discussed in **Chapter 4**. It develops an optimal design methodology for thermal piles used in GSHP systems. This approach enables rapid calculation of the ideal pitch length for double spiral tube GHEs and facilitates estimation of the most cost-efficient installation methods for thermal piles. Detailed calculation flows of this optimal design method are elucidated in this chapter.

The chapter also presents simulations of this design method under various conditions, including daily operational hours, undisturbed ground temperature, underground soil conductivity, underground depth, and the diameter of thermal piles—all critical factors in designing GSHP systems. The findings demonstrate that the spiral length of double spiral GHEs has a significant impact on its thermal efficiency. Several variables markedly affect the optimization process, with the optimal spiral length and total investment costs varying substantially under different conditions. Based on the simulation results, this chapter summarizes patterns in thermal pile design that can serve as future references. It provides practical insights and guidelines, thereby enhancing the efficient implementation of thermal piles in energy-efficient buildings.

The research presented in this thesis marks a substantial advancement in the field of thermal pile technology. It introduces innovative methodologies for designing and evaluating the performance of thermal piles, effectively bridging critical gaps in current practices. The empirical validation of these methodologies in real-world scenarios signifies a significant progression in this area of study. Furthermore, the development and empirical confirmation of new design and performance evaluation methods set the stage for more sustainable and efficient utilization of geothermal energy in the future.

6.2. Study Limitations

In this study, some limitations were encountered in the research presented in **Chapters 3**, **4**, and **5**:

Chapter 3 identifies two primary limitations. Firstly, the Ground Source Heat Pump (GSHP) units were not continuously operational during the measurement process; they were activated as needed and turned off otherwise. This intermittent operation may have influenced the data, particularly due to the system's frequent starts and stops. Secondly, while the new method simplified and expedited heat transfer calculations between the ground and the double spiral pipe, it resulted in less precise results compared to more time-intensive numerical models.

In **Chapter 4**, the study primarily focuses on the practical, long-term application of GSHP systems with innovative Ground Heat Exchangers (GHEs), rather than relying on computer simulations or lab-based experimental results. This approach provides a more realistic assessment of the thermal performance of double-spiral tube GHEs under actual usage conditions. However, the study faced several limitations, including missing data during holidays due to temporary system shutdowns, unnecessary energy consumption during inactive heating or cooling periods, and the system's non-continuous operation, which differed from the steady conditions typically observed in laboratory environments. These factors, along with varying room occupancy and operational durations, may have impacted the heat extraction/injection coefficients of double spiral tube GHEs employed by the GSHP units.

Chapter 5 faced challenges due to experimental constraints, making it impractical to empirically validate the study by constructing double-spiral GHEs identical to those modeled. Available data were limited to previous studies on zero-energy buildings using GSHP systems. Although the study effectively demonstrated the applicability of the new coefficient of heat extraction/injection, it was unable to conduct comprehensive research on other GHE types commonly used in thermal piles, such as single- and double-U-tube configurations, due to time constraints.

6.3. Future Study

In the context of thermal piles with large diameters, particularly for U-tube Ground Heat Exchangers (GHEs), the potential exists to increase the number of pipes within the pile cross-section. This enhancement can lead to a more efficient performance, especially when more pipes are installed within the borehole. This approach is not limited to double spiral tube GHEs. Previous studies have conducted thermal performance analyses on various configurations, including single U-tube and double U-tube, among other multiple pile heat exchangers. Additionally, research has extended beyond prestressed high-strength concrete (PHC) piles to include steel piles. These steel piles often incorporate U-tube GHEs immersed in anti-freeze fluid or water. All these diverse configurations offer promising directions for future research endeavors.

Acknowledgment

I am profoundly grateful to everyone who supported me throughout the journey of writing this thesis.

First and foremost, I extend my deepest appreciation to Prof. Takao Katsura, my supervisor. At the beginning of my doctoral program, I faced significant challenges due to the extensive specialized knowledge required, a field in which I was initially quite inexperienced. Prof. Takao Katsura's guidance and assistance were invaluable in helping me overcome these challenges and advance my research. His support extended beyond academia, aiding significantly in my adaptation to life in Japan, which in turn positively impacted my academic endeavors.

I also extend heartfelt thanks to Prof. Katsunori Nagano, another esteemed and engaging professor in our lab. His encouragement and commendations during our discussions were a powerful source of motivation throughout my academic journey.

Special thanks go to Dr. Shigeyuki Nagasaka. Much of the extensive fieldwork for this research was conducted by him. He laid many of the theoretical foundations for this study and provided a wealth of measurement data.

My gratitude also extends to all members of the Environmental System Research Laboratory. Your assistance and support, both academically and personally, were indispensable. You helped me transition from being a newcomer to comfortably adapting to my surroundings.

Lastly, the sincerest gratitude goes to my parents. Their unwavering support, both financial and emotional, has been the bedrock of my personal and academic growth. Without their enduring encouragement, none of my achievements would have been feasible.